File

I.O.S.

INTERNAL DOCUMENT
53

GEOSTROPHIC, GRADIENT AND ACTUAL WIND FIELDS IN THE NORTH SEA DURING THE 1953 STORM SURGE

S. Ishiguro

1979

NATURAL ENVIRONMENT RESEARCH COUNCIL
INSTITUTE OF OCEANOGRAPHIC SCIENCES

INSTITUTE OF OCEANOGRAPHIC SCIENCES

Wormley, Godalming,
Surrey, GU8 5UB.
(042-879-4141)

(Director: Dr. A. S. Laughton)

Bidston Observatory,
Birkenhead,
Merseyside, L43 7RA.
(051-652-2396)
(Assistant Director: Dr. D. E. Cartwright)

Crossway,
Taunton,
Somerset, TA1 2DW.
(0823-86211)
(Assistant Director: M.J. Tucker)

INTERNAL
DOCUMENT
NO. 53

GEOSTROPHIC, GRADIENT AND ACTUAL WIND FIELDS IN THE NORTH SEA DURING THE 1953 STORM SURGE

S. Ishiguro

1979

Contents

Abstract

In relation to the investigation of the highest possible storm surge, the meteorological conditions around the British Isles from 29th January to 2nd February 1953, which caused the highest recorded surge in the North Sea, have been re-examined.

A set of isobar maps has been edited from the best available sources, and the values of atmospheric pressure at the sea surface digitized at 100 km grids. From these data, the geostrophic wind and gradient wind were computed with the frictional corrections, and they were compared with the observed wind data at 13 coastal and off-shore stations.

The computed gradient wind agrees with the observed wind in both speed and direction. The computed geostrophic wind is practically the same as the gradient wind when its speed is not high. When the speed is high (say $\geq$15 km/s or 30 kt), the geostrophic wind becomes significantly higher than the observed wind speed. The stress force at the sea surface, which generates a major part of the surge, estimated from the geostrophic wind is more than twice that estimated from the gradient wind, in nearly half of the sea surface area for more than 12 hours. This suggests the importance of the gradient wind in the dynamic treatment of a storm surge, particularly for a high wind speed.

This paper includes the full data of the pressure and wind fields. The computation of the data was carried out by the meteorological input-data processing system which is built into the new electronic model. Therefore, the data also shows an example of its output.

1. Introduction

The storm surge in the North Sea which occurred around the end of January 1953 is unique in its height and the scale of damage it caused, and therefore this has been well documented from various aspects in the countries involved. Reconstructions of the surge by solving the dynamic equations with meteorological data have been made by using a numerical model by W. Hansen (1959), and by using an electronic model by S. Ishiguro (1963, 65, 66).

The author is still interested in this particular surge, from the point of view of estimating the highest possible surge, since this is the highest recorded surge in the North Sea. This surge is being re-analysed shortly using the author's new electronic model*.

This paper describes the meteorological conditions of the North Sea from 29th January to 2nd February 1953, based on newly arranged data for the dynamic analyses of the surge, but without referring to the surge itself. In addition to a set of digitized pressure-field data for a model input, the geostrophic wind+ and gradient wind++ (both with the frictional corrections) are computed, and they are compared with available observed wind data.

The computation and display of the output were carried out by the meteorological input-data processing system (MIP)** which is a part of the new electronic model. The data in this paper also shows, therefore, an example of the output of the processing system.

---

* An electronic system, consisting of analogue and digital elements, by which the hydrodynamic equations of tides and storm surges can be solved without step-by-step computations (i.e. the differential equations, and not the difference equations) with a high speed (typically 10 milli seconds for a 10-day surge). The system can be applied to most shallow seas.

** See Appendix for the outline.

\+ The horizontal equilibrium wind, blowing parallel to the isobars, which represents an exact balance between the horizontal pressure gradient force and the horizontal component of the Coriolis force.

++ The horizontal equilibrium wind, blowing parallel to curved isobars of radius of curvature, whose centripetal acceleration represents the net inward horizontal force acting per unit mass of air.

2. Sources of the pressure field data

Although data representing details of the atmospheric pressure field and wind field at the sea-surface is required for the dynamic analysis of a storm surge, little observed data is available for a storm before about 1970. Therefore, the pressure field on the sea has been interpolated or extrapolated from the data observed at coastal stations, and then the wind field computed from the pressure field.

For the main sources of the pressure field data of the 1953 storm surge, two unpublished sets of material have been used:-

(1) UK Meteorological Office (1953): Hourly Weather Maps, from 29th January to 2nd February.

(2) Royal Netherlands Meteorological Institute (un-dated): A set of 3-hourly isobar maps, 36 pp.

(1) is hand-written data on maps, for weather forecasts, which was prepared immediately after the weather information was obtained. The data is concerned mainly with the west of the British Isles and its land area, and data for the North Sea, notably its east area, was omitted from the maps. (2) is also hand-written diagrams, and seems to have been prepared for the surge investigation soon after the event, and is very useful for filling in the missing information in (1).

Other than the two above-mentioned sets of material, information from ships in the sea at that time was checked as far as it was possible. According to the Meteorological Office, however, not many ships sent weather data, and the accuracy of their data was not necessarily comparable with that of land stations.

The following publications, which contain the information of the pressure field (although less frequent or shorter period than the two above documents), are also used as references:-

(3) UK Meteorological Office (1953): The Daily Weather Report, Nos. 33307 to 33311.

(4) Koninklijk Nederlands Meteorologisch Institut (1960): Meteorologische en Oceanografische Aspecten van Stormvloden op de Nederlands Kust, p.16-40.

(5) UK Meteorological Office (1975): Weather in Home Fleet Waters, Vol. 2, Part 1, p.142.

(6) Kruhl, H. (1954): Zur Dynamik polarer Kaltluftausbrüche am Beispiel des Holland-Orkans von 30.1. bis 1.2.1953, Ann. d. Meteorol. 6. Jg., H. 3/4, 1953/54.

(7) Rodewald, M. (1953): Der grosse Norderseesturm von 31. Januar und 1. Februar 1953, Die Naturwissenschaften, Jg. 40.

3. Treatment of the data

3.1 Grid scheme

The new electronic model uses square grids for both the meteorological system and the hydrodynamic system of the sea. The sizes of grids in the two systems can be chosen arbitrarily and independently. However, the present arrangement of the model for the sea around the British Isles uses a 100-km square grid scheme for the meteorological system, and a 50-km square grid scheme for the hydrodynamic system of the sea.

The meteorological grid scheme matches with the 100-km square grid scheme used for the numerical computer-model of the Meteorological Office, so that the transformation of data becomes simple. The coordinate of the Meteorological Office grid scheme is specified by

$$1(1 + \sin \phi) = 0.5 + (x^2 + y^2)\, A$$

$$\tan (\theta - 55^{\circ}) = x/y$$

where

x,y = Sequential number of a 100-km square grid, taking its origin on the north pole, and x along Longitude 55°E, y along Longitude 35°W.

ϕ = Latitude of the grid

θ = Longitude of the grid

$A = 0.3655667 \times 10^{-4}$

For the convenience of the author's new electronic model, the details of the above-mentioned meteorological grid scheme have been slightly modified, by separating the grids into two types: 'pressure reference grids' and 'wind reference grids'. Fig. 1 shows the relationship of the two types of grid, taking four adjacent pressure reference grids and one wind reference grid. Fig. 22 (page 28) shows the location of the two types of grids separately, with their alpha-numeric reference numbers. Note, the pressure reference grids in this scheme are the same as the grids in the Meteorological Office scheme, but they are referred to by using a different number system.

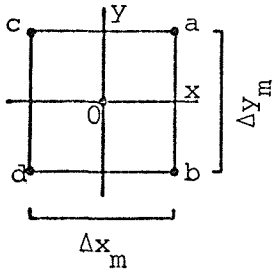

a,b,c,d: Pressure reference grids

0: Wind reference grid (centre of square abcd)

$\Delta x_m = \Delta y_m$ = 100 km

Fig. 1 Meteorological grid used in this paper

3.2 Atmospheric pressure

By combining the material from (1) and (2), and other references shown in chapter 2, and also checking their continuity with time, a set of 3-hourly isobar maps with 1-mb intervals was made first. Any doubtful data was examined as far as possible. Then the values of atmospheric pressure on the sea surface were digitized at each pressure reference grid.

The top part of Fig. 23 (pages 29 to 69) shows the set of edited isobar maps with digitized values. Each pressure value is shown by a 3-digit figure, for example,

857	means	985.7 mb
002	means	1000.2 mb
258	means	1025.8 mb

The full expression of pressure value is given for only one isobar in each map. In the completed maps, 1-mb or 2-mb intervals are used depending on the pressure gradient of each map. In the top right corner of each map, the date, time (GMT), and a map reference number which relates to Figs. 8 to 19 (pages 15 to 27) are given.

The digitized pressure values have been recorded on a tape.

3.3 Geostrophic wind

From the above-mentioned digitized pressure data, the geostrophic wind is computed by using the following equations:-

$$U_a = -\beta \frac{1}{\rho_a} \frac{1}{2\omega_E \sin\phi} (P_x \sin\delta + P_y \cos\delta)$$

$$V_a = \beta \frac{1}{\rho_a} \frac{1}{2\omega_E \sin\phi} (P_x \cos\delta - P_y \sin\delta)$$

$$P_x \equiv \frac{\partial p}{\partial x} = \{(p_a + p_b) - (p_c + p_d)\}/2\Delta x_m$$

$$P_y \equiv \frac{\partial p}{\partial y} = \{(p_a + p_c) - (p_b + p_d)\}/2\Delta y_m$$

where

U_a, V_a = X and y components of the geostrophic wind for each wind reference grid.

P_x, P_y = X and y components of atmospheric pressure gradient at each wind reference grid (0 in Fig. 1).

p_a, p_b, p_c, p_d = Atmospheric pressures at four adjacent pressure-reference grids (a, b, c and d in Fig. 1).

$\Delta x_m, \Delta y_m$ = Dimensions of a meteorological grid, in the x and y directions.

ϕ = Latitude of each wind reference grid.

ρ_a = Density of air = 1.25×10^{-3} gr cm^{-3}.

ω_E = Angular velocity of earth's rotation = 7.292×10^{-5} s^{-1}.

β = Coefficient for adjusting the geostrophic wind speed to the actual wind speed = 0.65.

δ = Angle for adjusting the geostrophic wind direction to the actual wind direction = 22°.

The computation has been carried out by the meteorological input-data processing system (see Appendix) from which the values of U_a, V_a, P_x, P_y and other related values are available simultaneously, in both the digital and analogue forms.

The bottom part of Fig. 23 (pages 29 to 69) are copies of a set of vector diagrams of the geostrophic wind obtained by the processing system which was set to the above equations. The tail of each vector arrow corresponds to each wind reference grid.

3.4 Gradient wind

The cyclonic gradient wind is computed from the above-mentioned geostrophic wind by using the following equation:-

$$V_r = \frac{V_g}{0.5 + \sqrt{0.25 + \frac{V_g}{2r\omega_E \sin \phi}}}$$

where

V_r = Cyclonic gradient wind speed.

V_g = Gradient wind speed = $\sqrt{U_a^2 + V_a^2}$

r = Radius of curvature of the isobar passing through each wind reference grid.

Fig. 2 shows an example of an isobar map, and Fig. 3 shows the values of the radius of curvature of the isobars in Fig. 2. The radius of curvature greater than 1500 km is not indicated in Fig. 3, since such values are not important from the practical point of view. For example, the depression in the top-right of Fig. 2 contains a large value of radius of curvature, but this is omitted from the diagram.

The anticyclonic gradient wind is omitted from this analysis, since the wind speed associated with an anticyclone in this storm case is small, although the curvature of its isobars is significant.

Fig. 4 shows an example of gradient wind vectors, plotted together with the geostrophic wind vectors.

Fig. 5 shows an example of the value of $(V_g/V_r)^2$ obtained from the values shown in Fig. 4. The values of V_g^2 and V_r^2 are proportional to the surge-generating force due to the geostrophic wind and gradient wind respectively. It is remarkable, for this storm case, that the ratio of the two values is more than 2 in a large area of the sea, the maximum ratio being nearly 3.

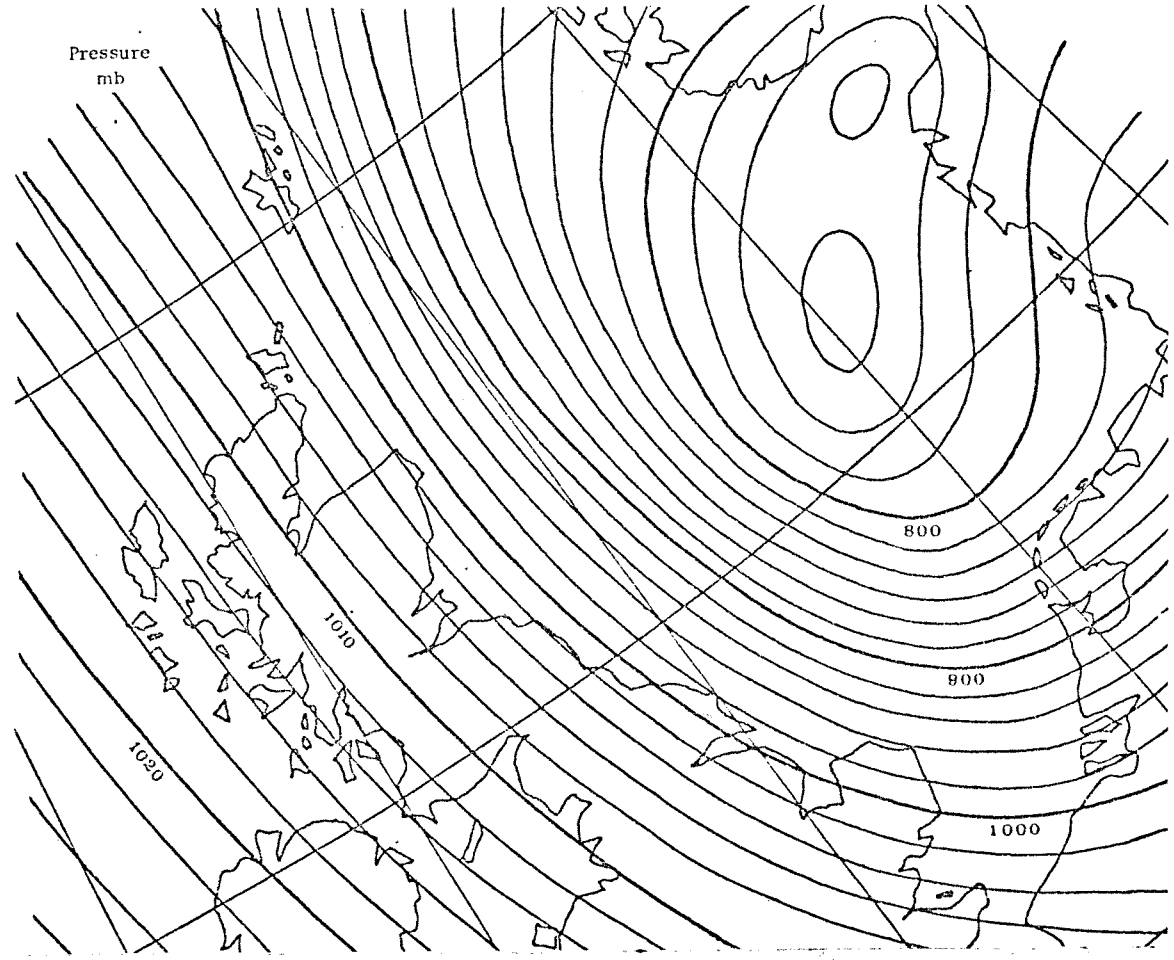

Fig. 2 An example of an isobar map.
The sea surface, 18.00 GMT, 31st January 1953.

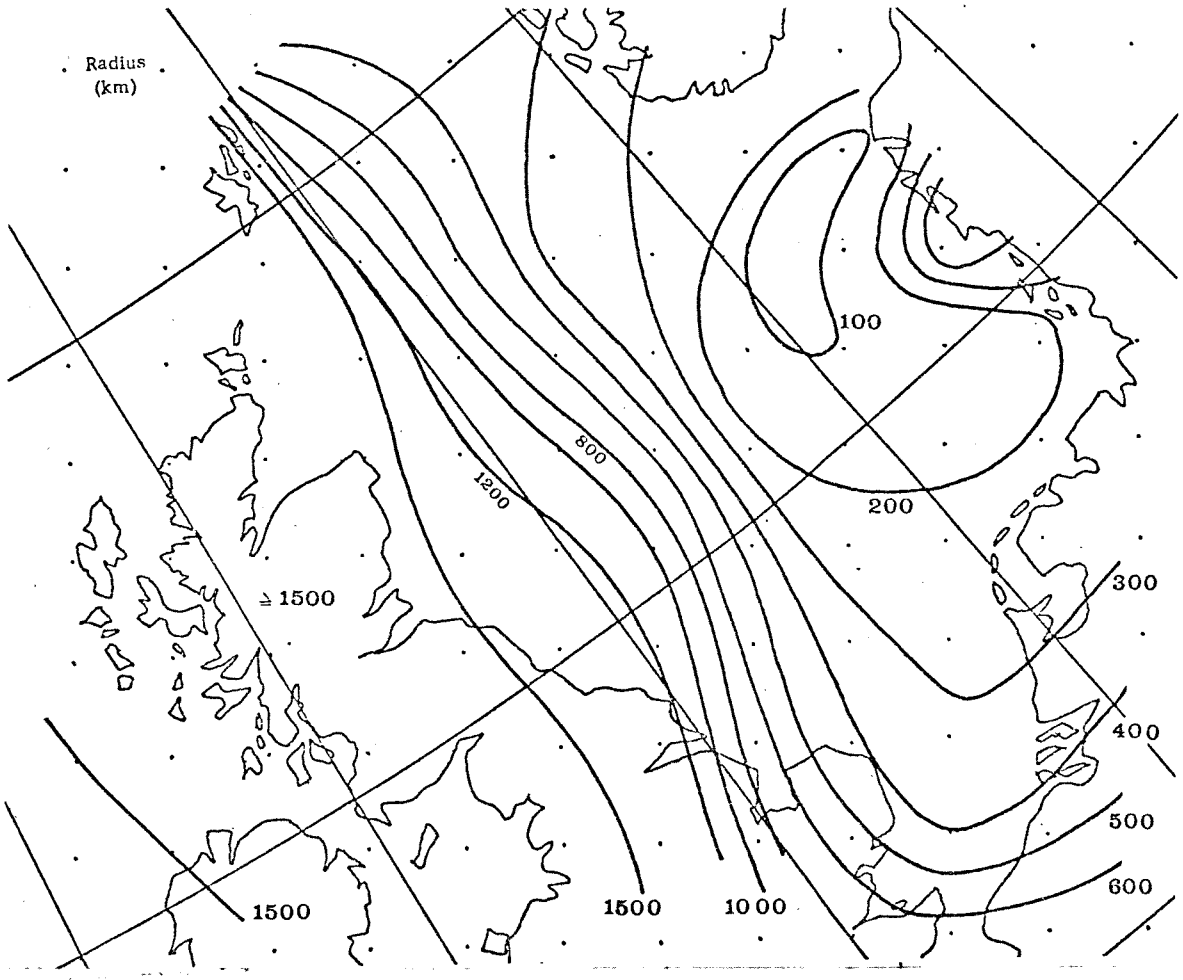

Fig. 3 An example of the radius of curvature of isobars.
The sea surface, 18.00 GMT, 31st January 1953.

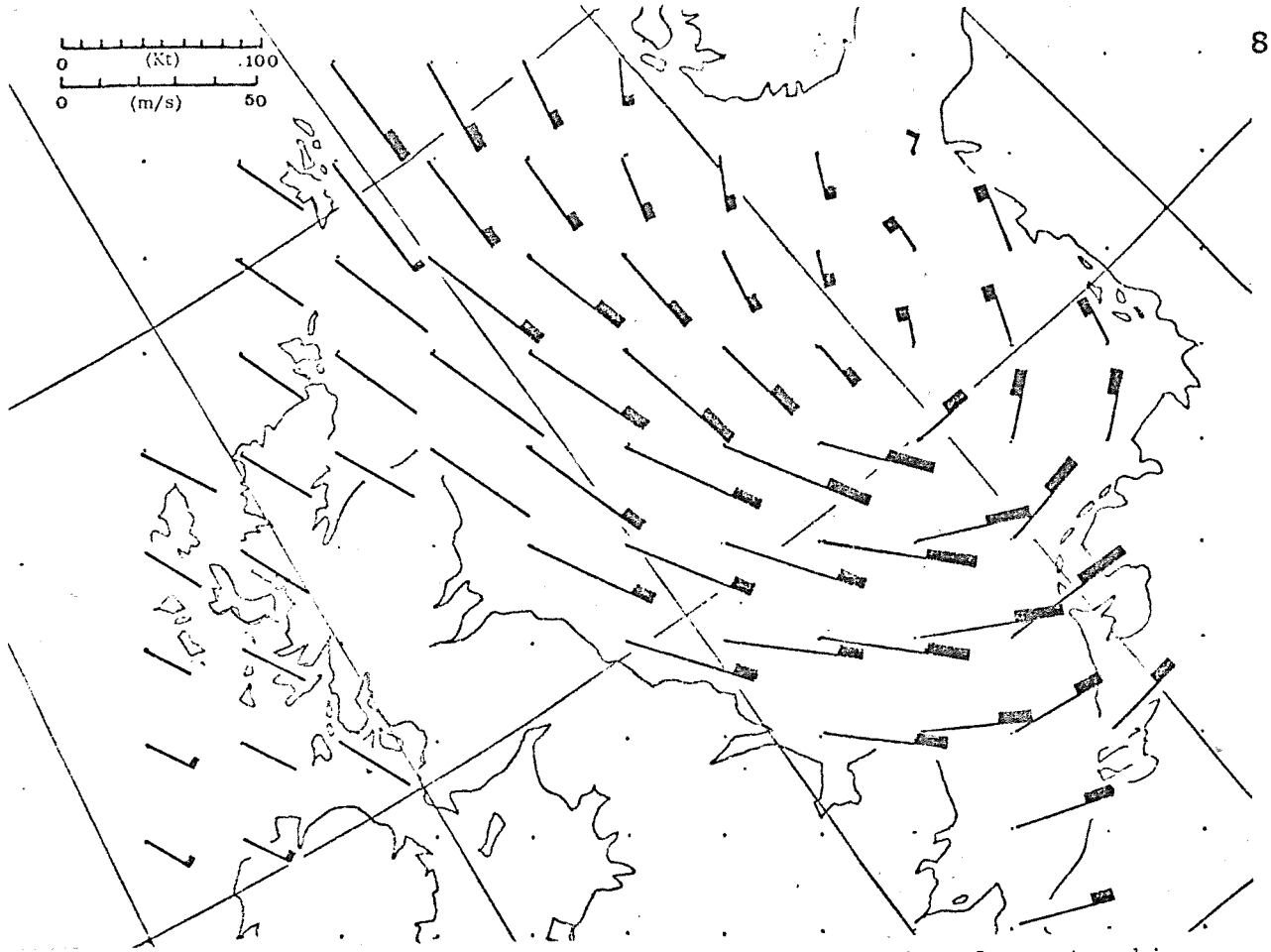

Fig. 4 An example of the gradient wind (thin line) and geostrophic wind (thin line plus thick line), both with the frictional corrections. Sea surface, 18.00 GMT, 31st January 1953.

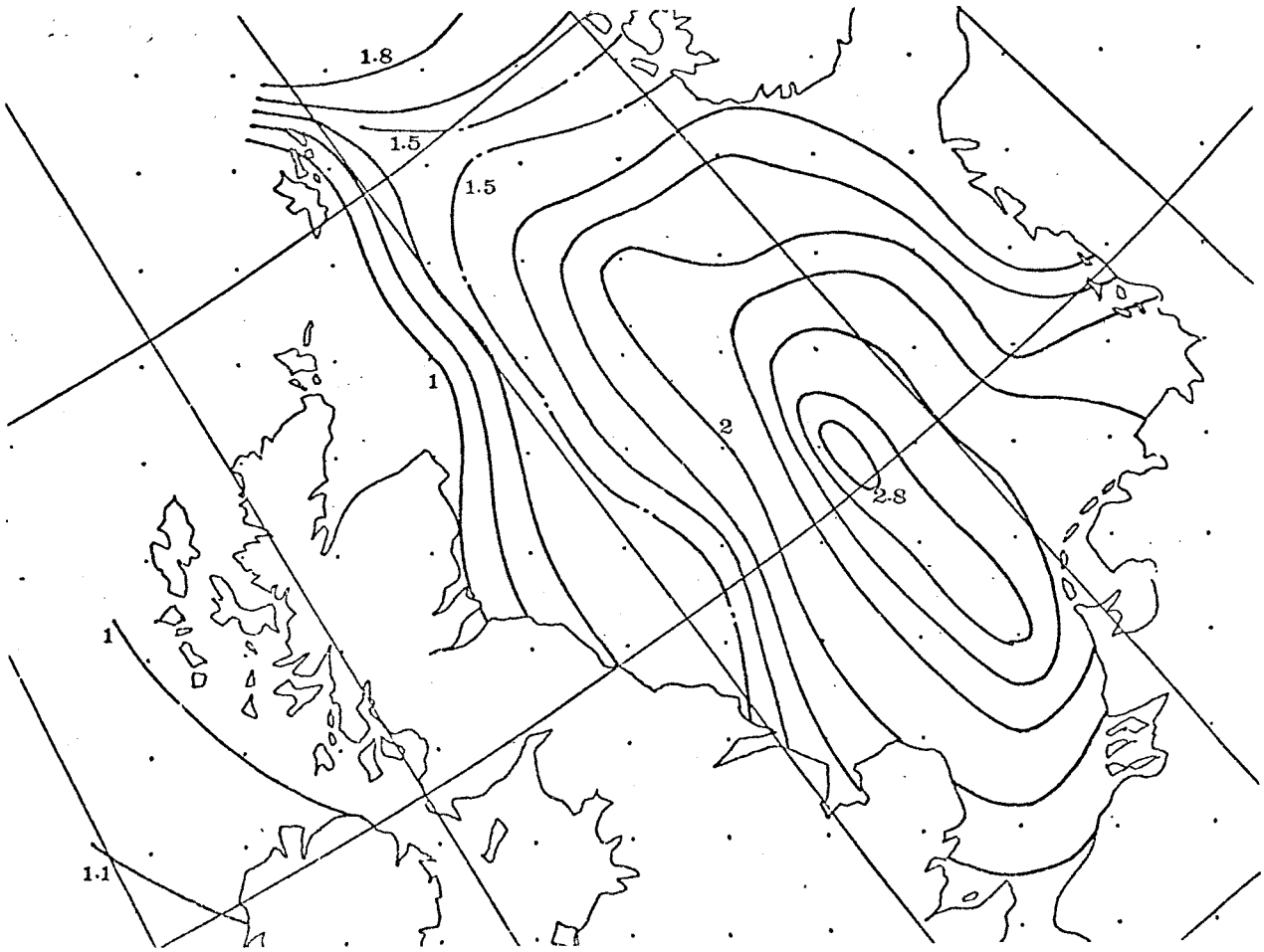

Fig. 5 Square of ratio of the geostrophic wind speed to the gradient wind speed, both with the frictional corrections. Sea surface, 18.00 GMT, 31st January 1953.

4. Comparisons of the computed wind with the observed wind

In order to evaluate the computed wind data, this is compared with the observed wind data, taking a few synoptic weather maps (area-variation) and the wind data at 13 stations (time-variation). The observed wind data is based on the documents shown in chapter 2, excluding (2).

4.1 Representation of the comparison

Fig. 6 shows an example of the area-variation comparison of the computed gradient wind and observed wind data for several coastal and offshore stations.

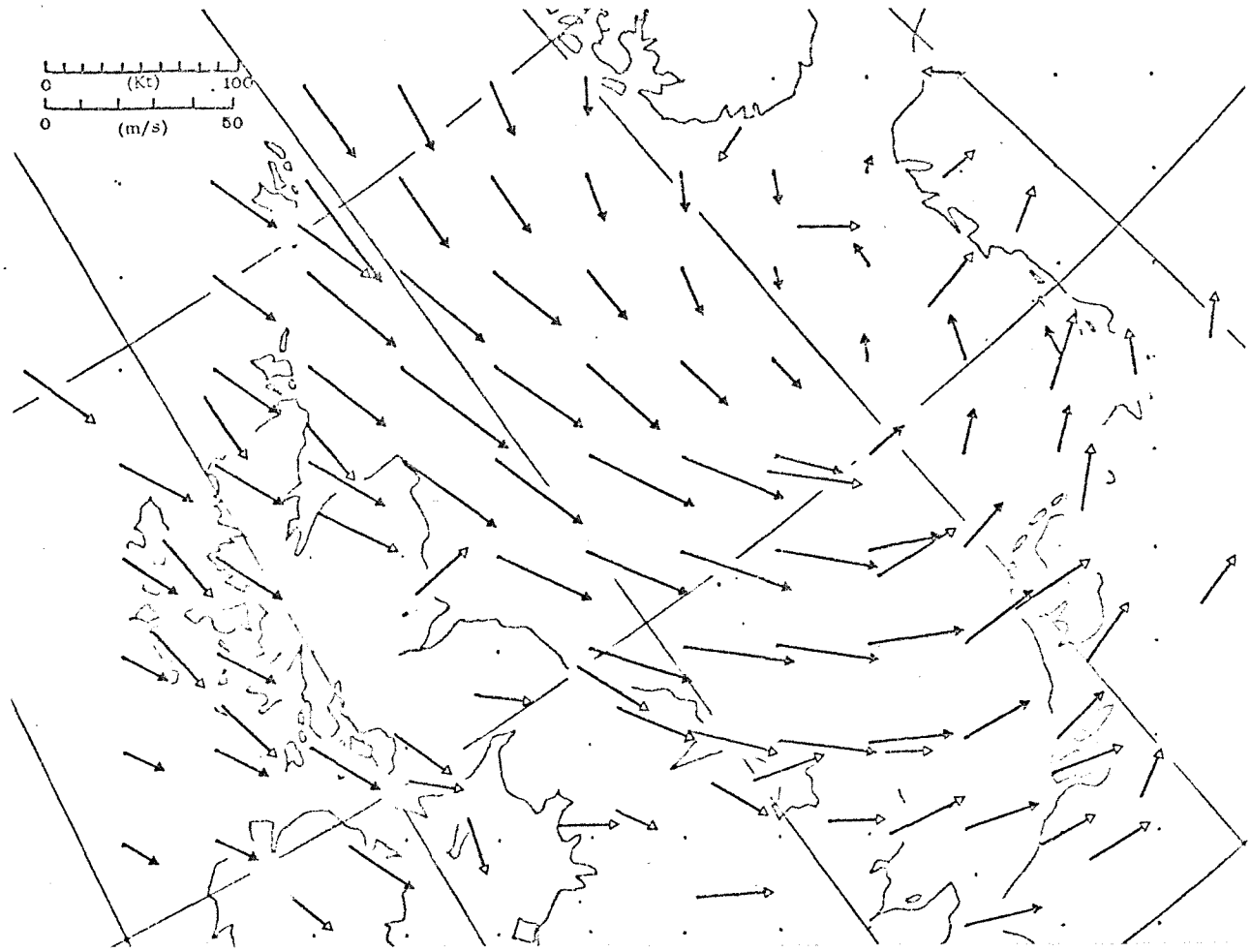

Fig. 6 An example of area-variation comparison of the computed gradient wind (▲) with the frictional corrections and the observed wind (△). Sea surface, 18.00 GMT, 31st January 1953.

Fig. 7 shows the locations of the 13 stations whose observed wind data has been used for the time-variation comparisons of the computed wind data. These stations were chosen, because their locations were expected to give good representations of the wind at the sea surface, and also the availability of wind data.

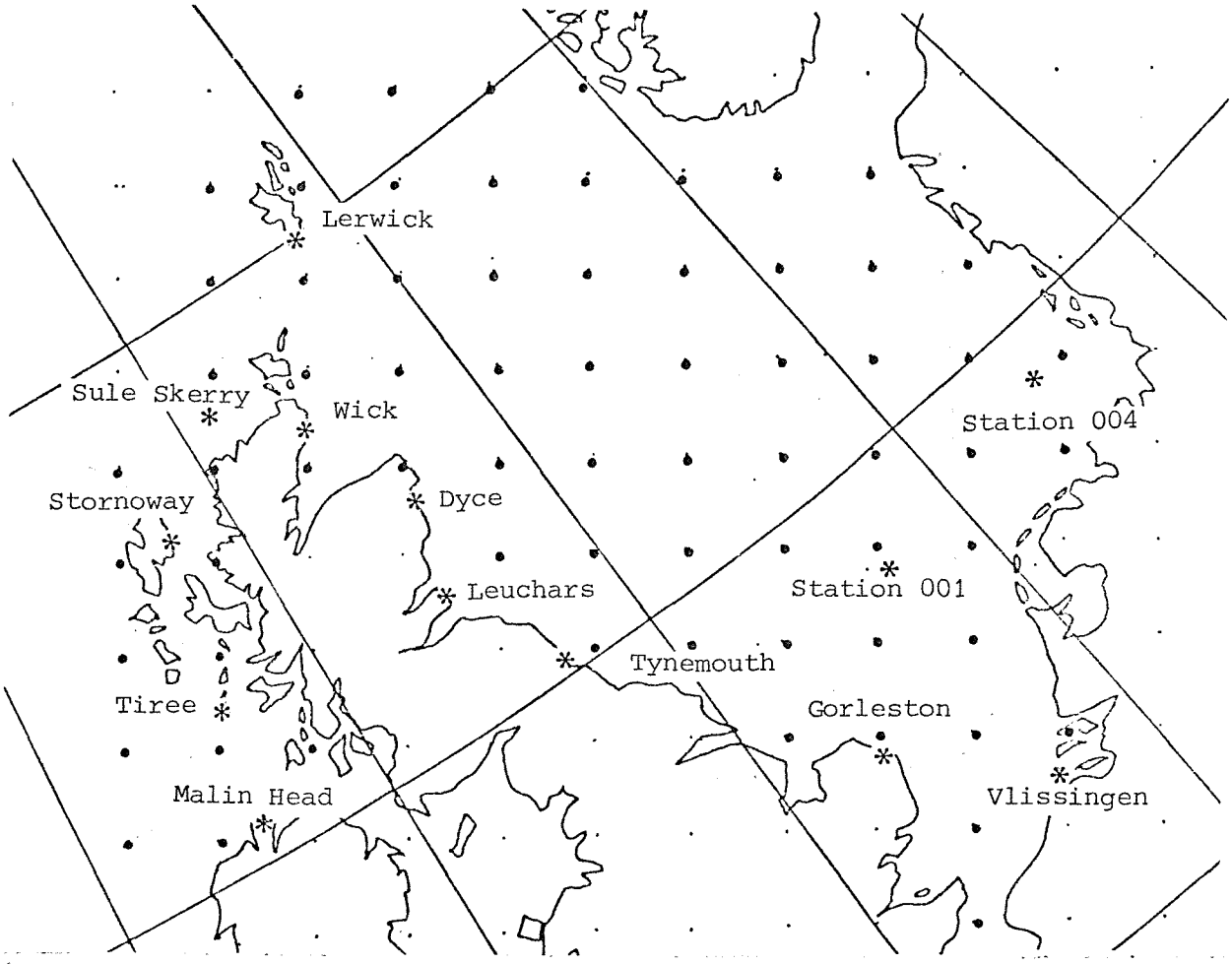

Fig. 7 13 stations whose wind data has been used for the evaluation of computed winds.

Figs. 8 to 20 (pages 15 to 27) show the comparisons of the computed wind data with observed wind data at the 13 stations. On a small map at the left side of each figure, the name and position of the station is shown with a circular scale referring to wind direction. On the same map, the nearest wind reference grid from which the computed data was obtained is shown, with its reference number (e.g. D21).

In the top part of each figure, the radius of curvature of the cyclonic isobar which passes through the grid is shown.

In the middle part of each figure, the speed of computed geostrophic wind, computed gradient wind and the observed wind are shown. If the speeds of the geostrophic wind and gradient wind are close, the latter only is shown in the figure. The observed wind speed data indicated by (O) is rounded to the nearest kt, and that indicated by (Δ) deviates by ±2.5 kt from the value shown in the figure, since they are indicated by the number of 'feathers' in the original weather maps.

In the bottom part of each figure, the computed and observed wind directions are shown. The direction of the geostrophic wind and gradient wind are not shown separately. The wind directions are indicated in the original documents by using values rounded to every 10°. 'Map Ref No' refers to the maps on pages 29 to 69.

4.2 Analysis of the comparison

Fig. 21 shows the difference between the speeds of the computed gradient wind and geostrophic wind with reference to the speed of the observed wind at the 13 stations, with short remarks.

The difference between the computed wind data and observed wind data does not directly show the error in the computation, because many factors contribute to the difference.

Observed wind data has:-

1 Characteristic deviations from the geostrophic or gradient wind, relating to the location of the station, its surrounding topography, the stability of air, the conditions of wind itself; and

2 Errors in measurement, coding or decoding (e.g. wind scale), communication, and documentation (e.g. analogue indication of wind direction).

Computed wind data has:-

3 Constant and uniform frictional corrections for the sea surface which ignore the variations due to factors such as the stability of air, and the effect of the coast;

4 Different grid locations from those of chosen stations (distance ranging from 50 to 100 km), in spite of the considerable gradient in wind speed and direction;

5 Errors originating in the pressure data which is interpolated or extrapolated from the observed data at the coastal stations; and

6 Errors in the approximations in the equations, and errors in the computing method*.

The difference between the computed and observed data, due to causes 1, 3 and 4 are considerable for some coastal stations. The worst example in the comparisons is the case of Leuchars - Grid J15, which has the largest distance between the station and grid, the greatest gradient of wind speed between the two points, and a mountainous hinterland of the station. The best example is the case of Vlissingen - Grid V19, which has the shortest distance between the two points, the smallest wind-speed gradient between the two points, the sea area to the windward side and flat land in the lee of the station, and an accurate wind record for the main part of the storm period.

Excluding the worst case, Leuchars - Grid J15, the peak value of differences between the computed gradient wind speed and observed wind speed is approximately ±10% of the maximum wind speed (48 m/s or 93 kt) involved in the whole computation. Taking the most suitable station for the comparison, Vlissingen, the peak value of difference between the computed gradient wind speed and the observed wind speed is about ±5% of the maximum wind speed in the computation. This percentage can be regarded as the error of computation, which is satisfactory for this application.

---

* For example, if an area surrounded by a closed isobar is similar to the area represented by a pressure reference grid, the computed wind speed and direction contain a large error.

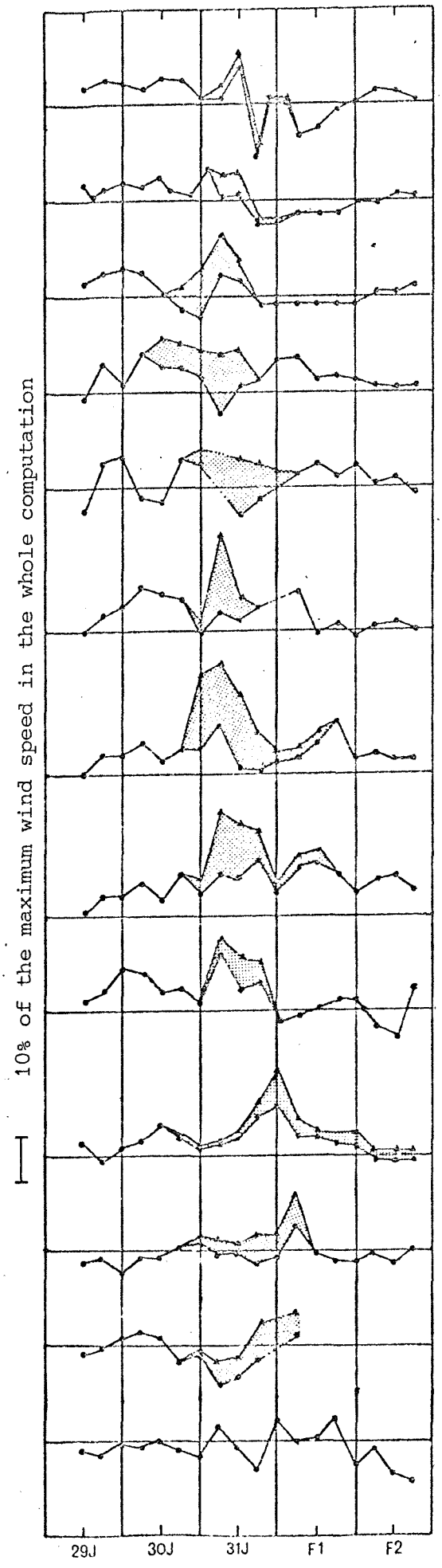

Malin Head - D21
The observed wind blew from the land side for the first 2 days, then from the sea. Midnight wind data is not available.

Tiree - D19
A part of a small group of islands. Land lies between 170° and 330°. The wind blew from the sea for most of the period.

Stornoway - B15
An island station surrounded by land, except between 30° and 60°. The wind was affected by land for the first 3 days.

Sule Skerry - D11
An offshore station. Land lies between 60° and 210°. The pressure gradient between the two points was considerable.

Lerwick - F7
An island station. The wind was affected by the island itself.

Wick - F13
The observed wind blew from the high mountains for the first 2 days, then from the sea.

Dyce - H13
The observed wind blew from the high mountains for the first 2 days, then from the peninsula.

Leuchars - J15
The observed wind blew from the high mountains for all the period. An unstable station for evaluating the sea-level wind.

Tynemouth - L17
The observed wind blew from the land side for the first 3 days, then from the sea.

Gorleston - R19
The observed wind blew from the land side for the first 4 days, then from the sea.

Vlissingen - V19
A station on the flat land coast. The observed wind blew from the sea all the period. The observed wind data for the 2nd and 3rd days are particularly accurate.

Station 001 - R15
An offshore station. The observed wind data have been documented less accurately, and are missing for the last 2 days.

Station 004 - V11
An offshore station near the flat land. The observed wind data have been documented less accurately. The speeds of geostrophic and gradient winds are similar.

Fig. 21 Difference of the computed gradient wind (●) and geostrophic wind (▲) with reference to the observed wind at the 13 stations. Shaded regions show the difference between the two computed winds.

The peak value difference of the computed geostrophic wind speed, with reference to the observed wind speed, is about +25% (always positive) of the highest wind speed involved in the whole computation, except for a few cases where the observed data on the documents are doubtful. This percentage is not satisfactory; in other words, the radius of curvature of cyclonic isobars have to be taken into account in the dynamic computation of a surge, particularly when the wind speed is high (say ≥15 m/s or 30 kt).

5. Conclusions

1 A set of isobar maps for the surface level of the North Sea and the north and west of Scotland from 29th January to 2nd February 1953 has been edited from the best available material, and the pressure values have been digitized for 100-km square grids. The data has been recorded on a tape, and is being used for the new electronic model.

2 From these pressure data, the geostrophic wind and gradient wind have been computed, taking account of the frictional corrections, and compared with the observed wind data at 13 coastal and off-shore stations.

3 Observed wind data at the coastal station does not satisfactorily represent the actual wind on the sea surface. The location of each coastal or offshore station is not exactly the same as the location of a grid under comparison. Observed data at coastal and offshore stations contains various errors, including errors due to the finite representation of values (e.g. wind scale). Therefore, the difference between the computed wind data and observed wind data does not directly show the errors in the wind computation.

4 By taking the best suitable station for this comparison (Vlissingen), the peak value of error of the computed gradient wind is estimated to be ±5% of the maximum wind speed involved in the whole computation, and $\pm 15^{\circ}$ in wind direction. These values are satisfactory for this application, and the frictional correction coefficient, $\beta = 0.65$ and $\delta = 22^{\circ}$ (see chapter 3.3), appeared to be correct in this storm case.

5 The computed wind, with the same frictional corrections, is practically the same as the gradient wind, when the wind speed is low. However, when the wind speed is high (say ≥15 m/s or 30 kt), and the radius of curvature of an isobar is small (say ≤1500 km), the speed of the geostrophic wind with cyclonic isobars becomes too high. The square of the ratio of the geostrophic wind speed to gradient wind speed, which is proportional to the surge-generating force, is more than 2 in the considerable area of the North Sea for more than 12 hours in this storm case. The maximum value of the ratio is nearly 3 at the middle of the sea. This suggests that the cyclonic curvature of isobars must be taken into account for the dynamic analysis of a storm surge, especially for a high wind speed.

6 If a computed storm surge height is compared directly with the observed surge height, it will be difficult to detect the cause of disagreement in the surge heights due to the geostrophic wind with curved isobars. In such a case, if some coefficient in the dynamic equations are adjusted to obtain a good agreement, the heights will not agree for other cases.

7 Most of the computations in this paper have been carried out by the meteorological input-data processing system (a part of the new electronic model). Therefore, this paper shows a successful operation of the processing system.

Acknowledgements

This work is a part of the project commissioned by the Ministry of Industry and the Ministry of Energy. The author wishes to thank the UK Meteorological Office, and the Netherlands Meteorological Institute for supplying their valuable material. The author also wishes to thank Miss Kathleen Reeves-Wilkin for helping with the data processing and drawing, and Miss Kim Barber for digitizing the isobars.

References

(1) to (7): see chapter 2.

(8) Hansen, W. (1957): Tellus, 8, 287-300.

(9) Ishiguro, S. (1963): Advisory Committee on Oceanographic and Meteorological Research, Paper 20(iv), 1-12.

(10) Ishiguro, S. (1965): Revue Pétroliére, No. 1073, Section 1, No. 110, 1-5.

(11) Ishiguro, S. (1966): Advisory Committee on Oceanographic and Meteorological Research, Paper 25(iii), Storm surge in the North Sea, 1-57.

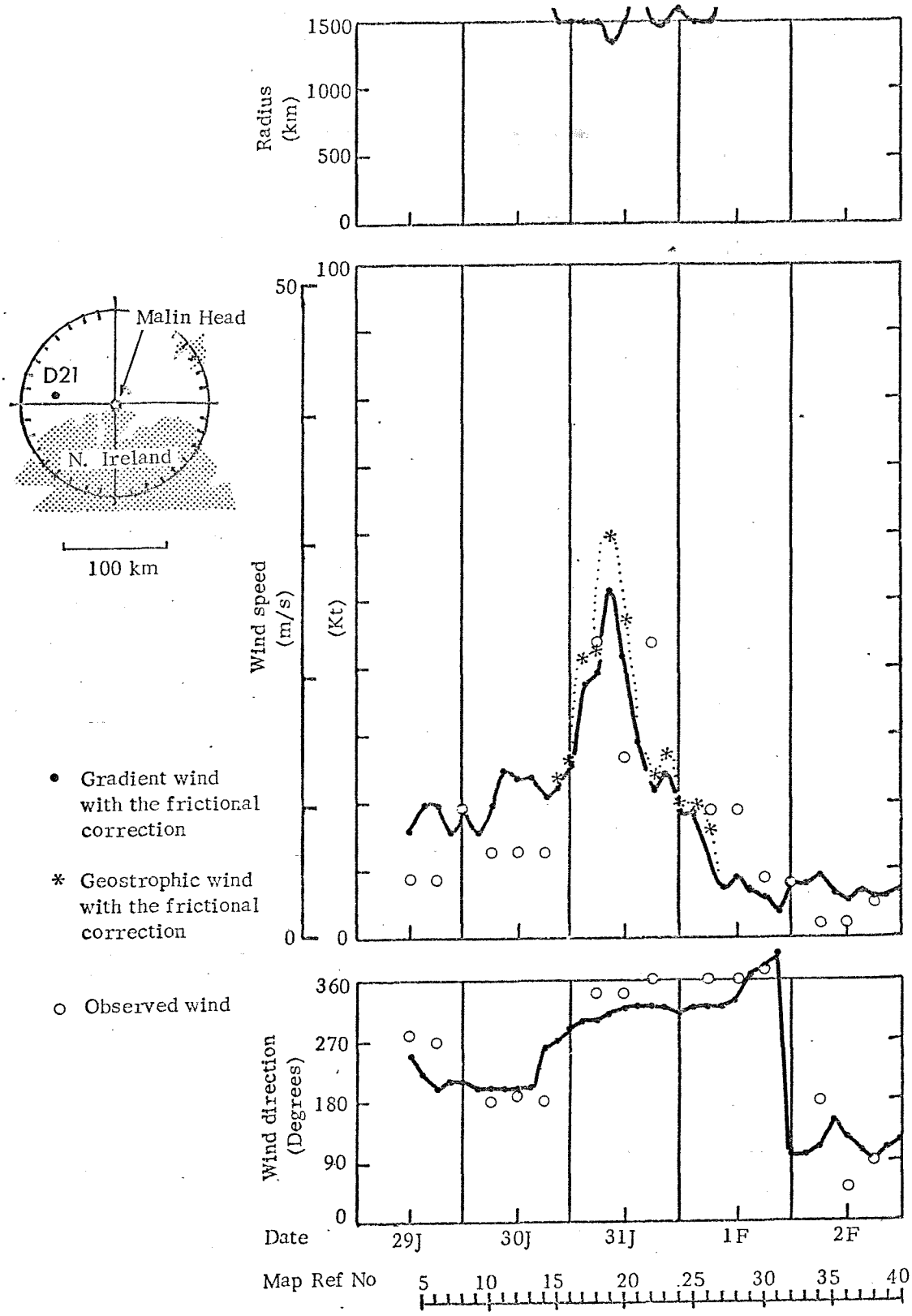

Fig. 8 Computed wind for grid D21, observed wind at Maline Head, and the radius of curvature of a cyclonic isobar passing through the grid.

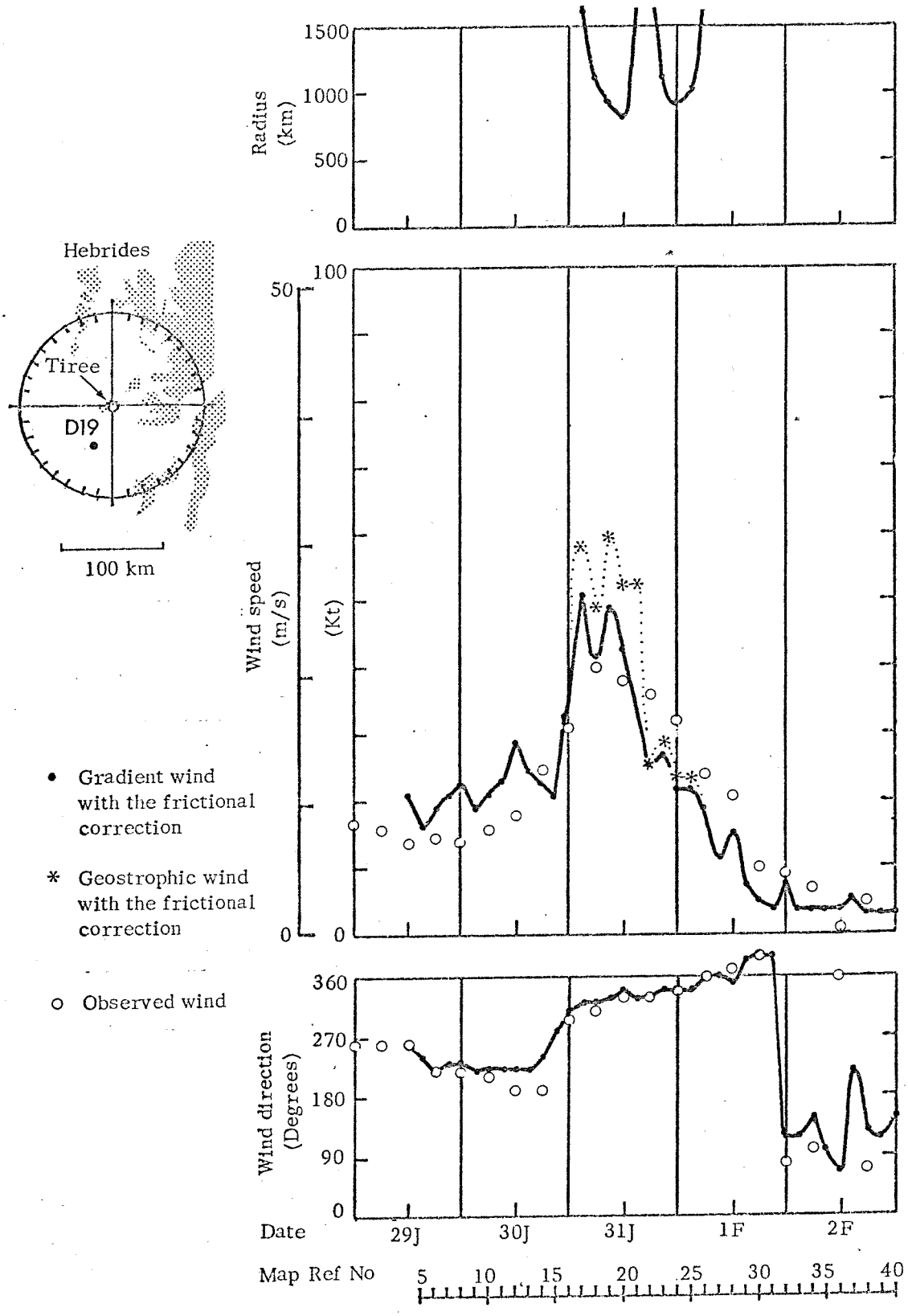

Fig. 9 Computed wind for grid D19, observed wind at Tiree, and the radius of curvature of a cyclonic isobar passing through the grid.

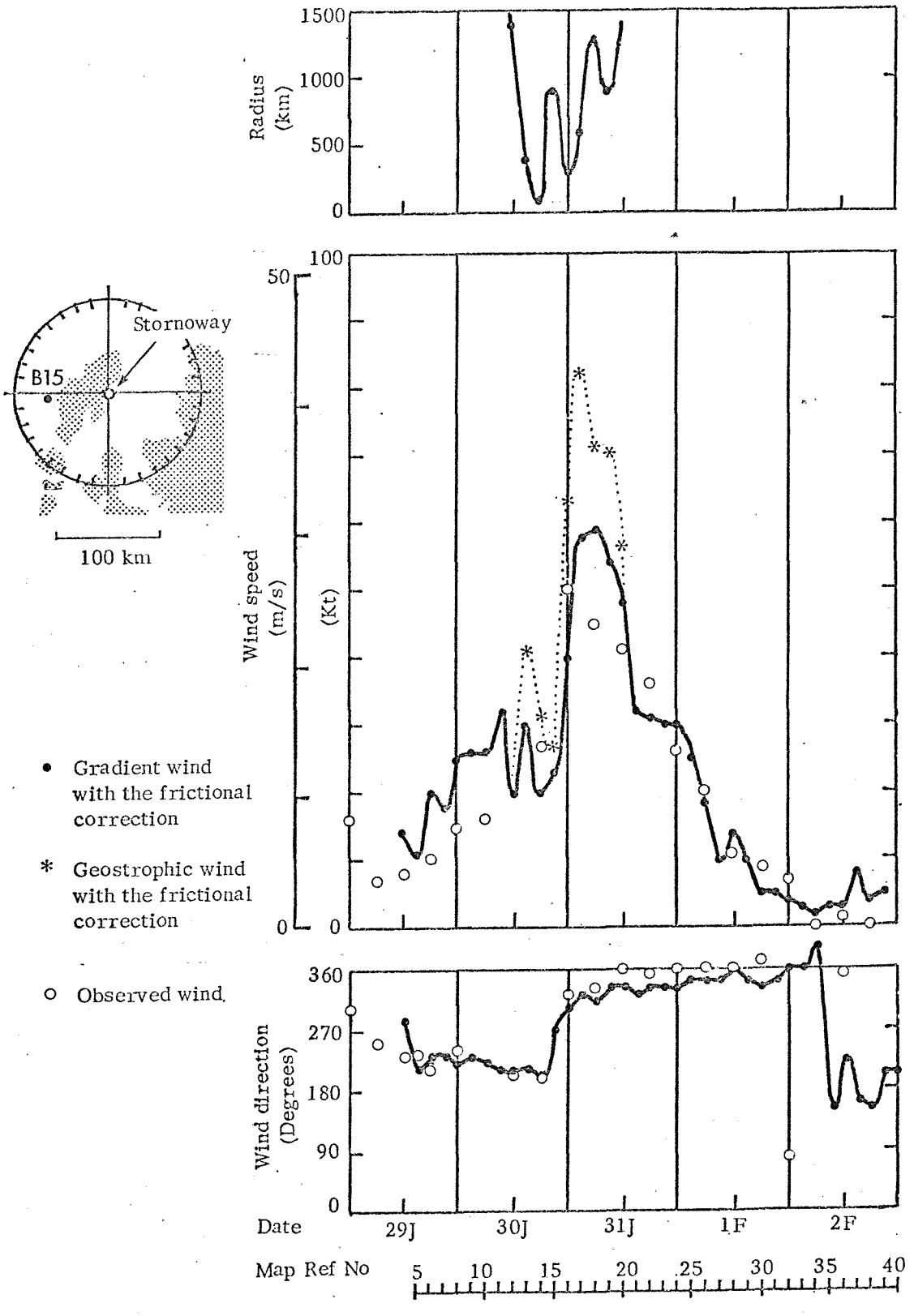

Fig. 10 Computed wind for grid B15, observed wind at Stornoway, and the radius of curvature of a cyclonic isobar passing through the grid.

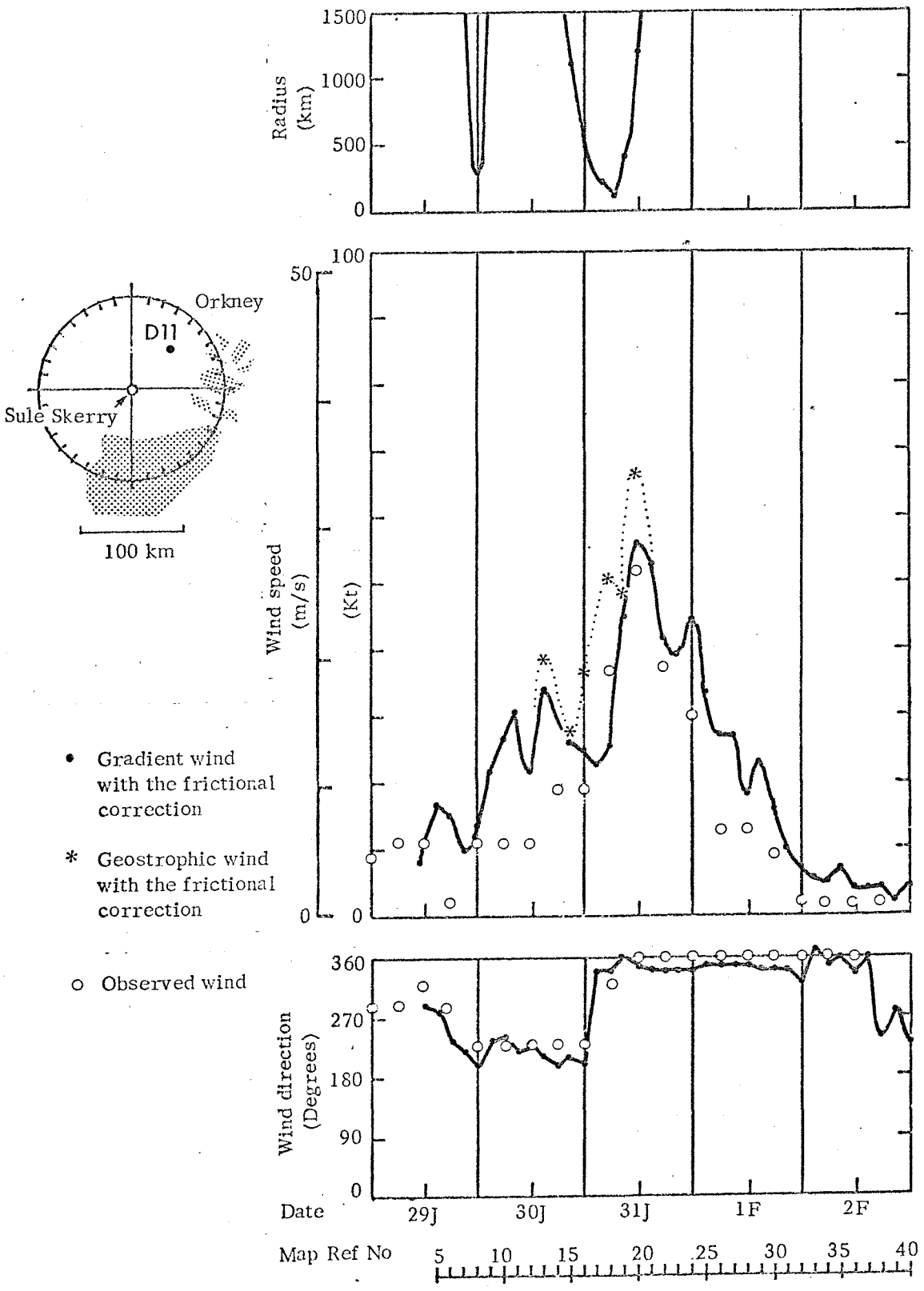

Fig. 11 Computed wind for grid D11, observed wind at Sule Skerry, and the radius of curvature of a cyclonic isobar passing through the grid.

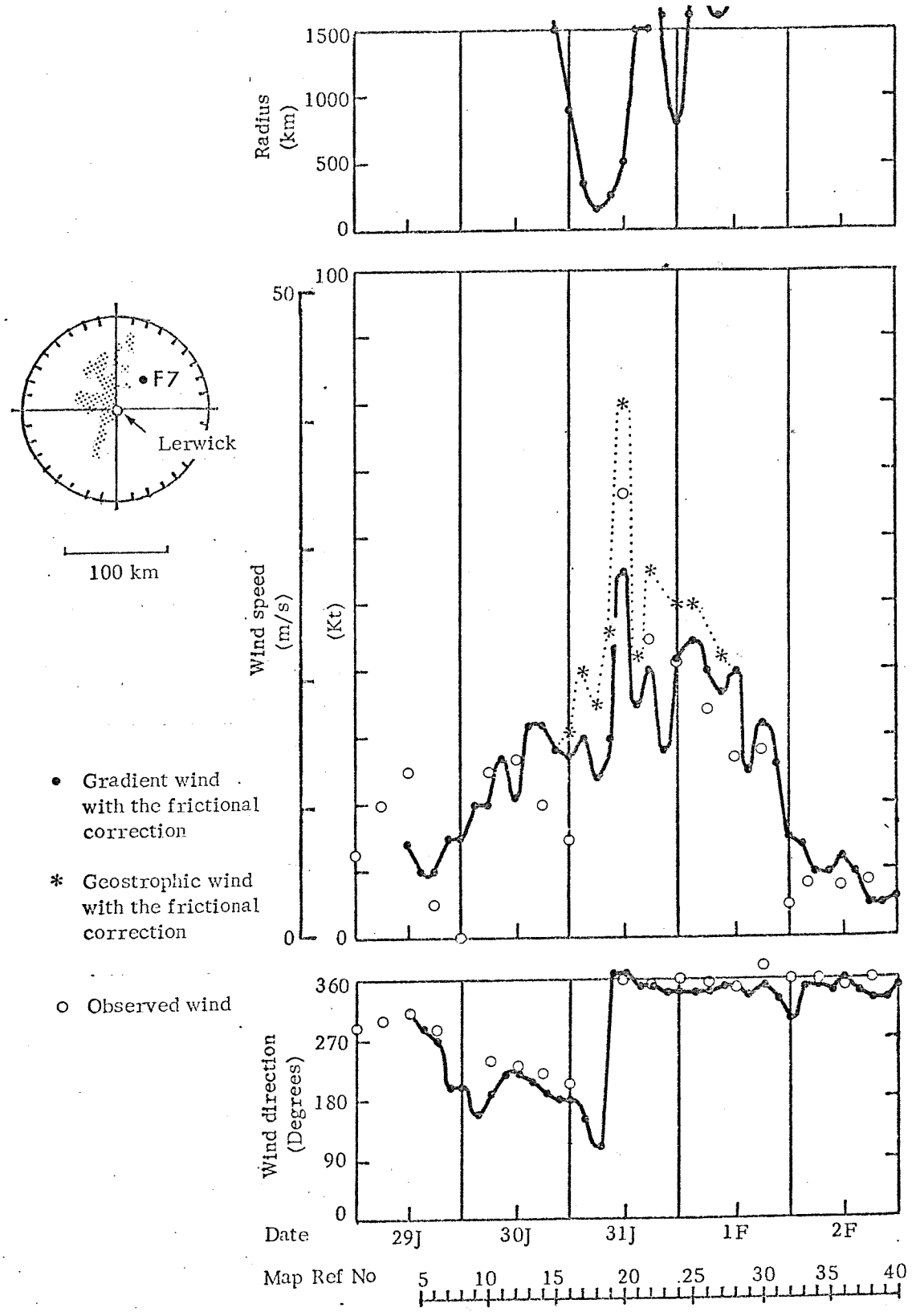

Fig. 12 Computed wind for grid F7, observed wind at Lerwick, and the radius of curvature of a cyclonic isobar passing through the grid.

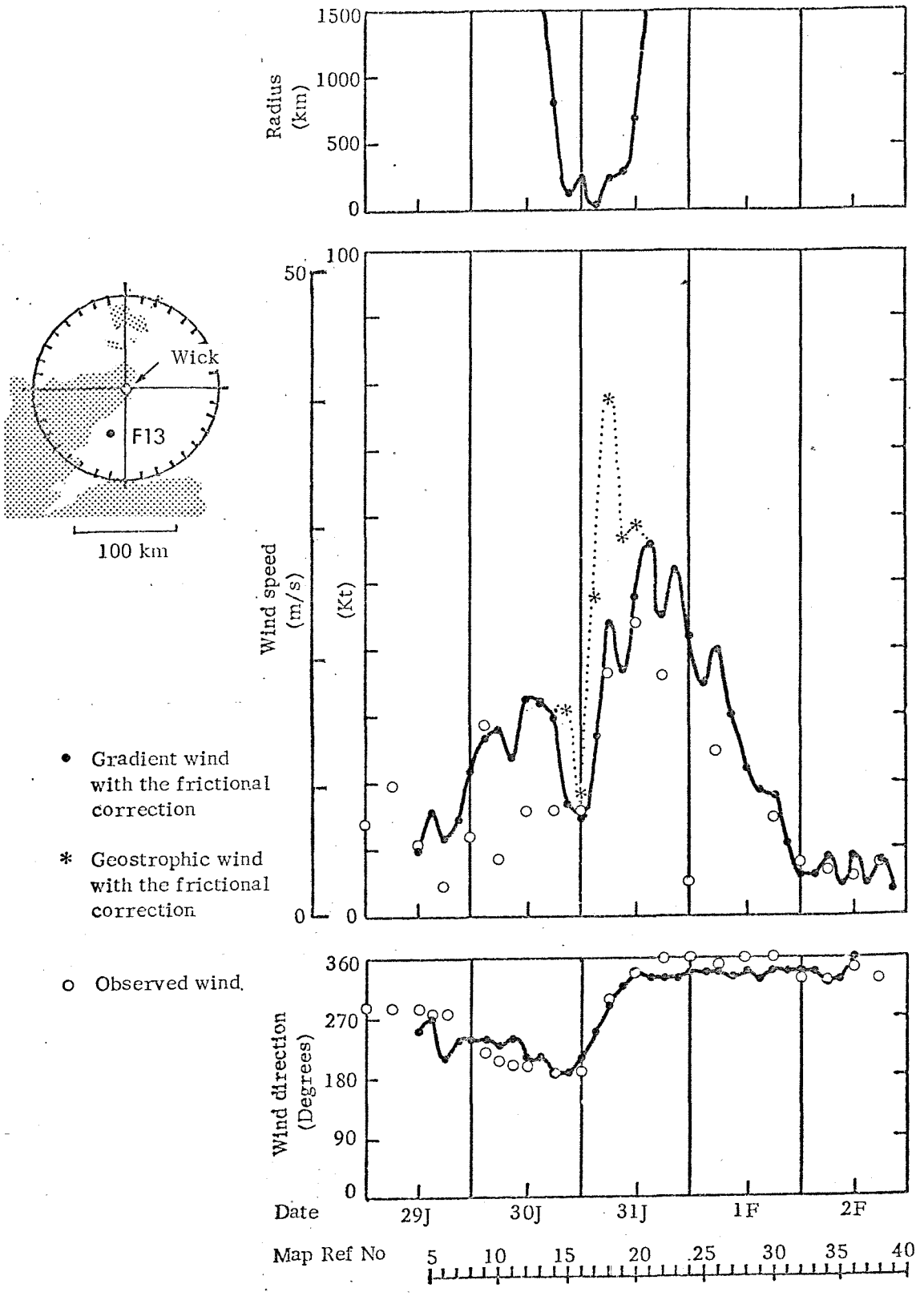

Fig. 13 Computed wind for grid F13, observed wind at Wick, and the radius of curvature of a cyclonic isobar passing through the grid.

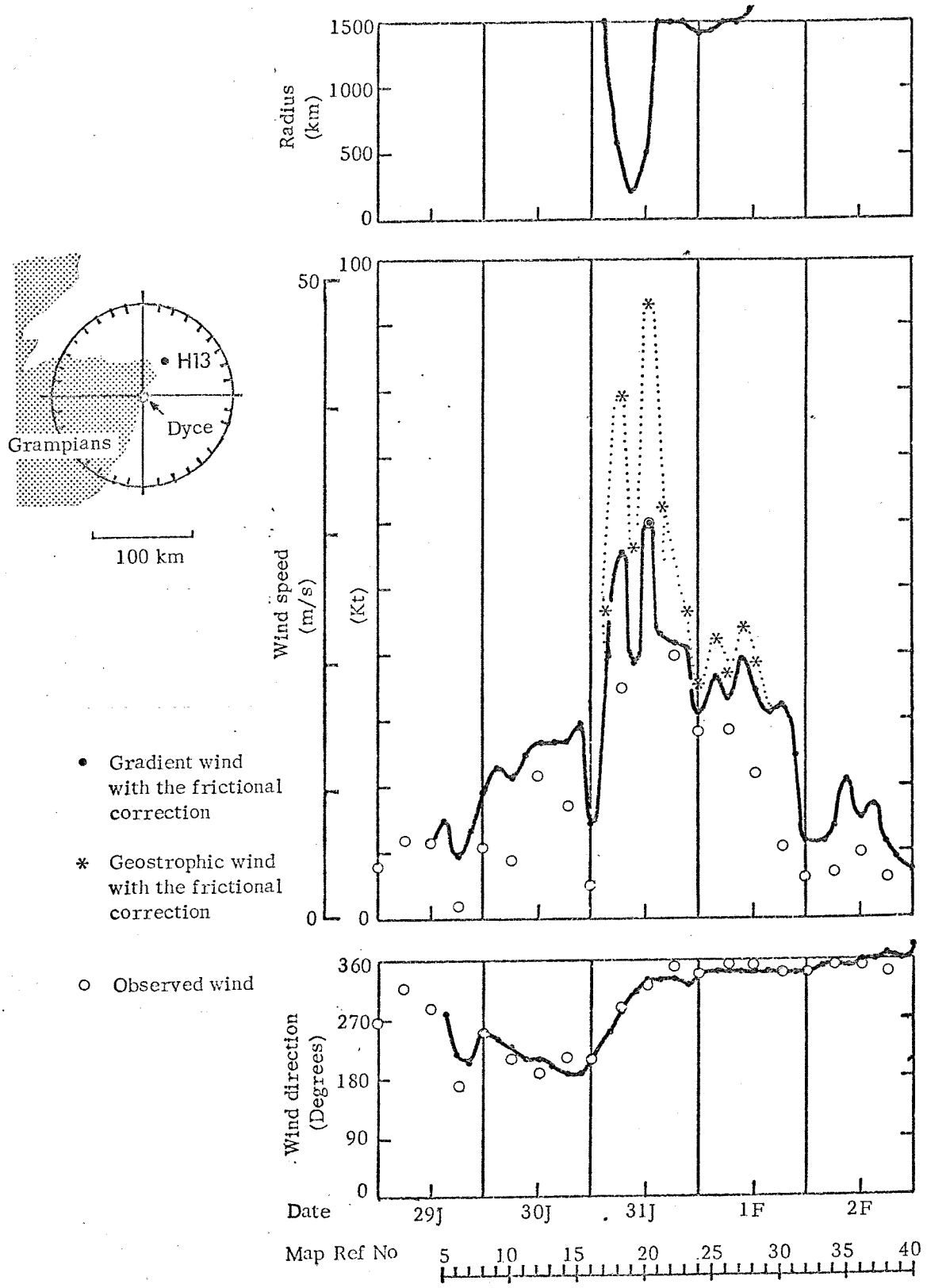

Fig. 14 Computed wind for grid H13, observed wind at Dyce, and the radius of curvature of a cyclonic isobar passing through the grid.

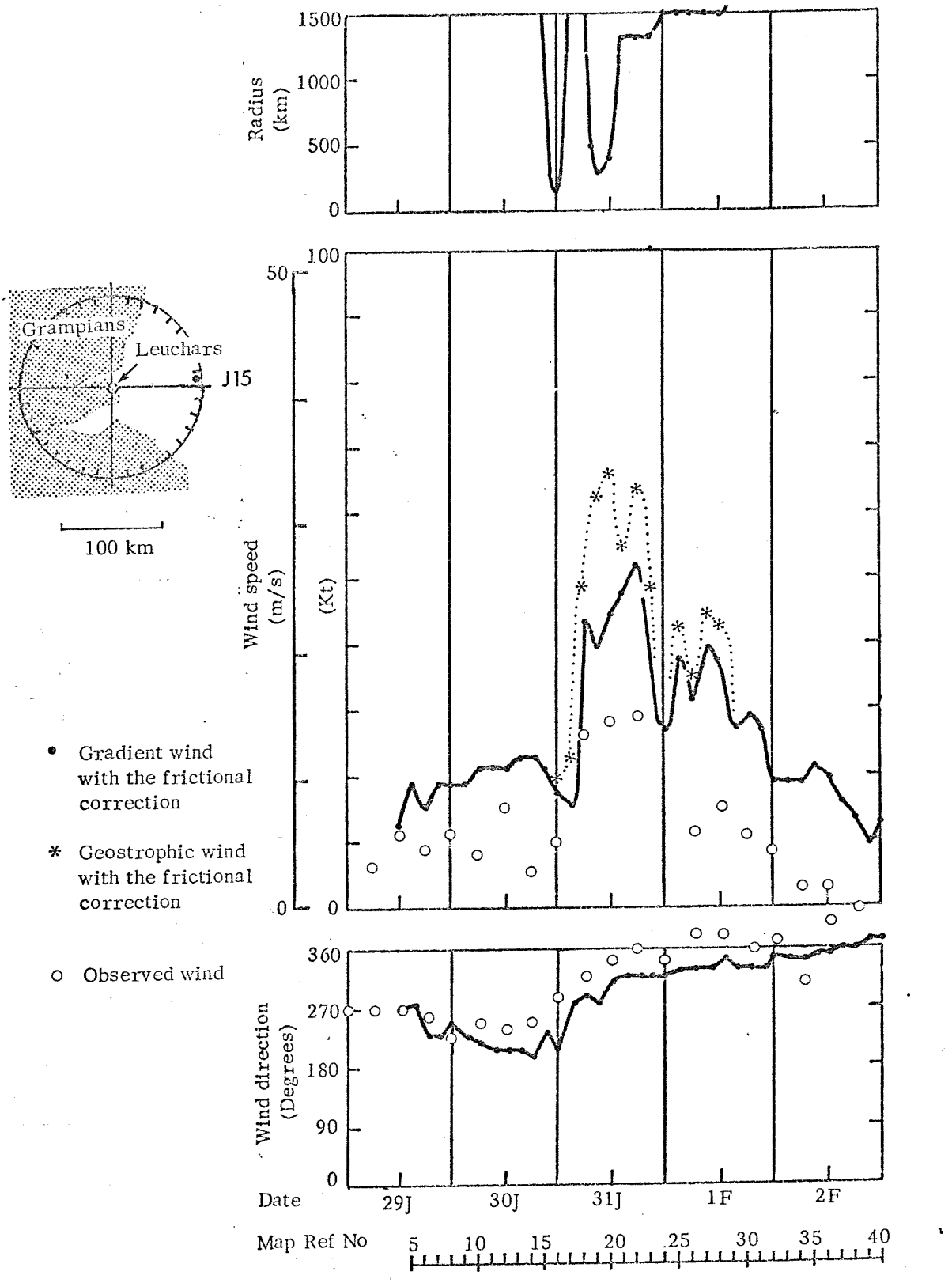

Fig. 15 Computed wind for grid J15, observed wind at Leuchars, and the radius of curvature of a cyclonic isobar passing through the grid.

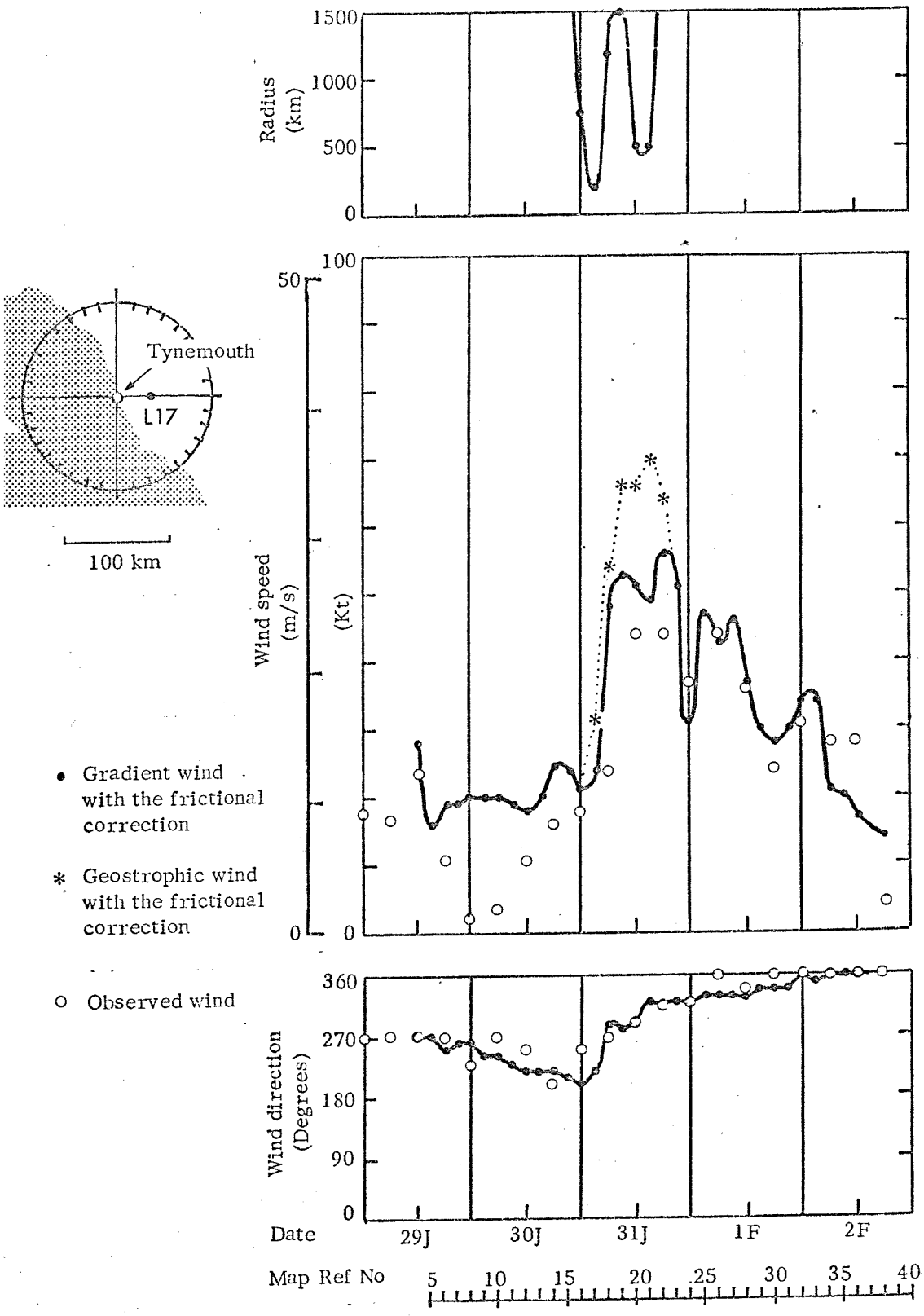

Fig. 16 Computed wind for grid L17, observed wind at Tynemouth, and the radius of curvature of a cyclonic isobar passing through the grid.

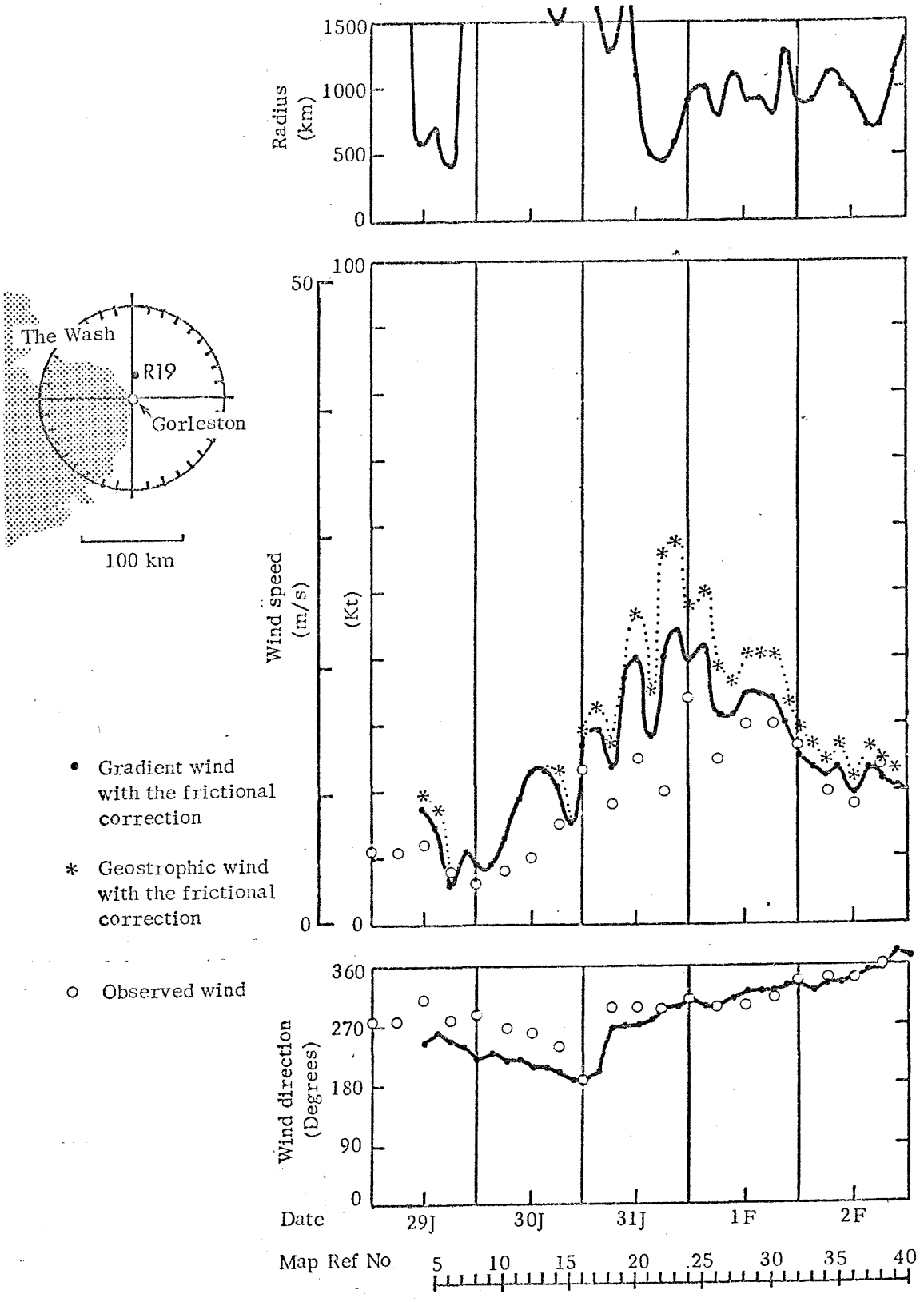

Fig. 17 Computed wind for grid R19, observed wind at Gorleston, and the radius of curvature of a cyclonic isobar passing through the grid.

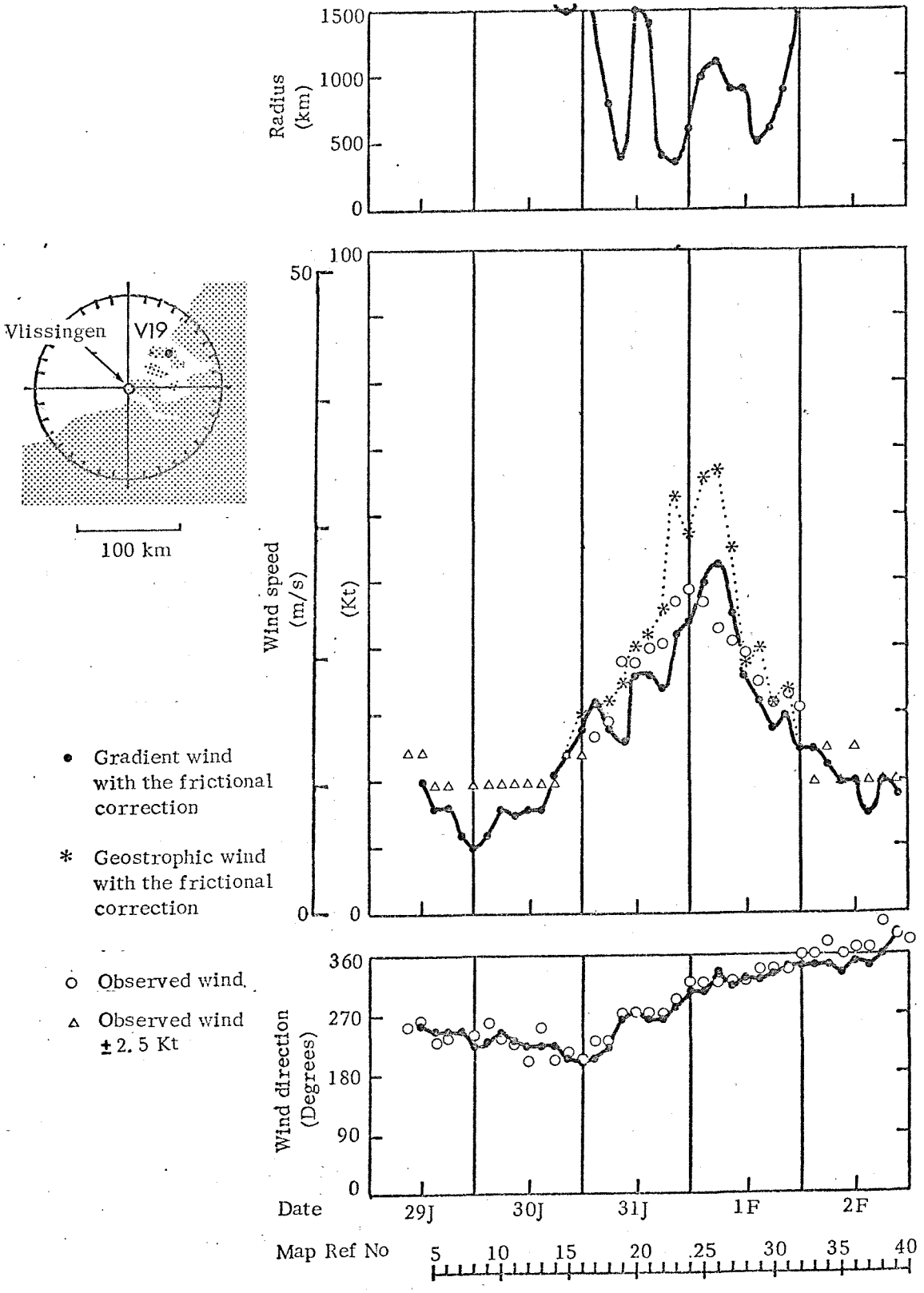

Fig. 18 Computed wind for grid V19, observed wind at Vlissingen, and the radius of curvature of a cyclonic isobar passing through the grid.

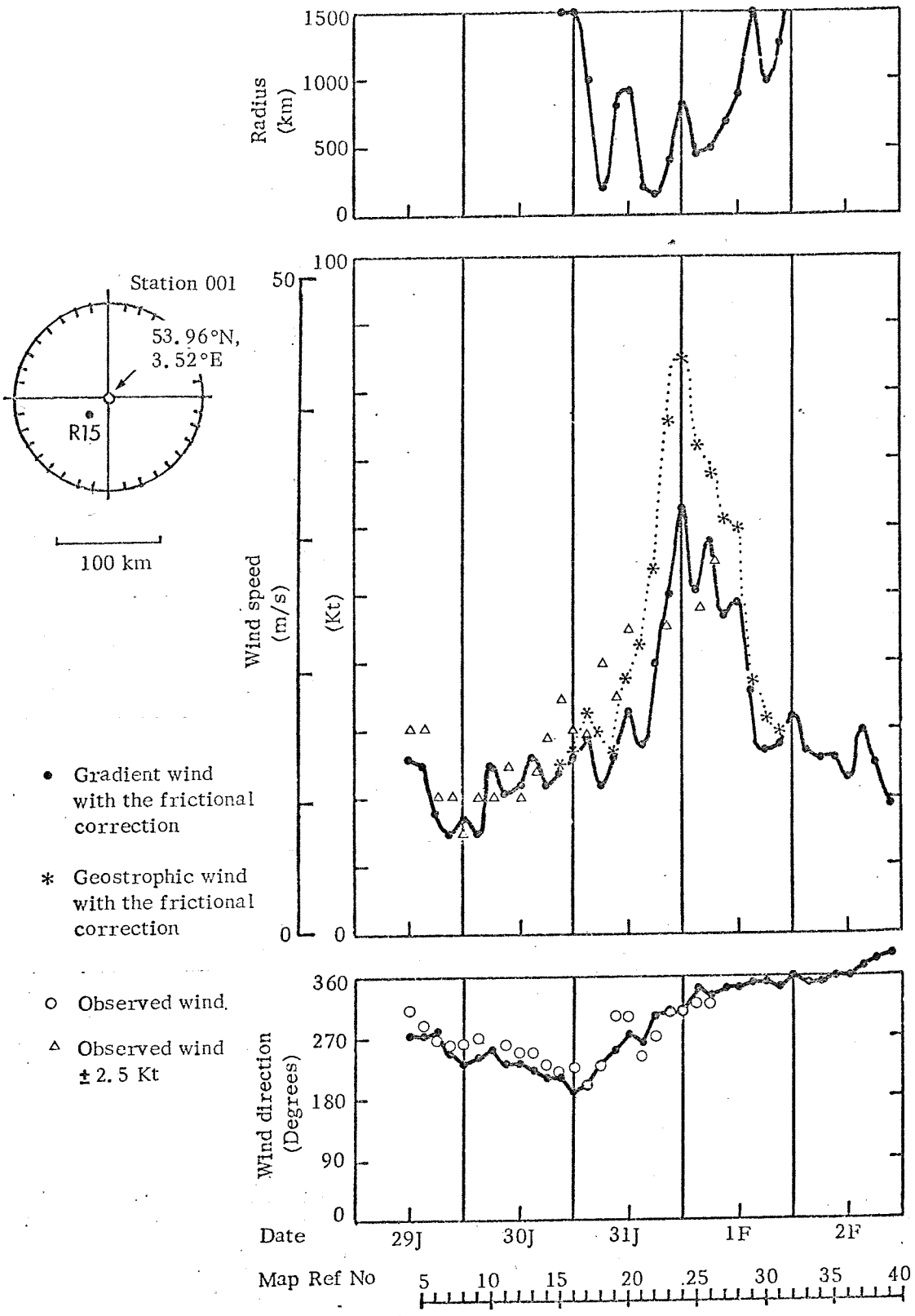

Fig. 19 Computed wind for grid R15, observed wind at Station 001, and the radius of curvature of a cyclonic isobar passing through the grid.

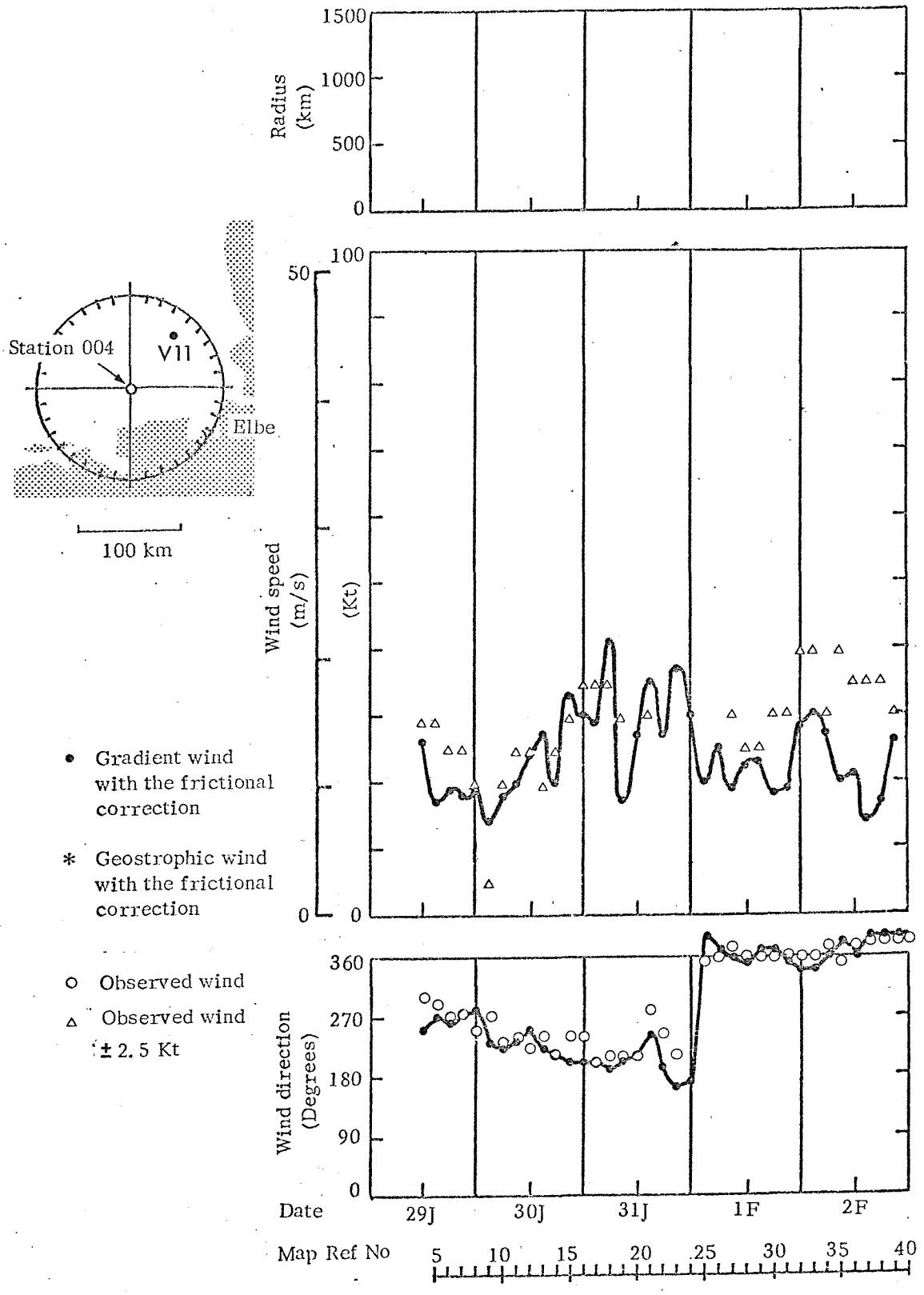

Fig. 20 Computed wind for grid V11, observed wind at Station 004, and the radius of curvature of a cyclonic isobar passing through the grid.

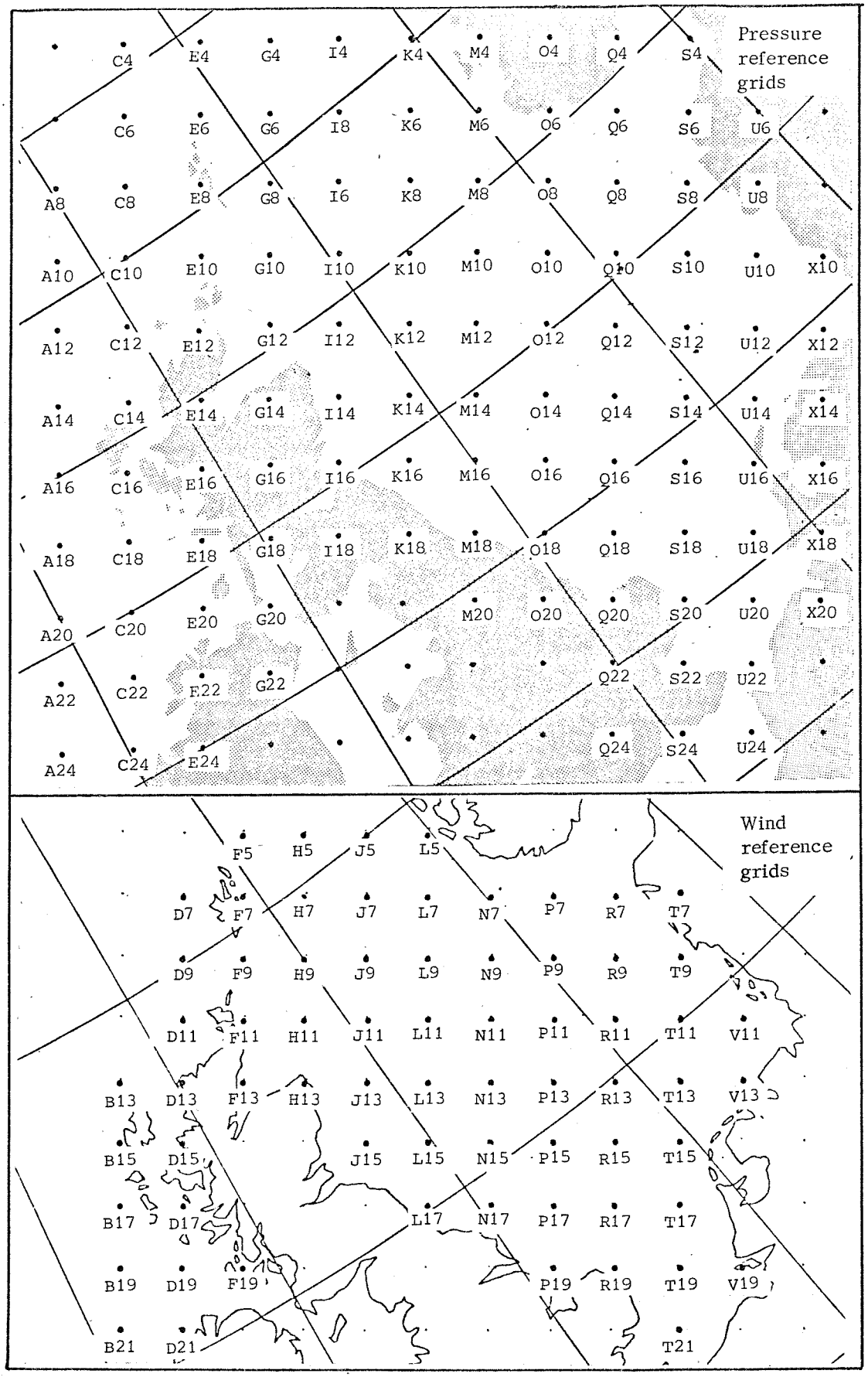

Fig. 22 Locations of 'pressure reference grids' and 'wind reference grids'.

Fig. 23 Isobars with digitized values (top) and the computed geostrophic wind (bottom), both at the sea surface level, from 12.00 GMT, 29th January to 12.00 GMT, 3rd February 1953 (from pages 29 to 69).

29. 1 | 1953
No. 4 | 12.00

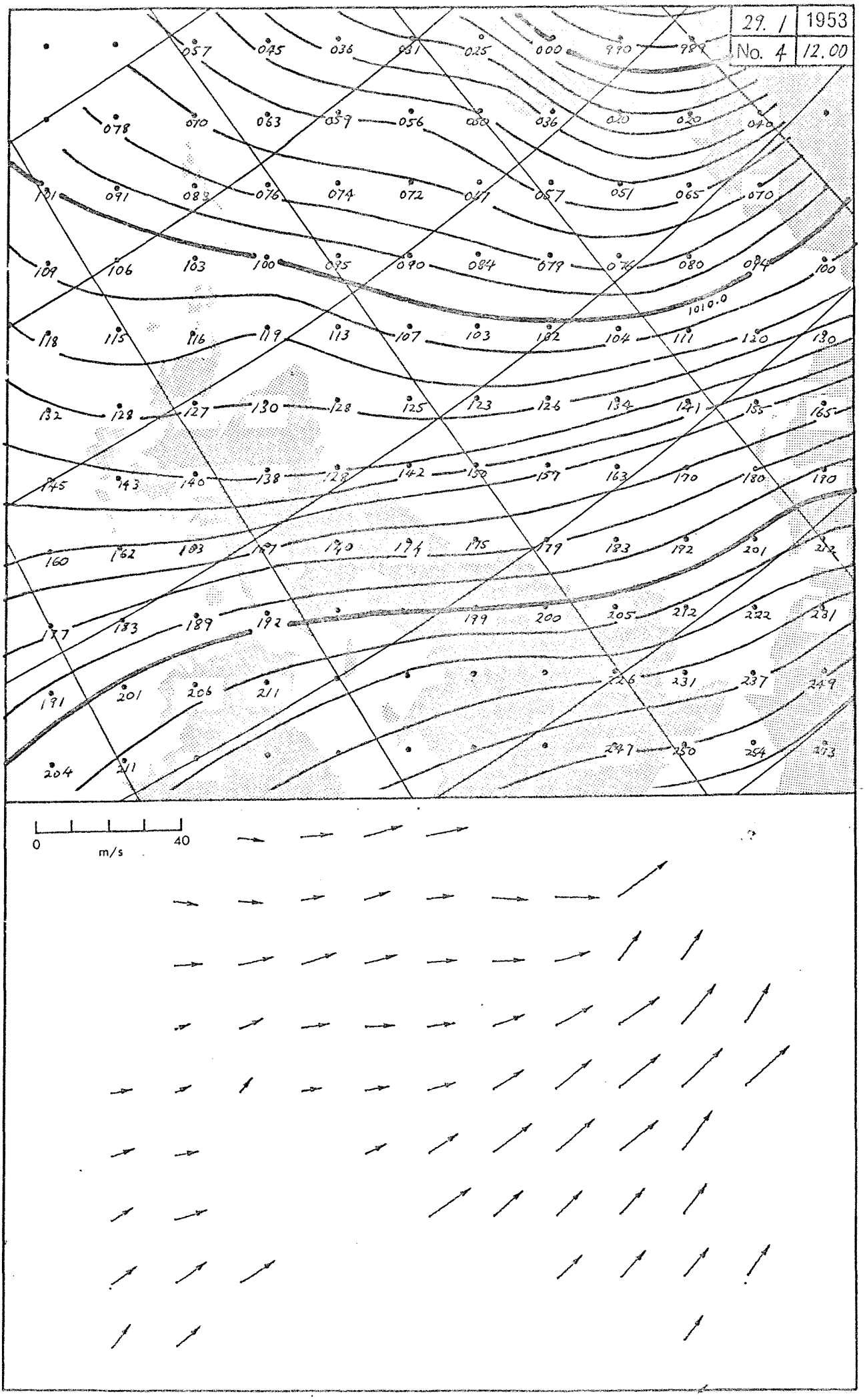

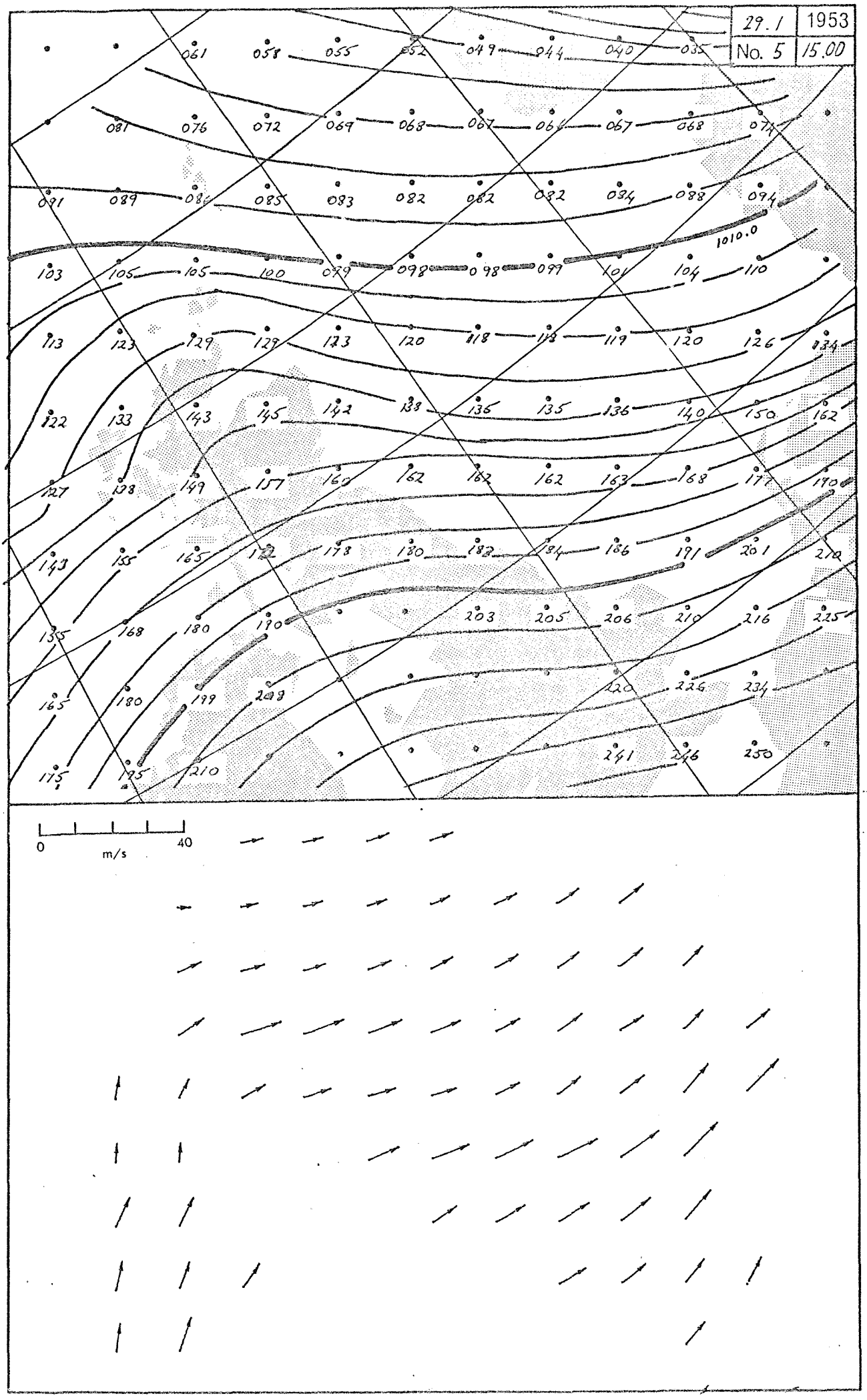
29.1
1953
No. 5
15.00
1010.0
0
m/s
40

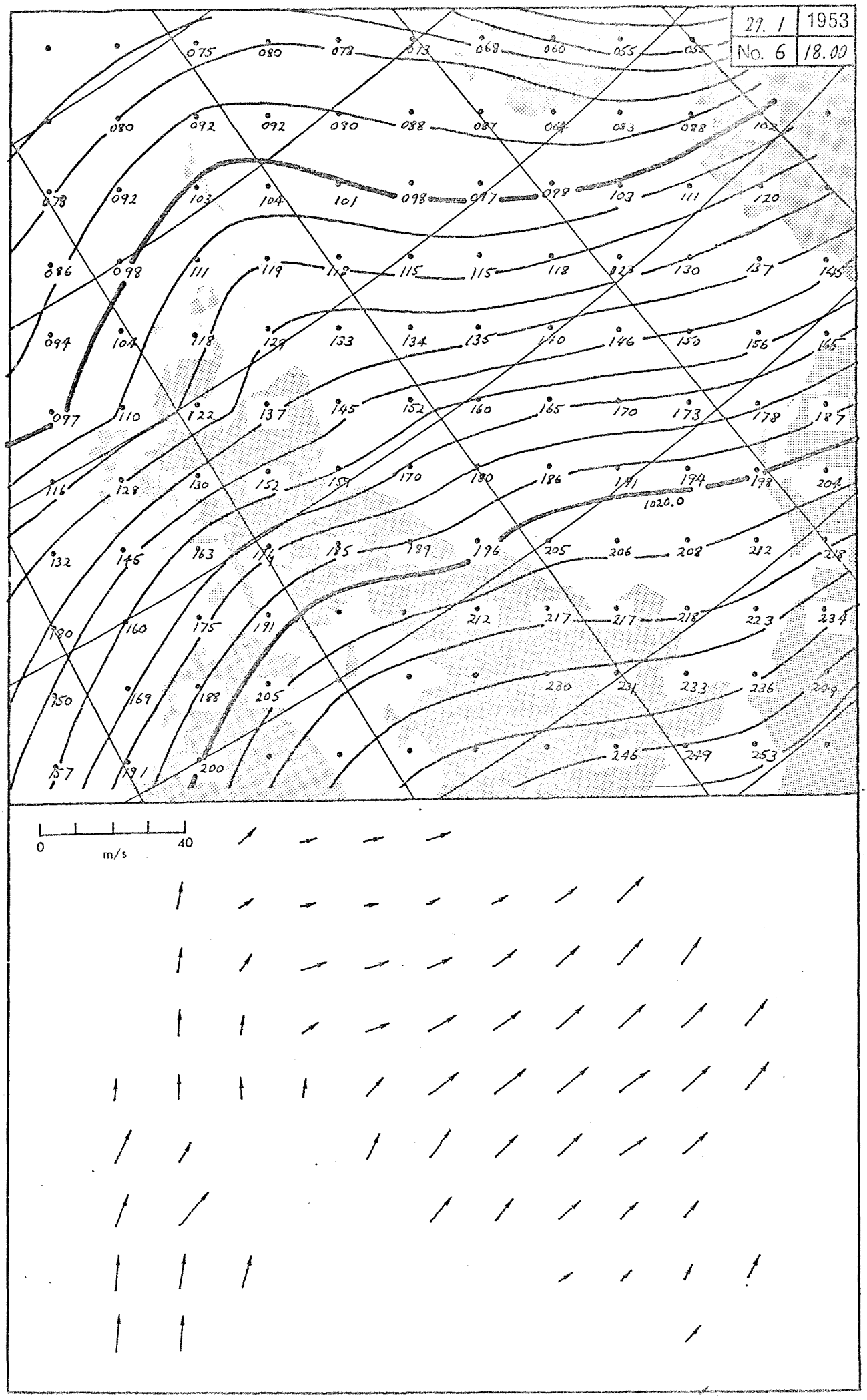
27. 1
1953
No. 6
18.00
1020.0
0
40
m/s

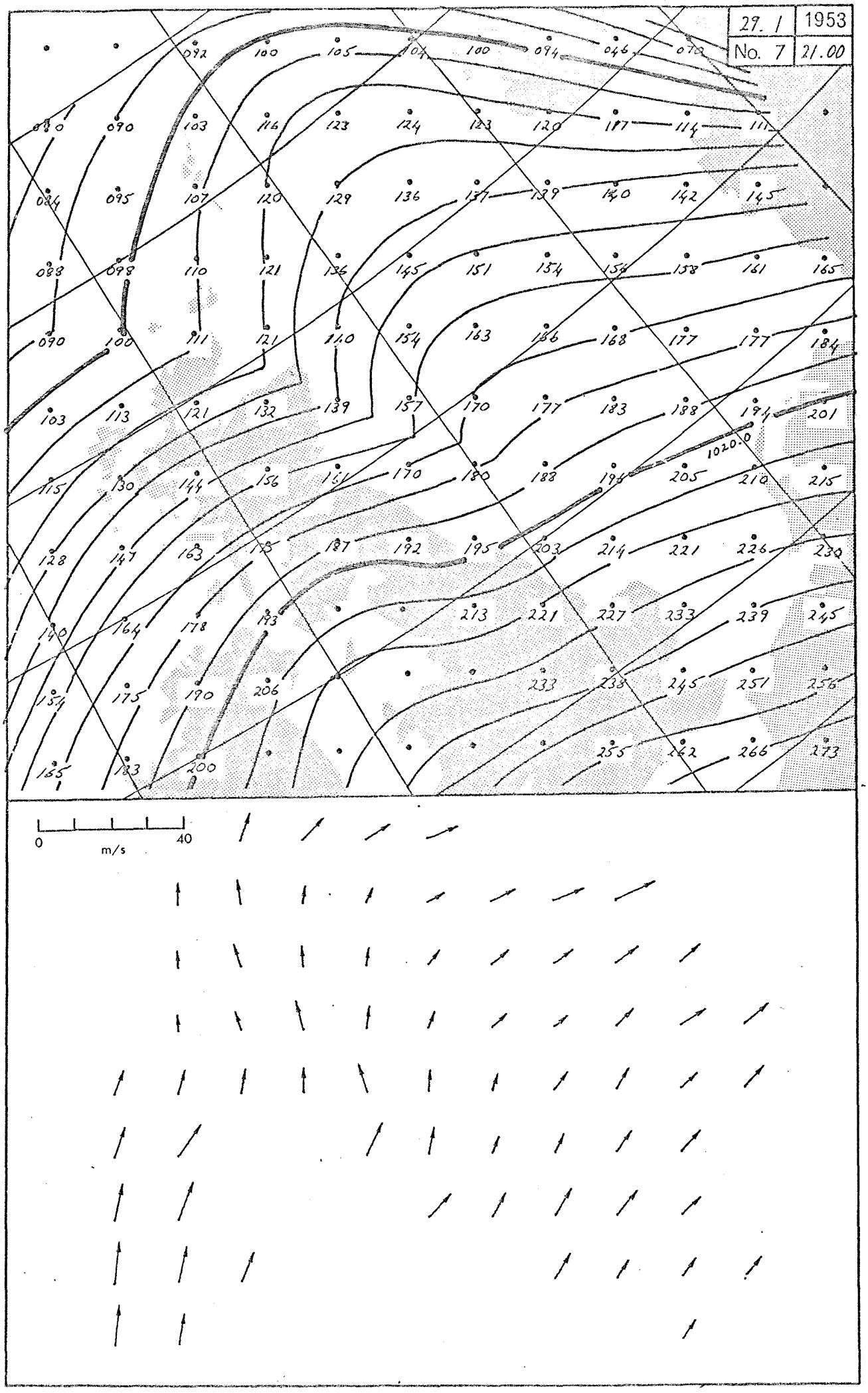
29. 1
1953
No. 7
21.00
1020.0
0
40
m/s

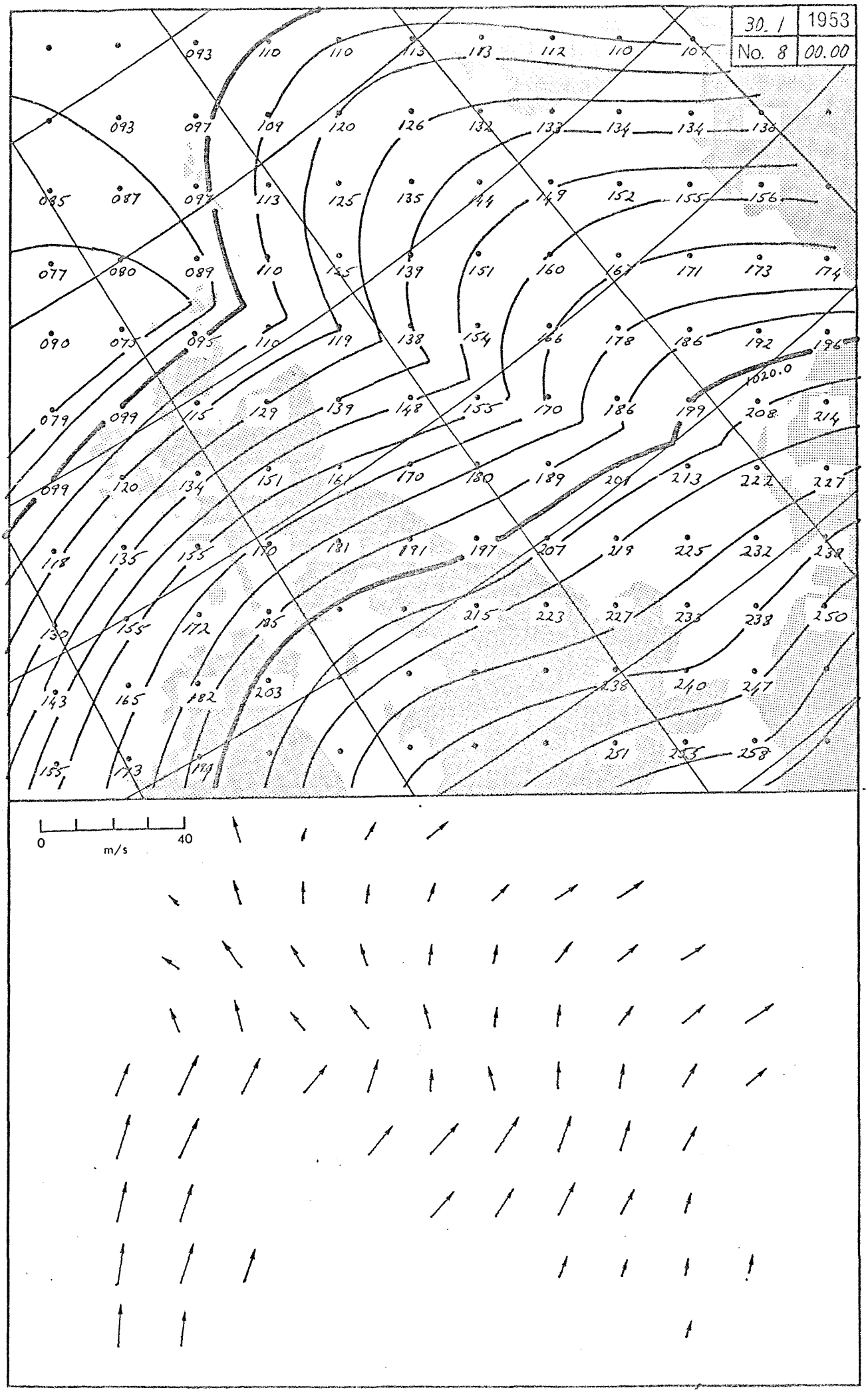
30. 1
1953
No. 8
00.00
1020.0
0
m/s
40

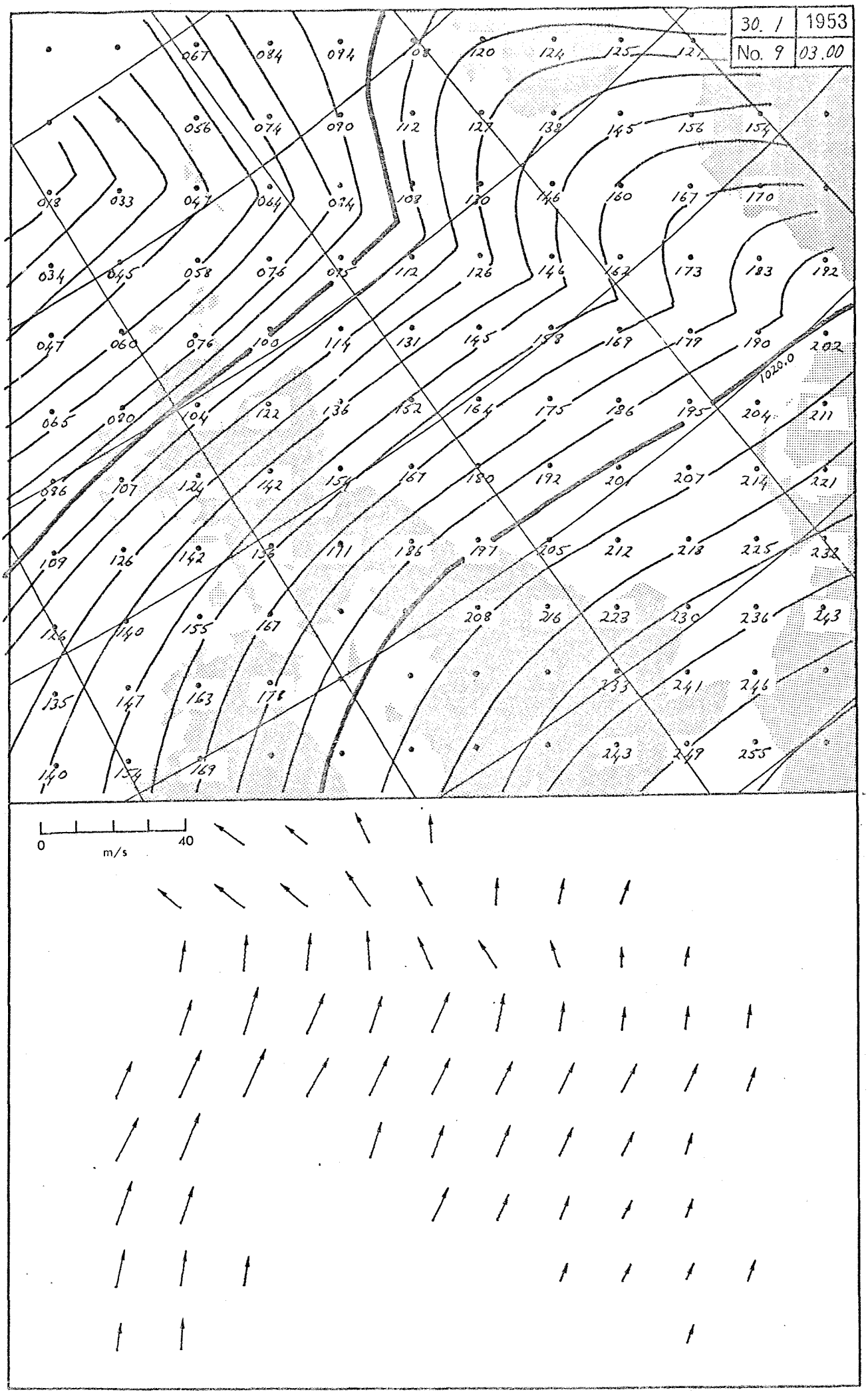
30. 1
1953
No. 9
03.00
1020.0
0
40
m/s

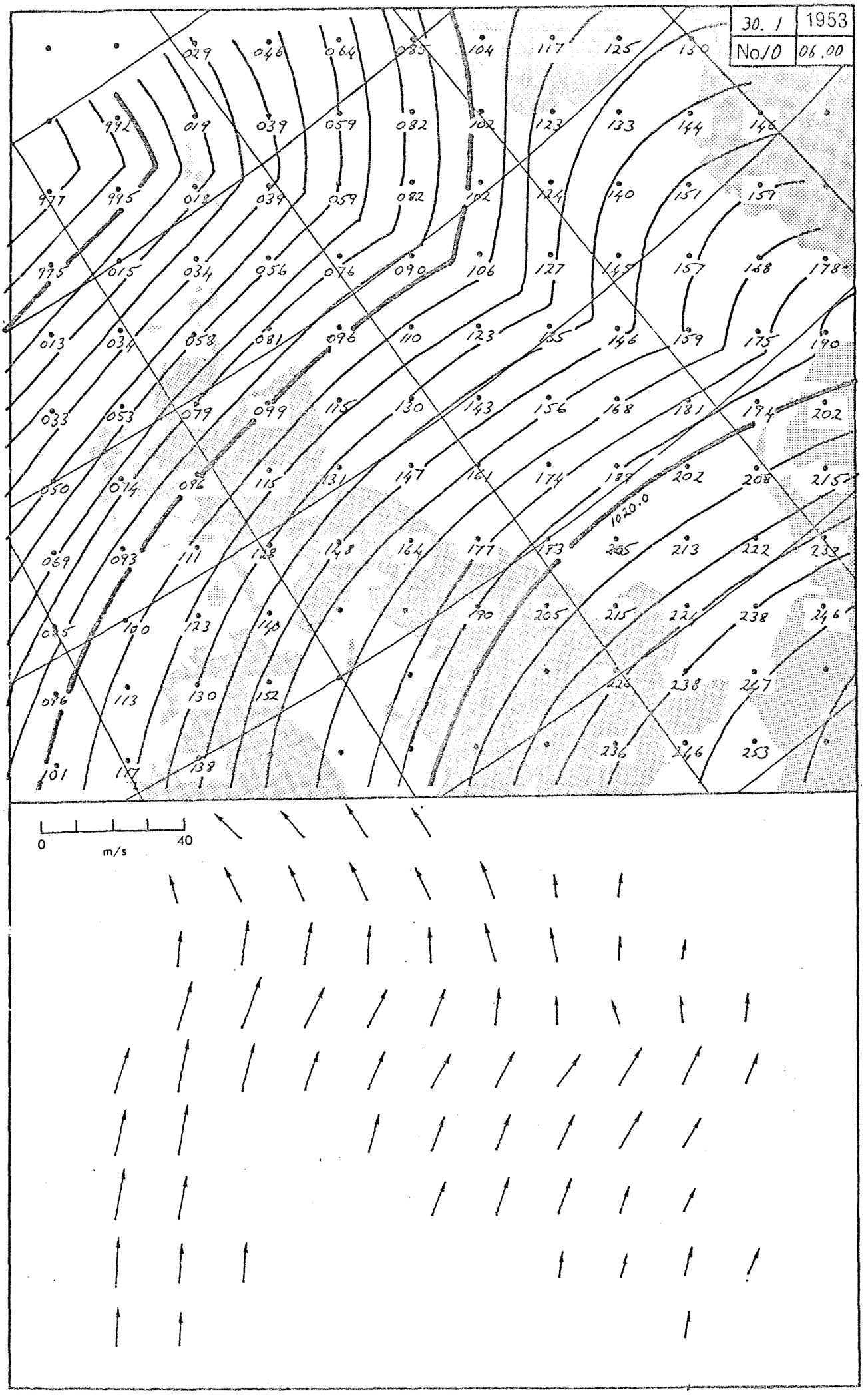
30. 1
1953
No.10
06.00
1020.0
0
40
m/s

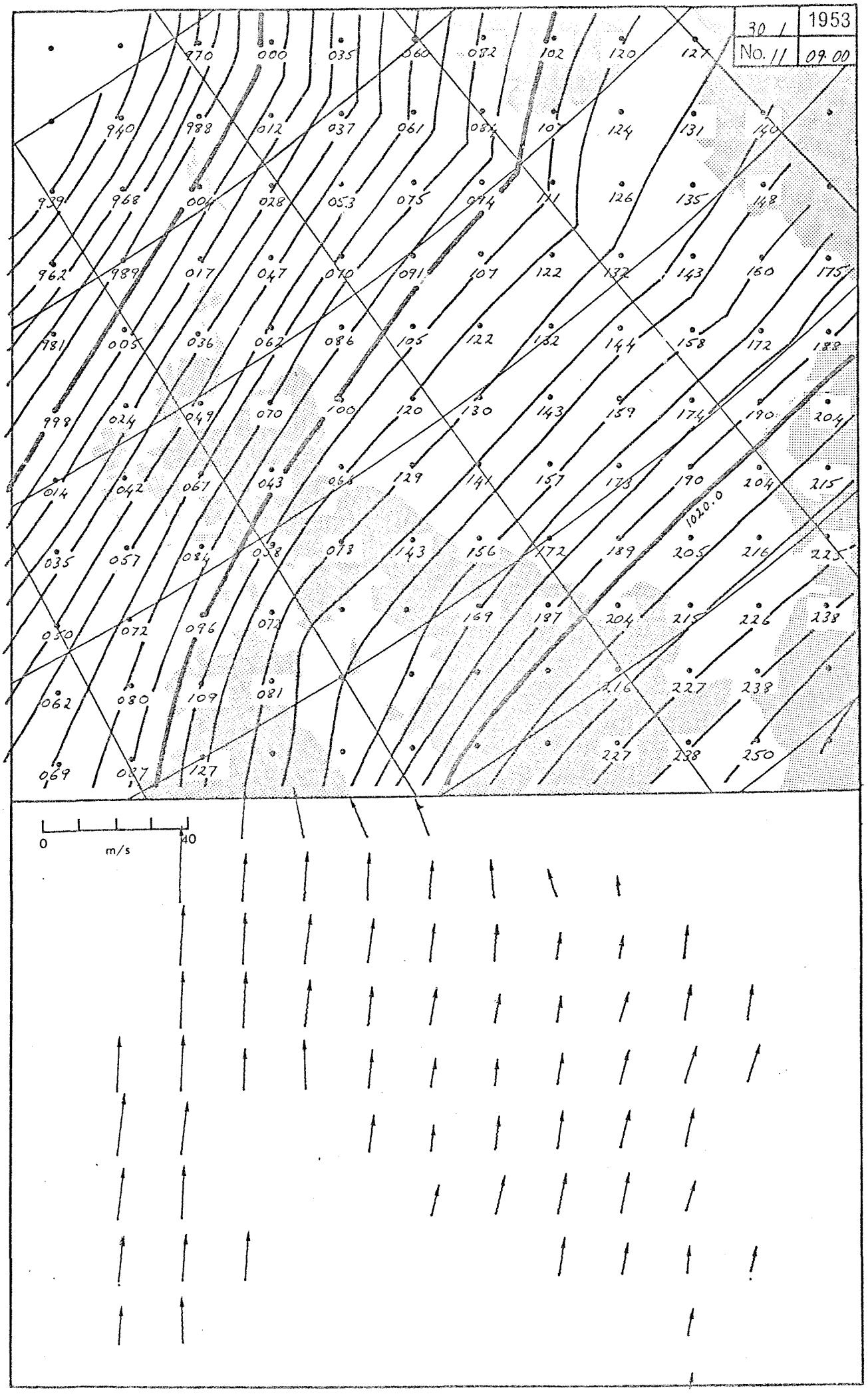
30 / 1953
No. 11 09.00
1020.0
0
m/s
40

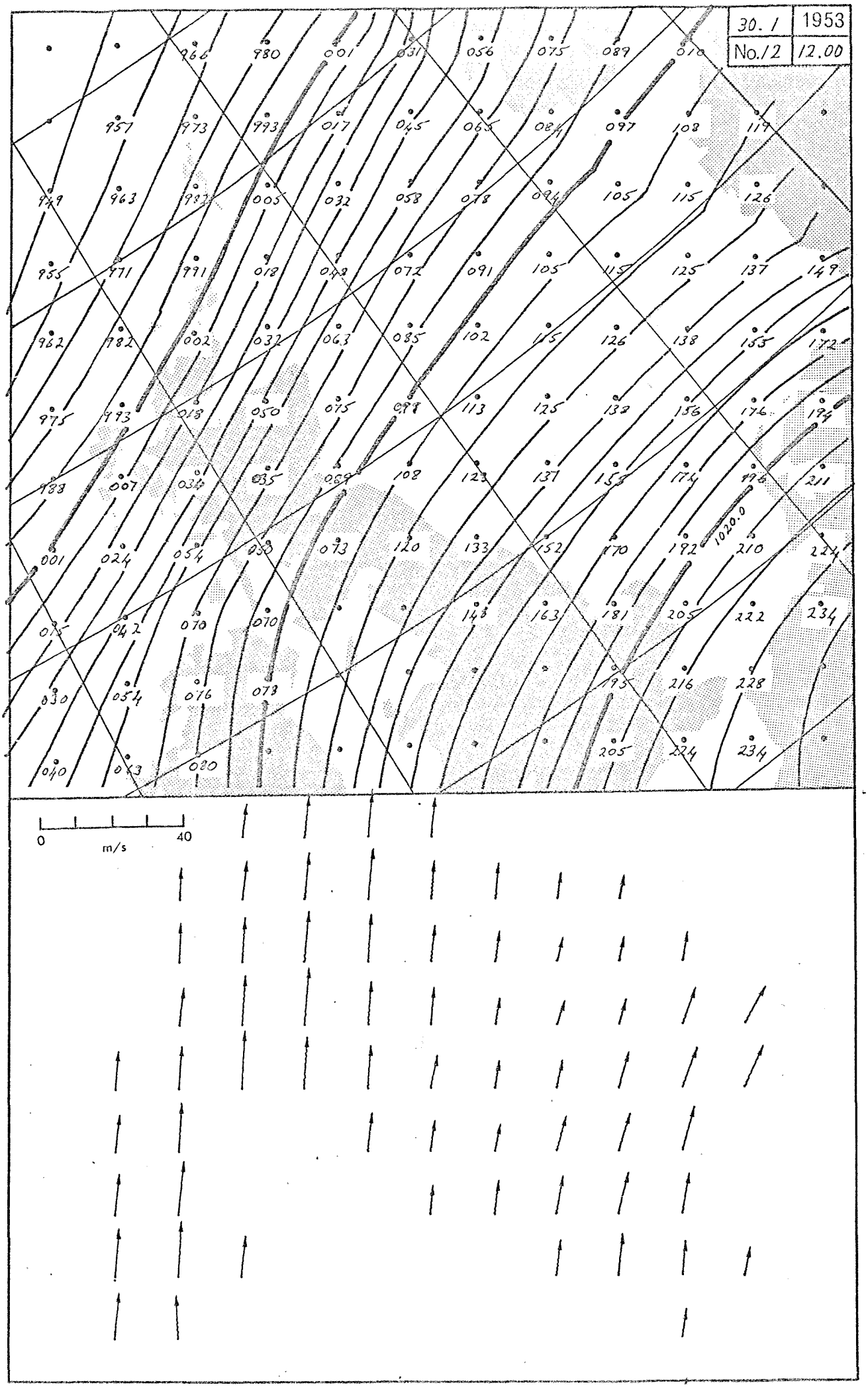
30. 1
1953
No./2
12.00
1020.0
0
40
m/s

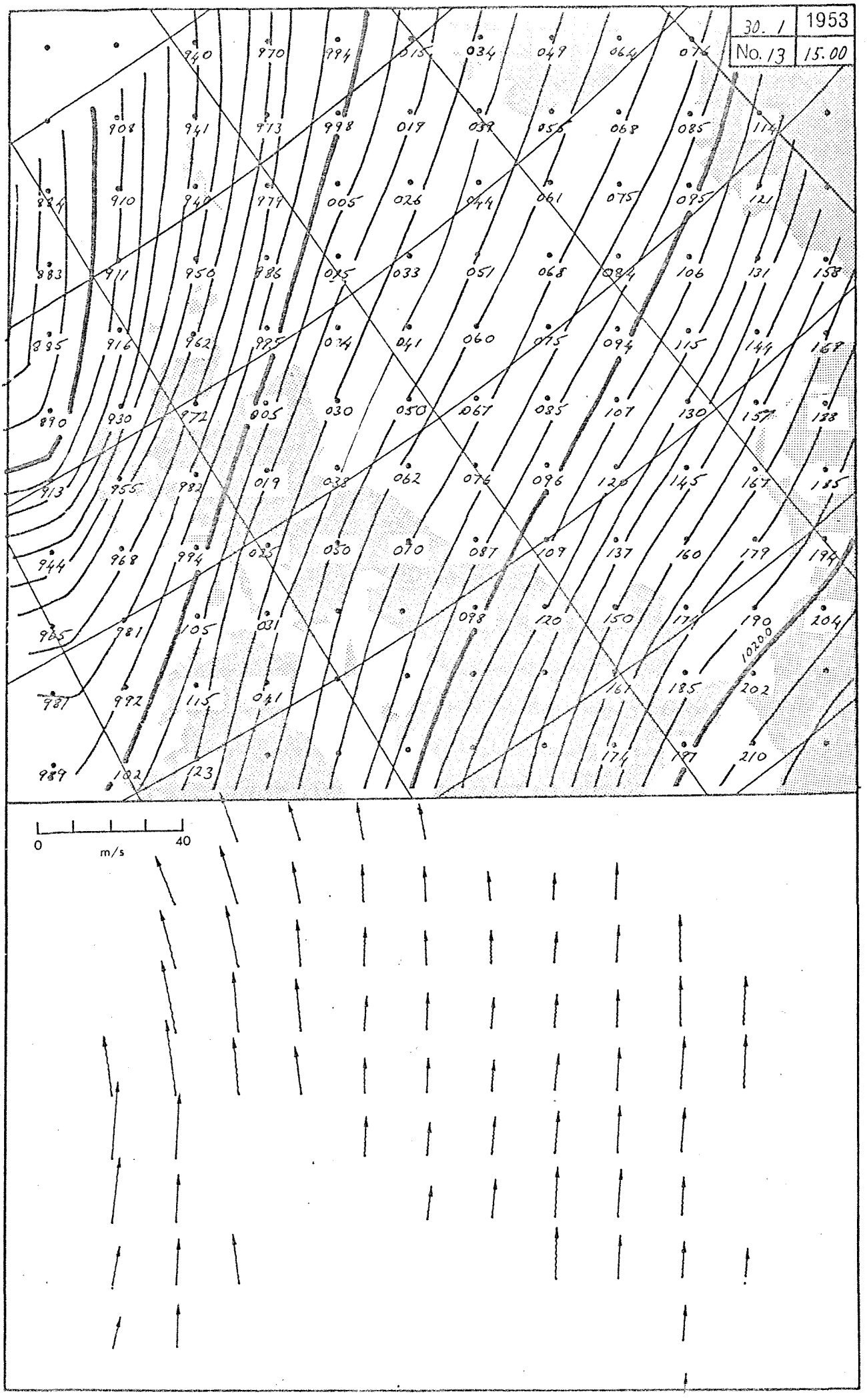
30. 1
1953
No. 13
15.00
0
40
m/s

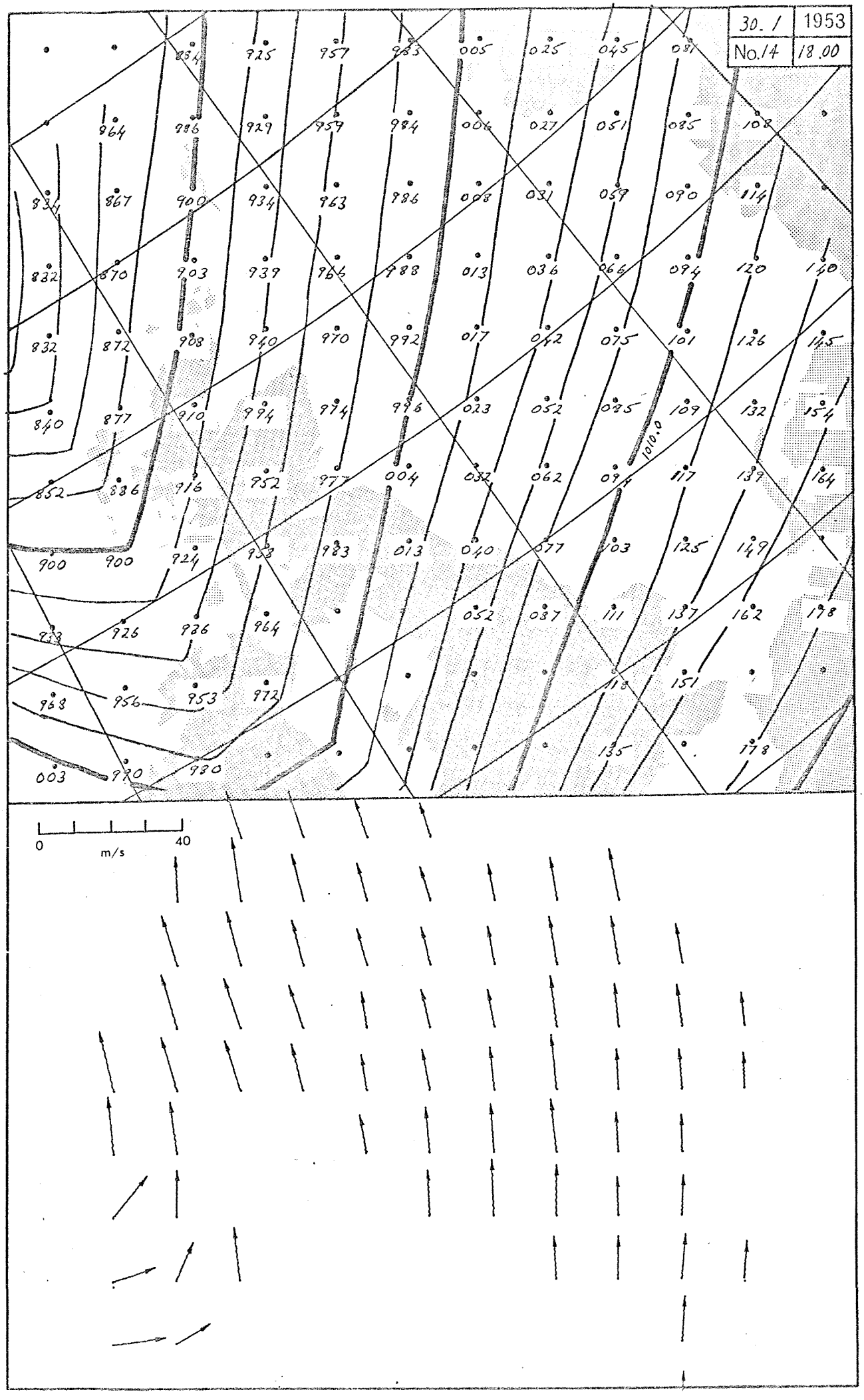
30. 1
1953
No.14
18.00
1010.0
0
40
m/s

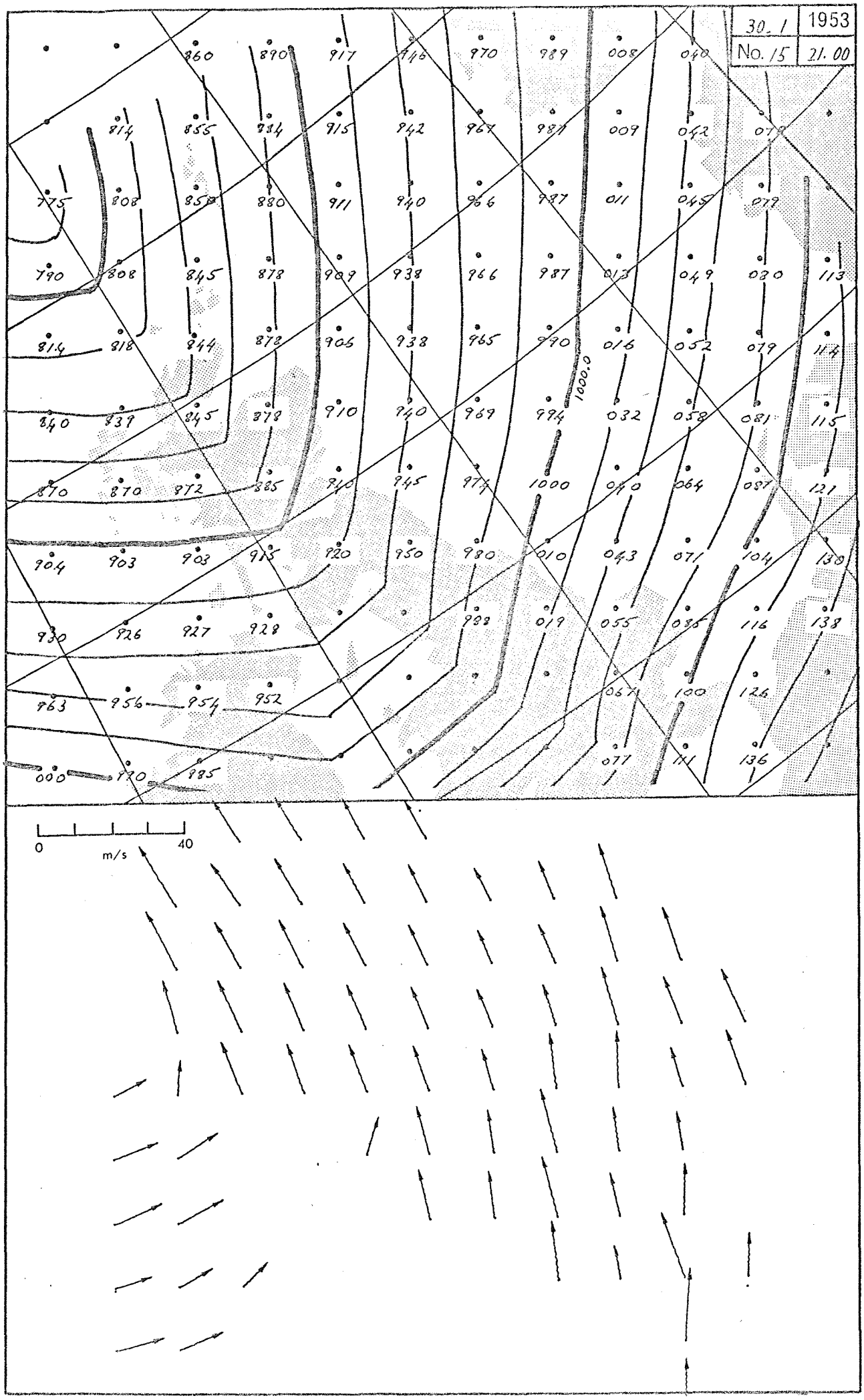
30. 1
1953
No. 15
21. 00
1000.0
0
40
m/s

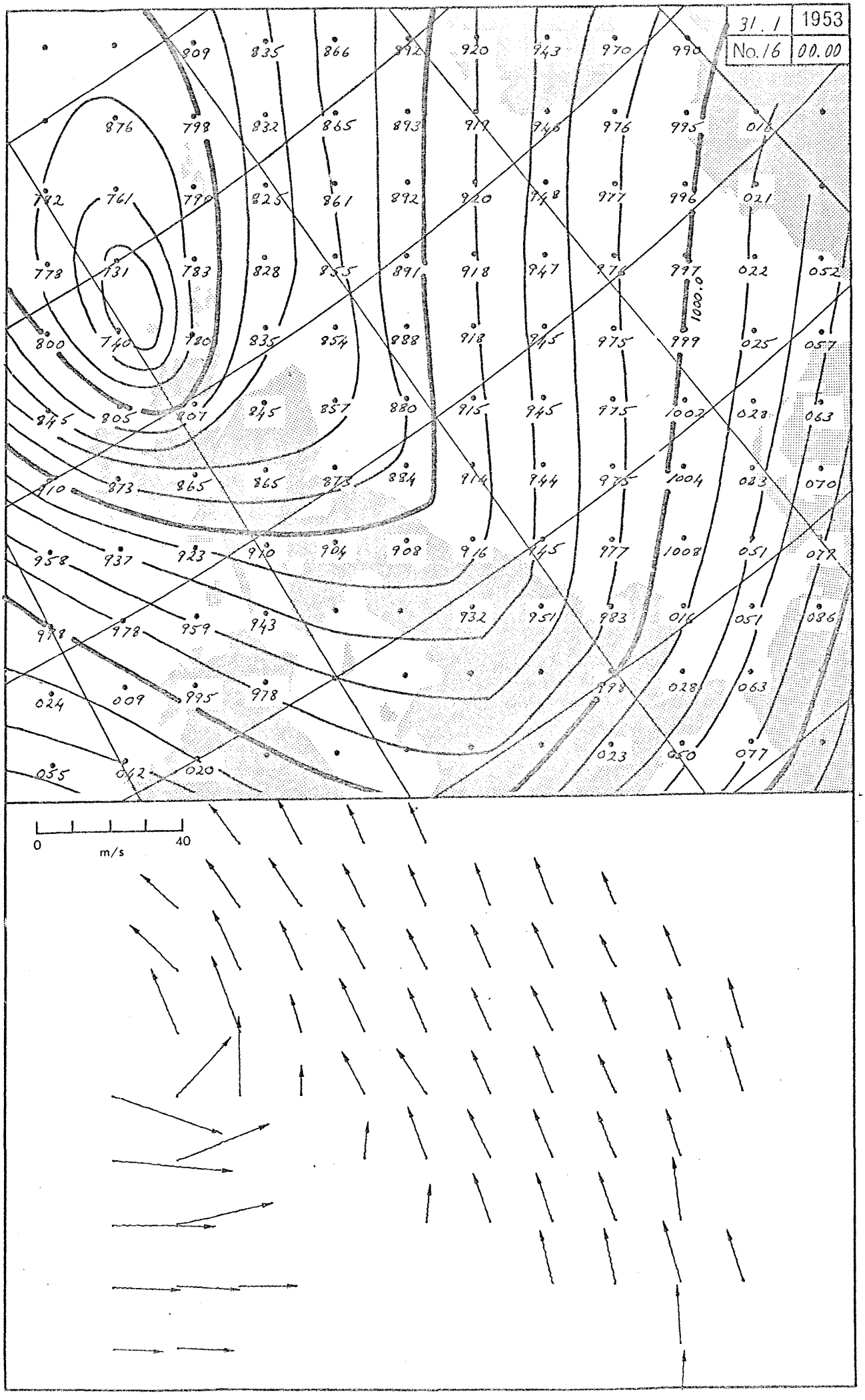
31. 1
1953
No. 16
00.00
1000.0
0
40
m/s

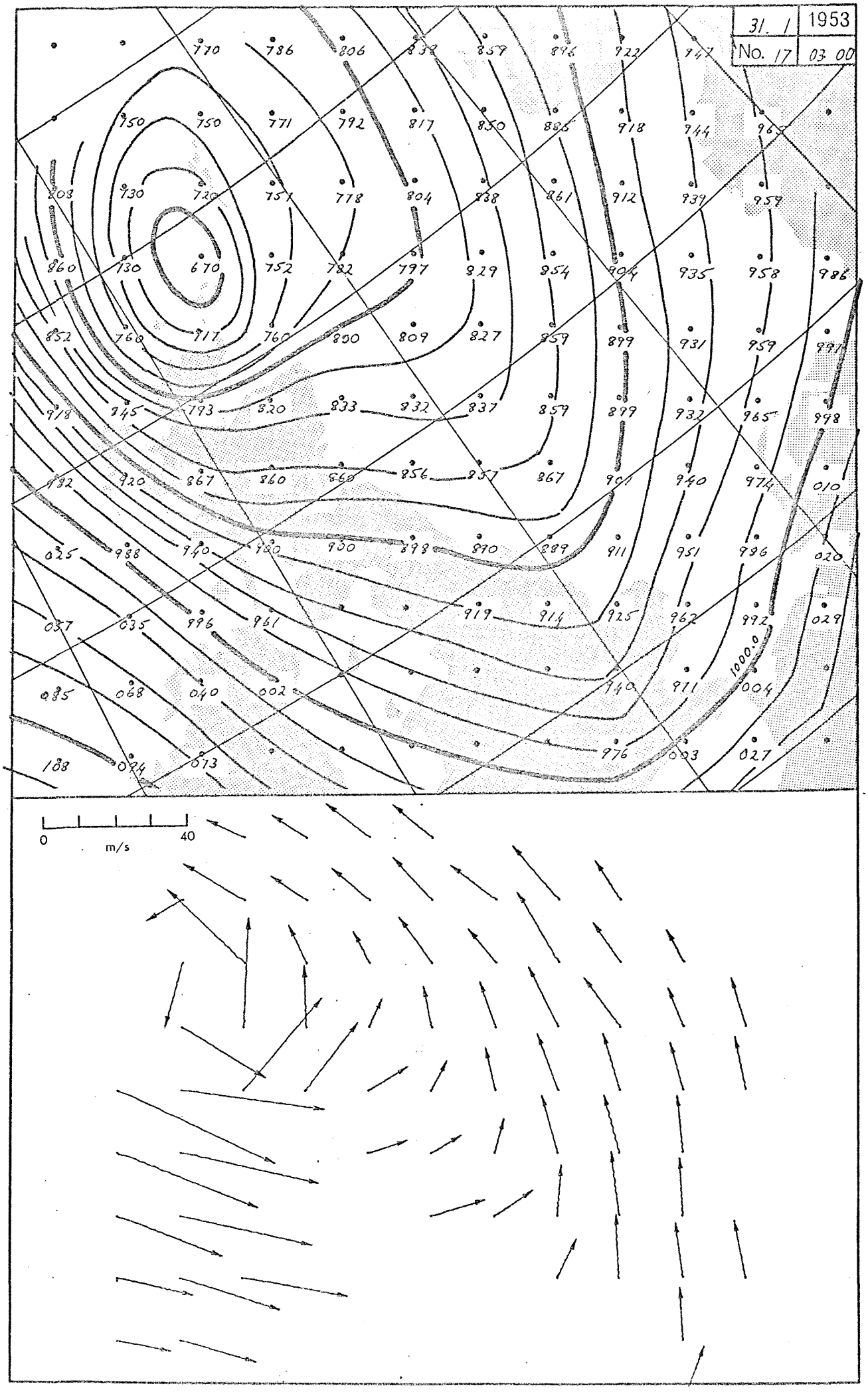
31. 1
1953
No. 17
03 00
0
40
m/s

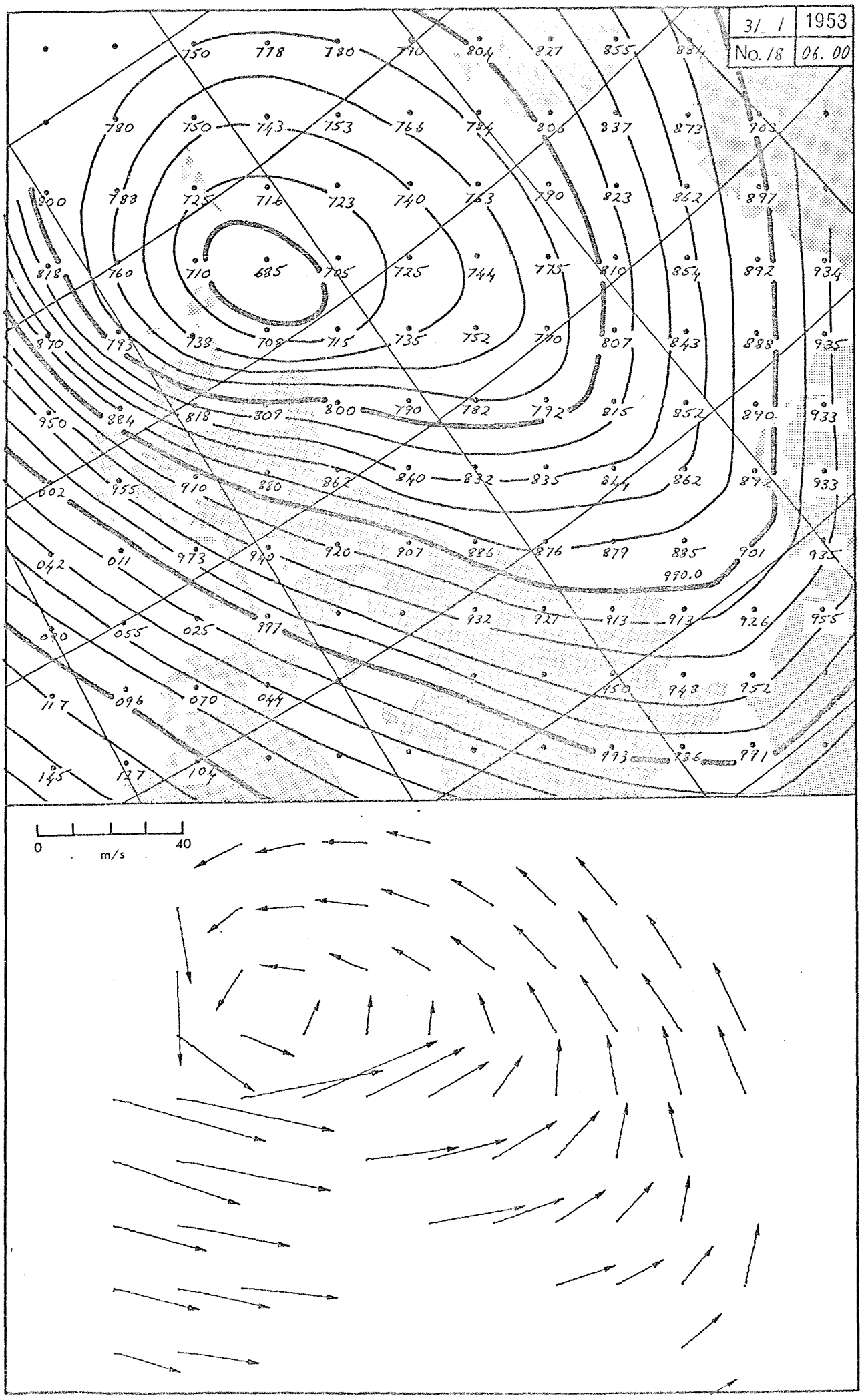
31 / 1
1953
No. 18
06. 00
0
40
m/s

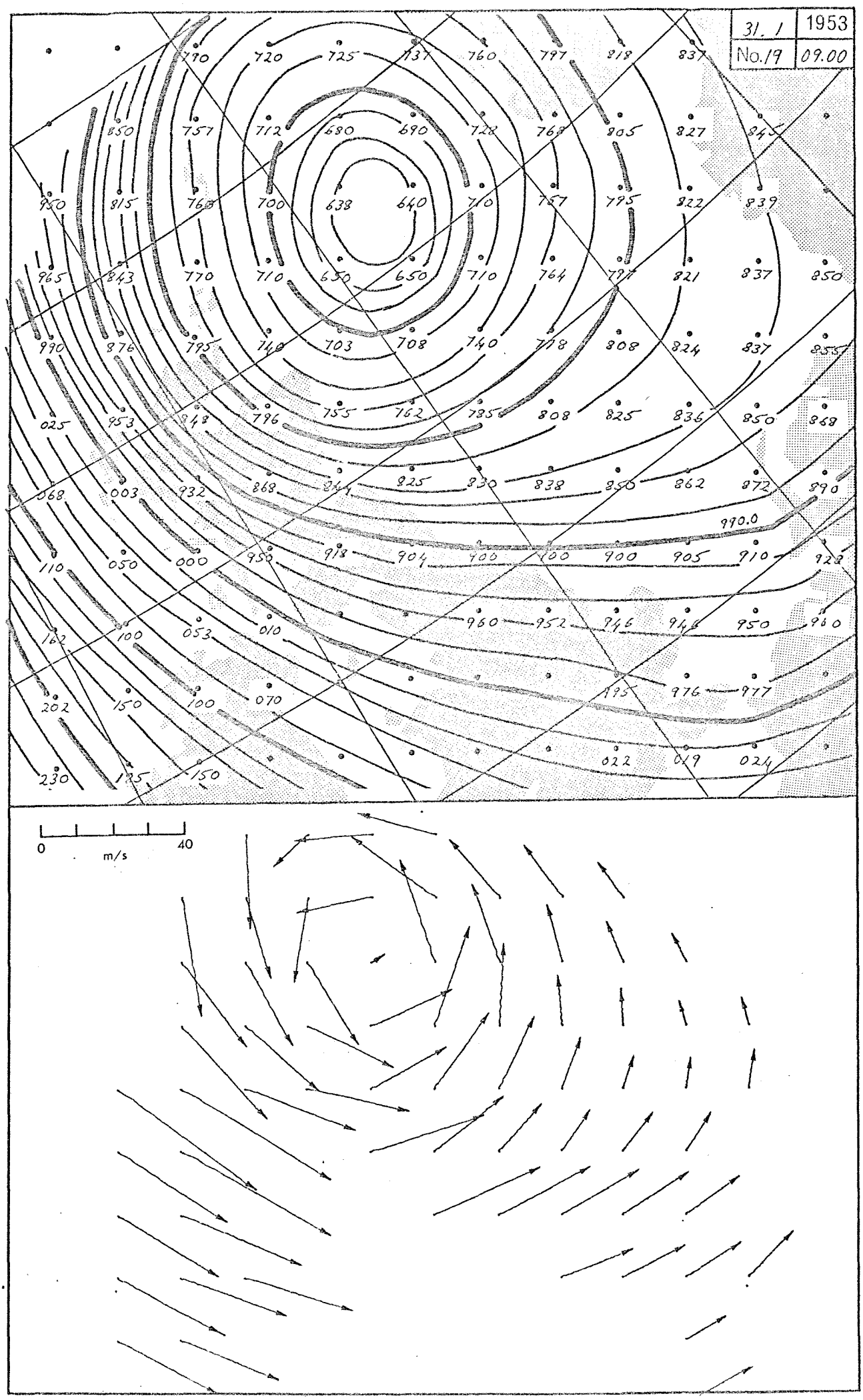
31. 1
1953
No.19
09.00
990.0
0
40
m/s

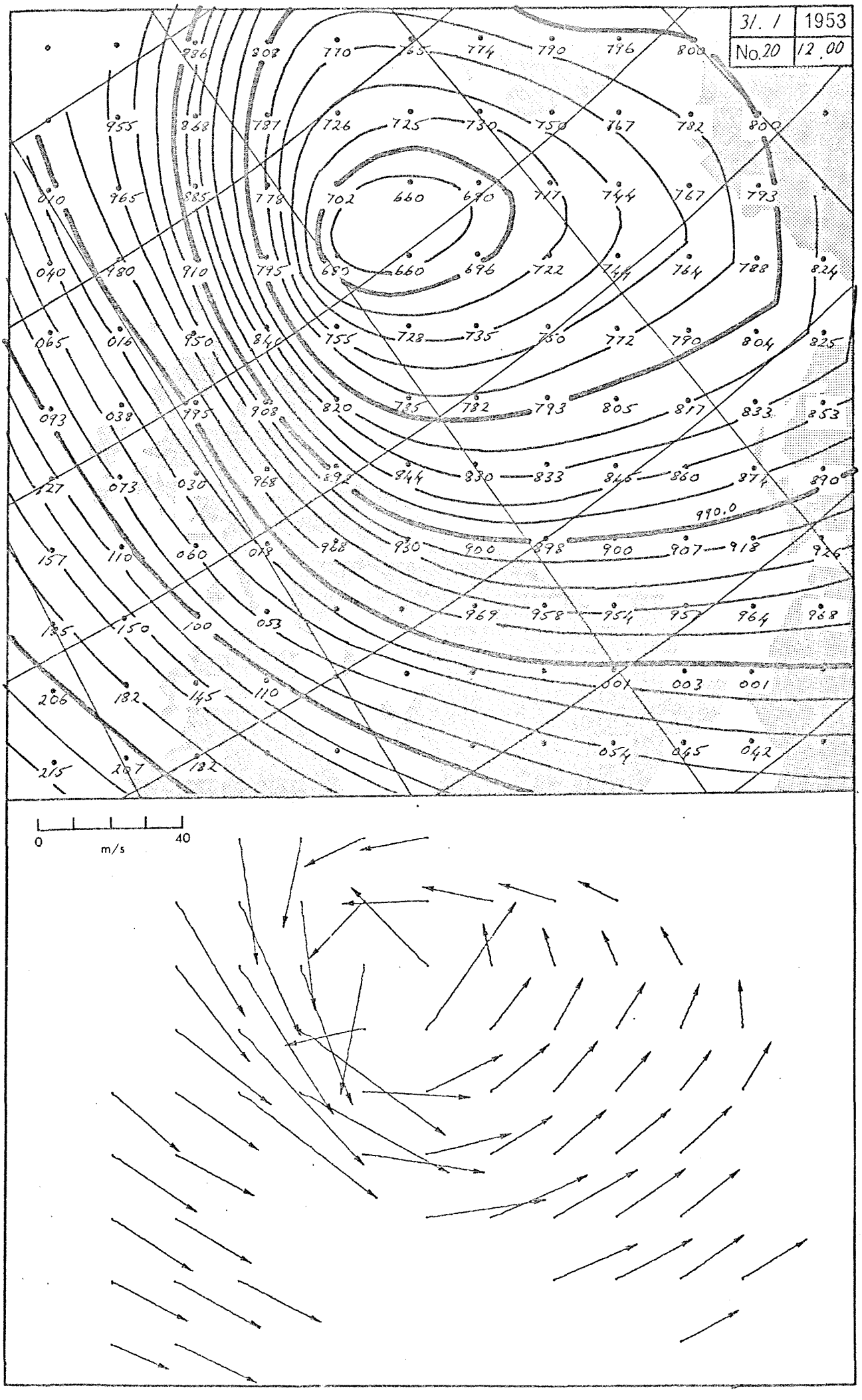
3/. /
1953
No.20
12 .00
0
m/s
40

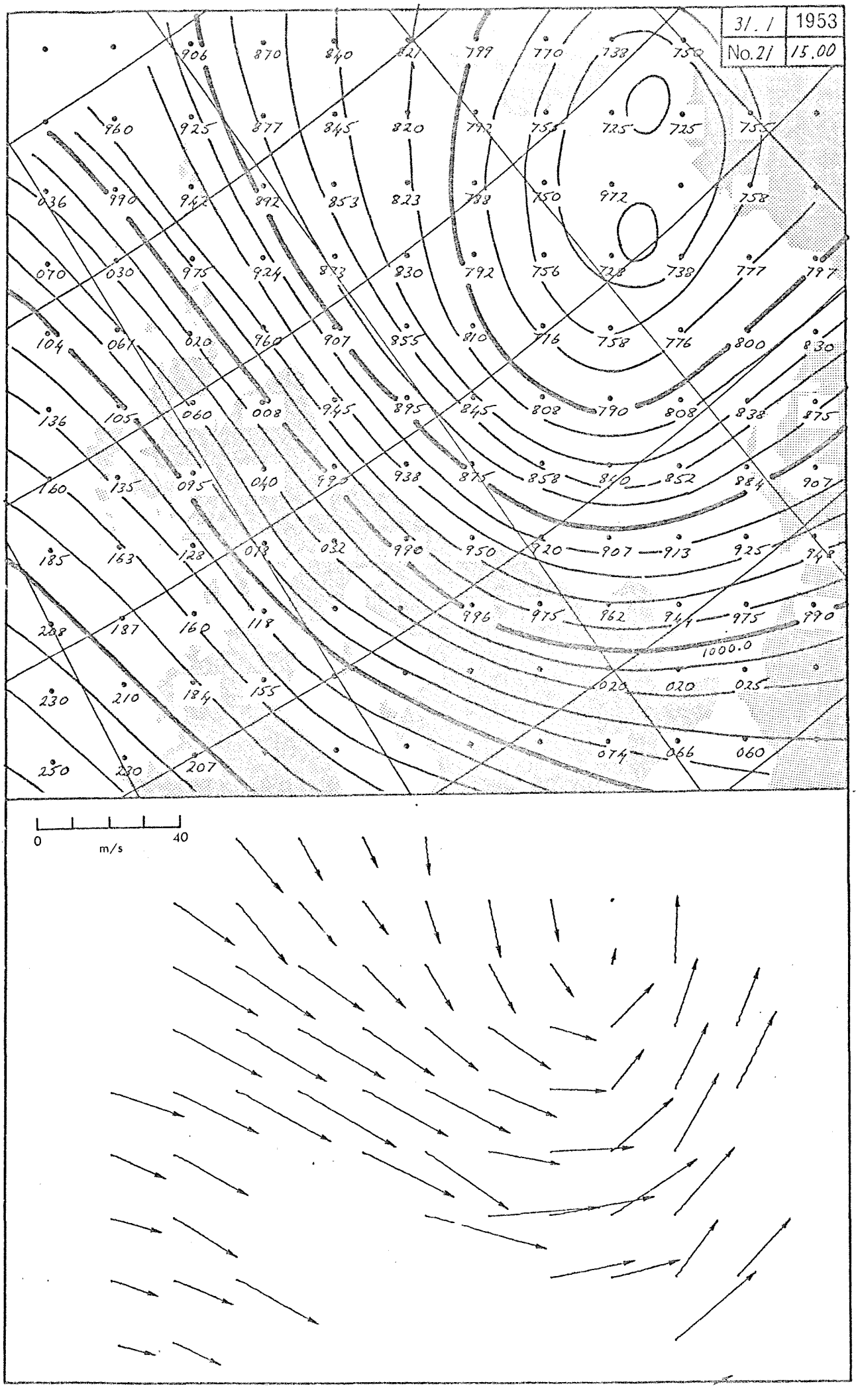
31. 1
1953
No. 21
15.00
1000.0
0
m/s
40

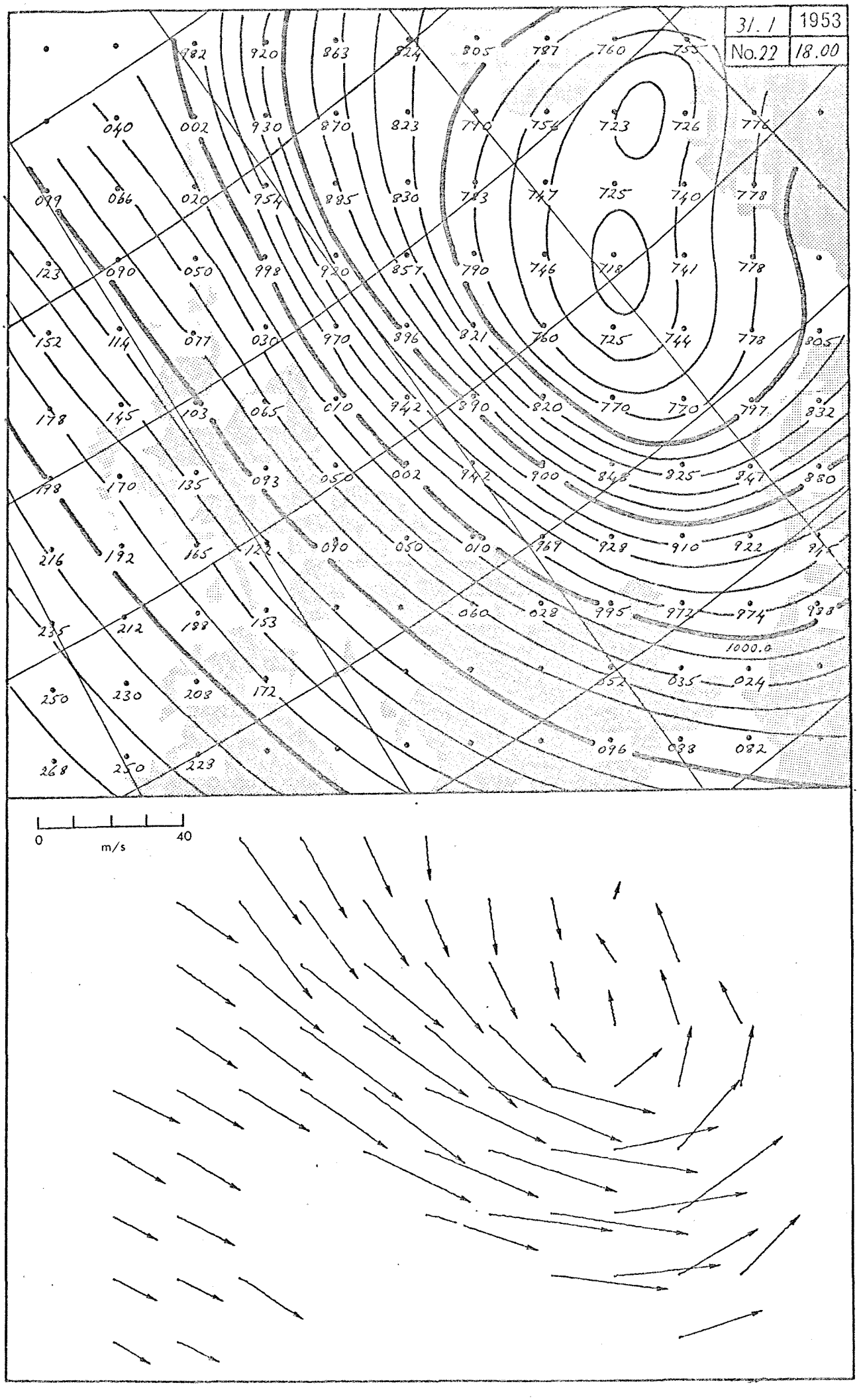
31. 1
1953
No.22
18.00
1000.0
0
40
m/s

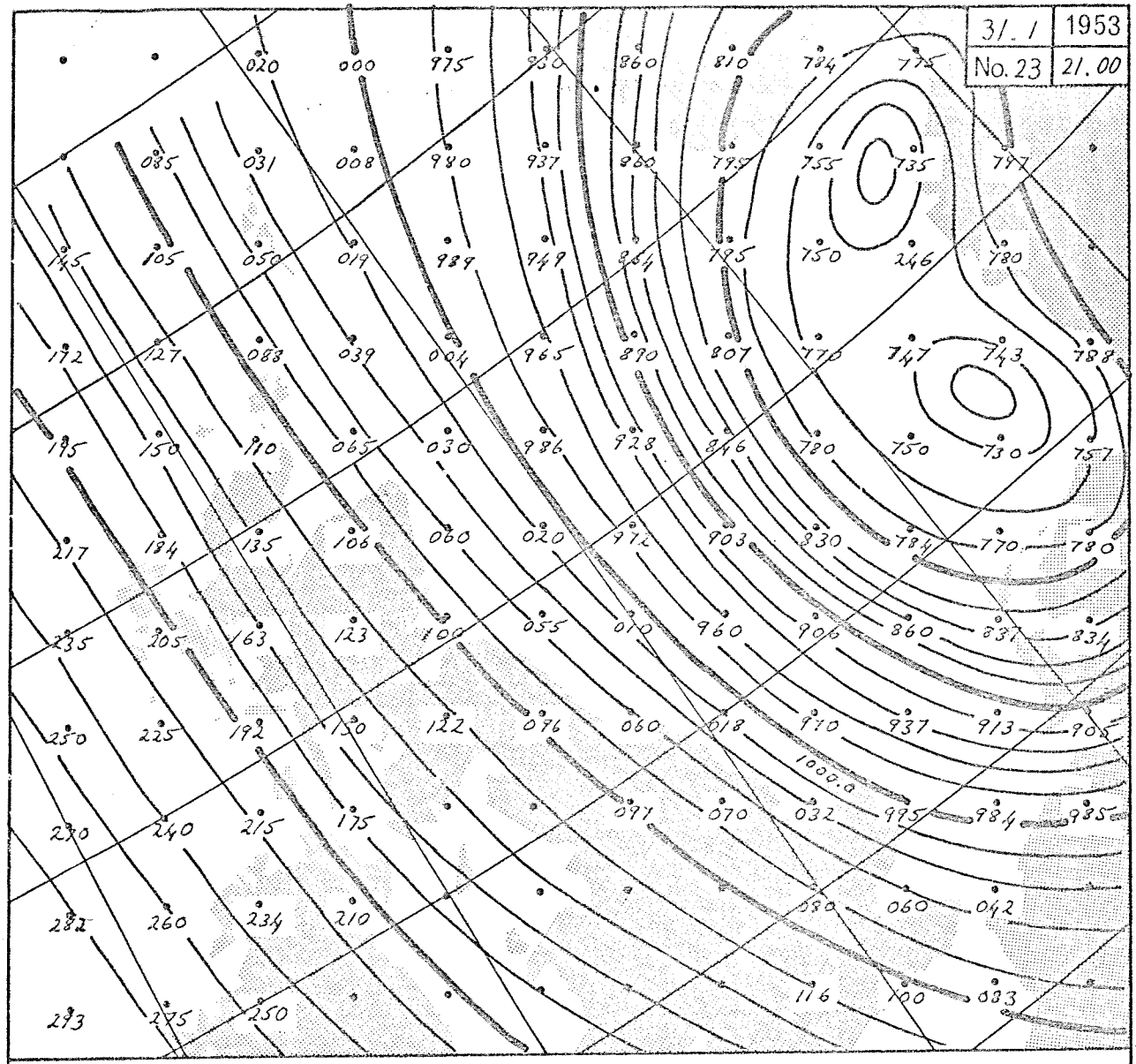
31. 1
1953
No. 23
21. 00

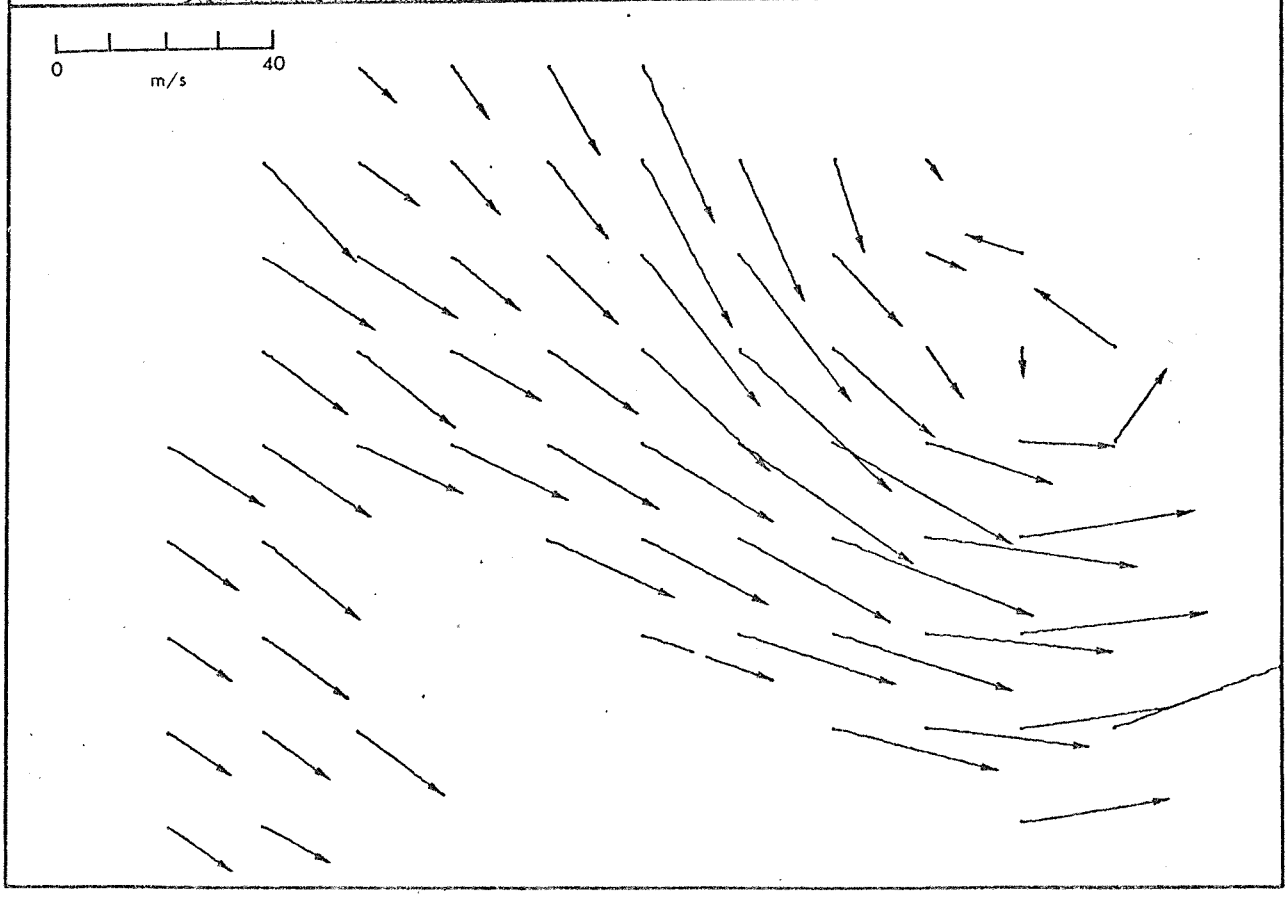
0
40
m/s

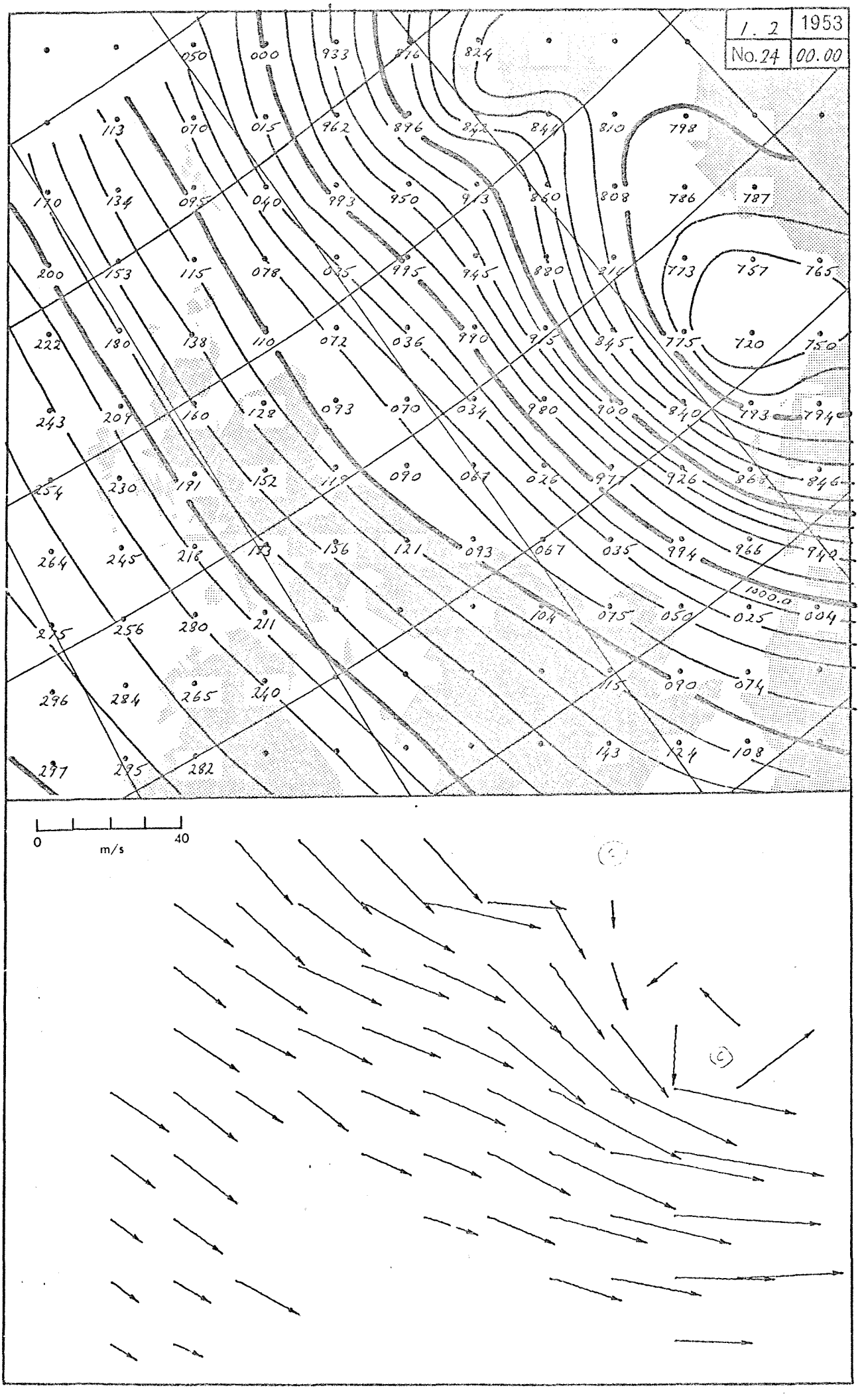
1. 2
1953
No. 24
00.00
1000.0
0
m/s
40

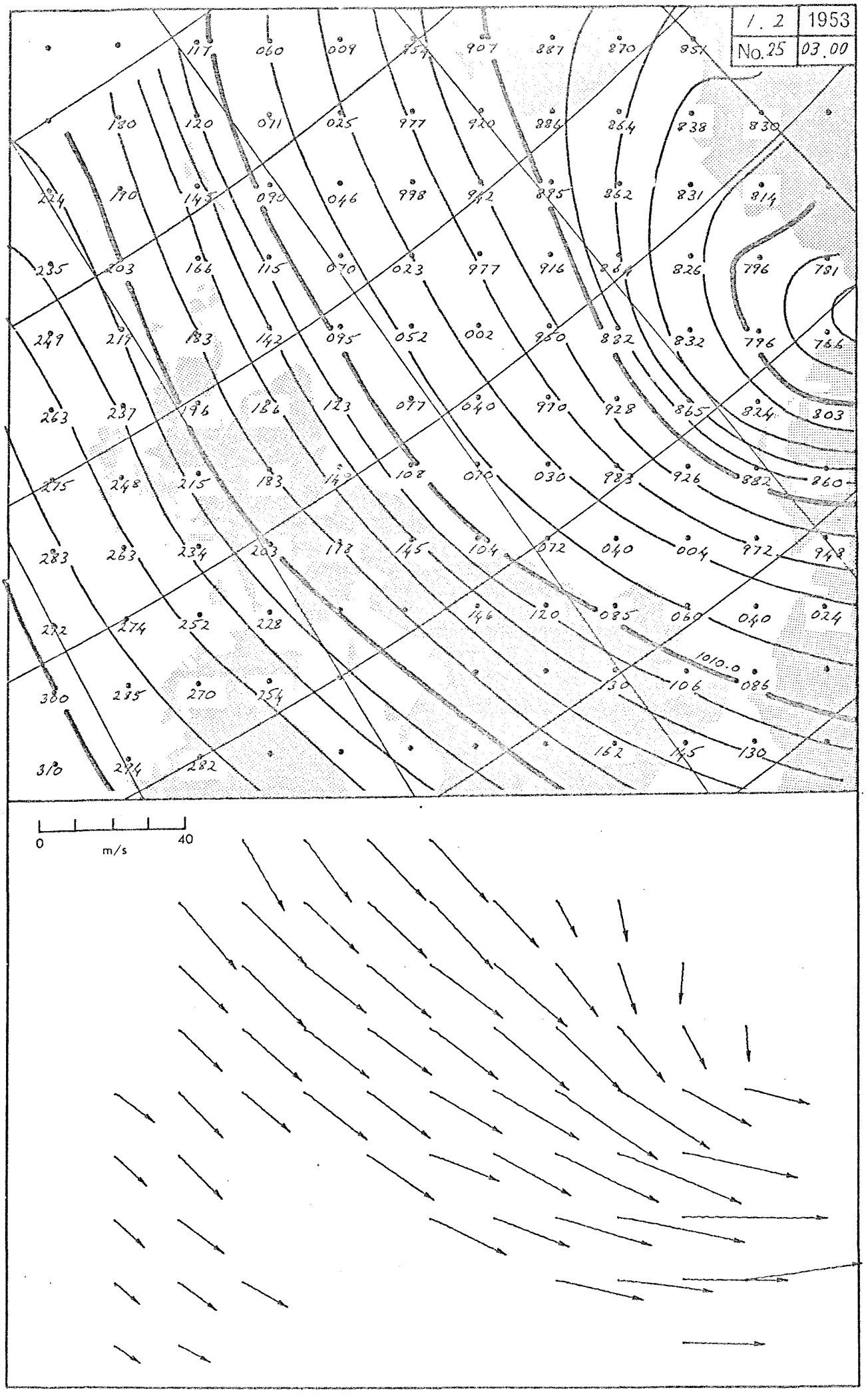
1. 2
1953
No. 25
03.00
0
m/s
40

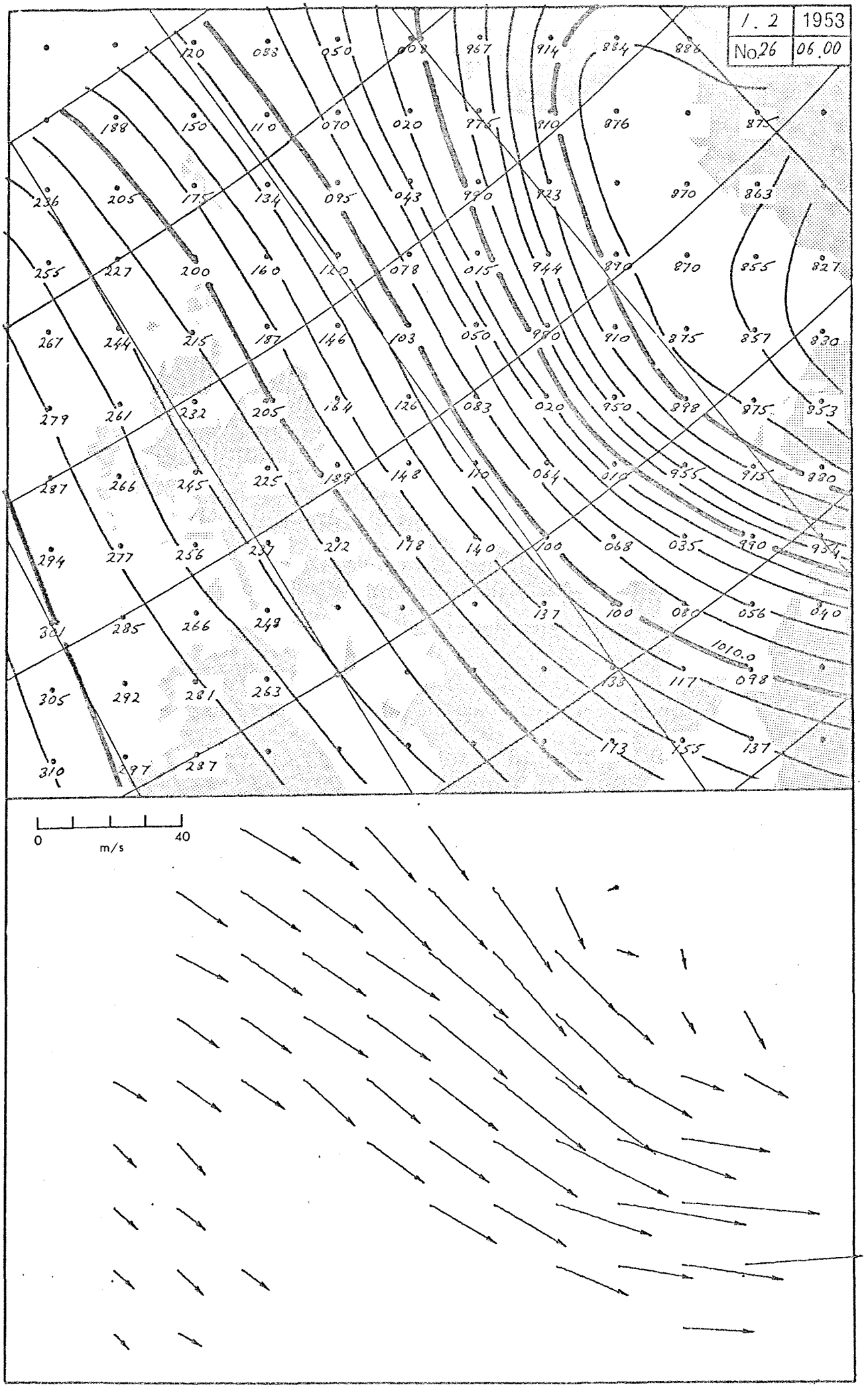
1. 2
1953
No.26
06.00
0
m/s
40

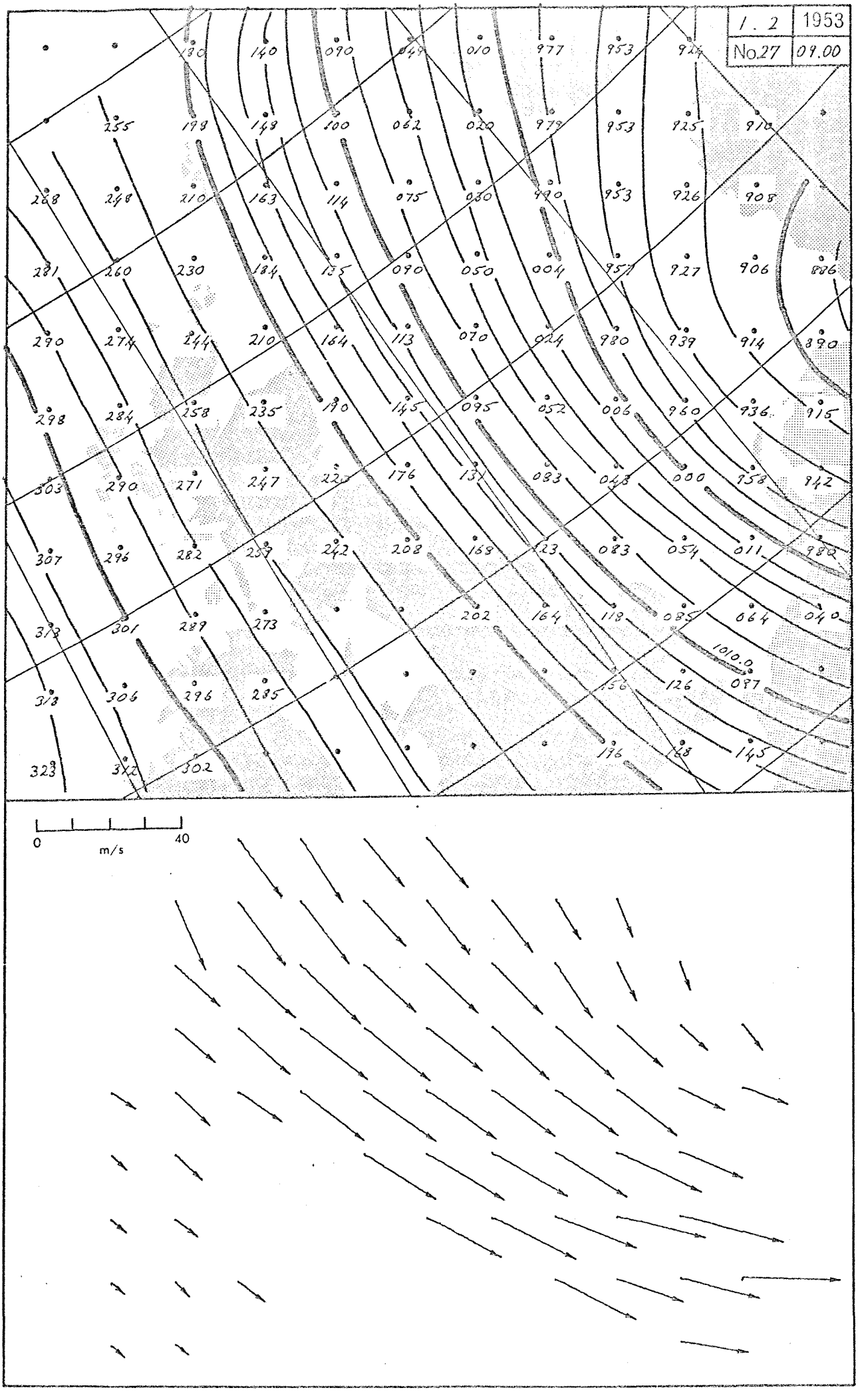
1. 2
1953
No.27
09.00
0
m/s
40

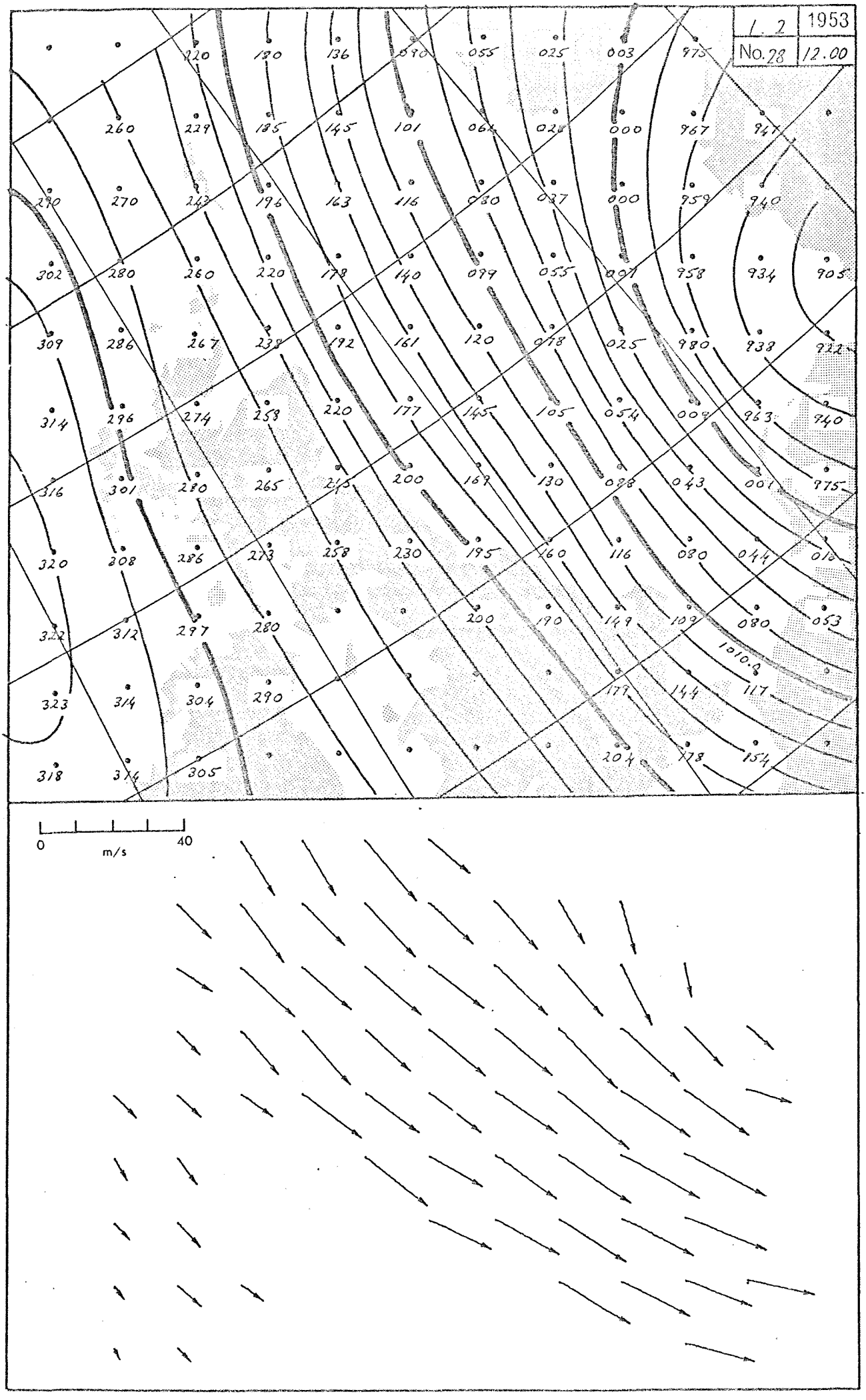
1953
12.00
0
40
m/s

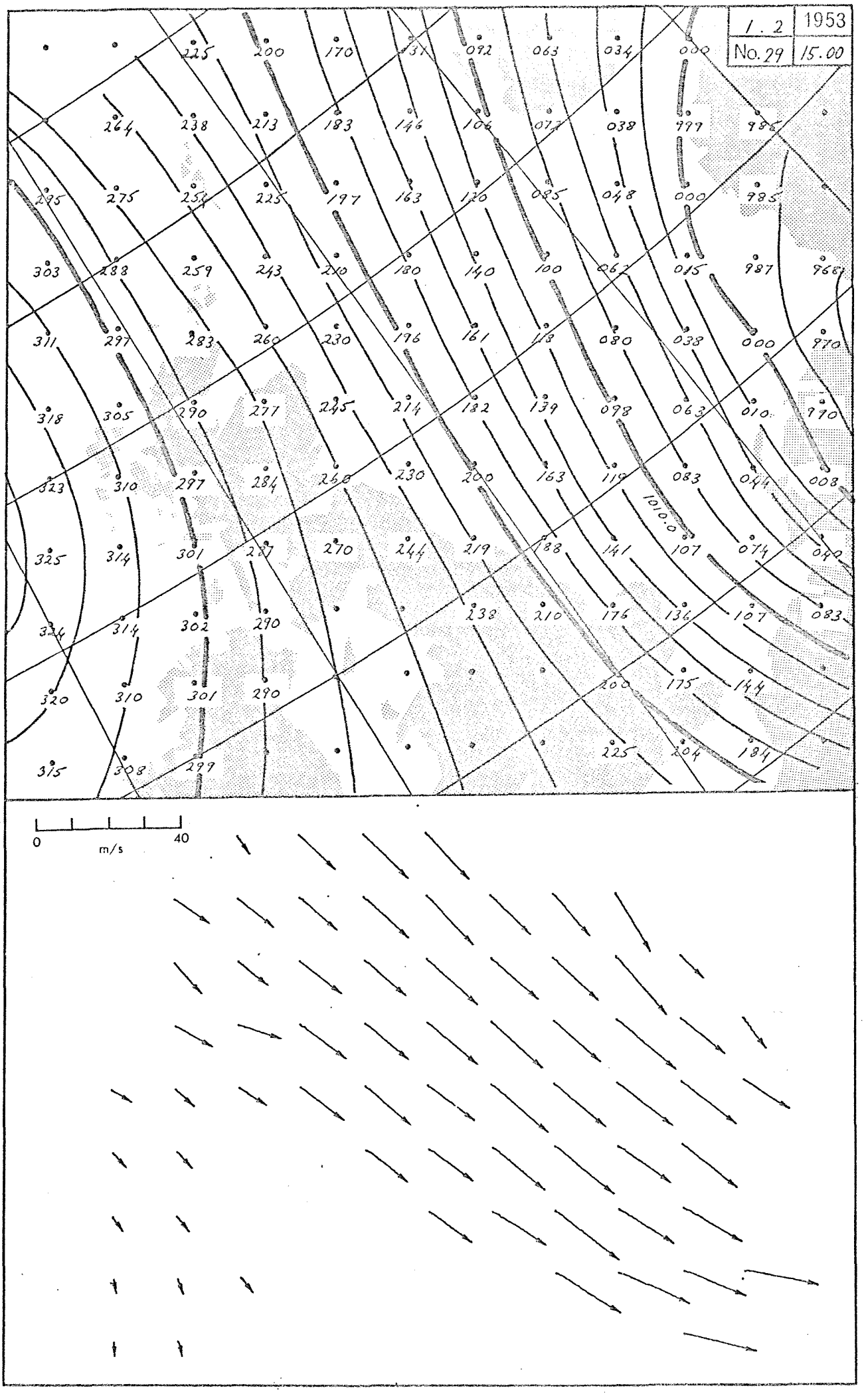
1 . 2
1953
No. 29
15.00
1010.0
0
40
m/s

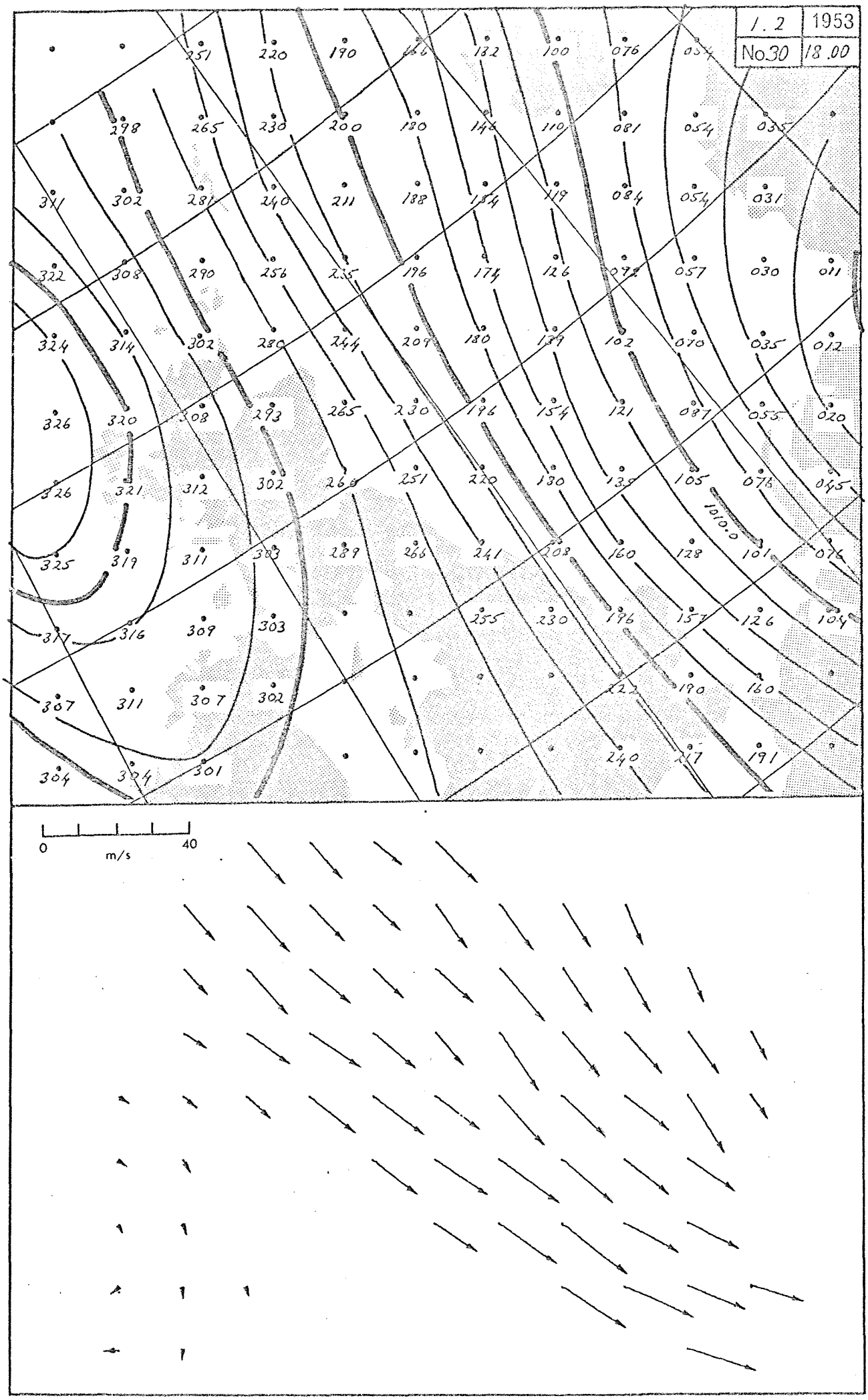
1. 2
1953
No.30
18.00
1010.0
0
m/s
40

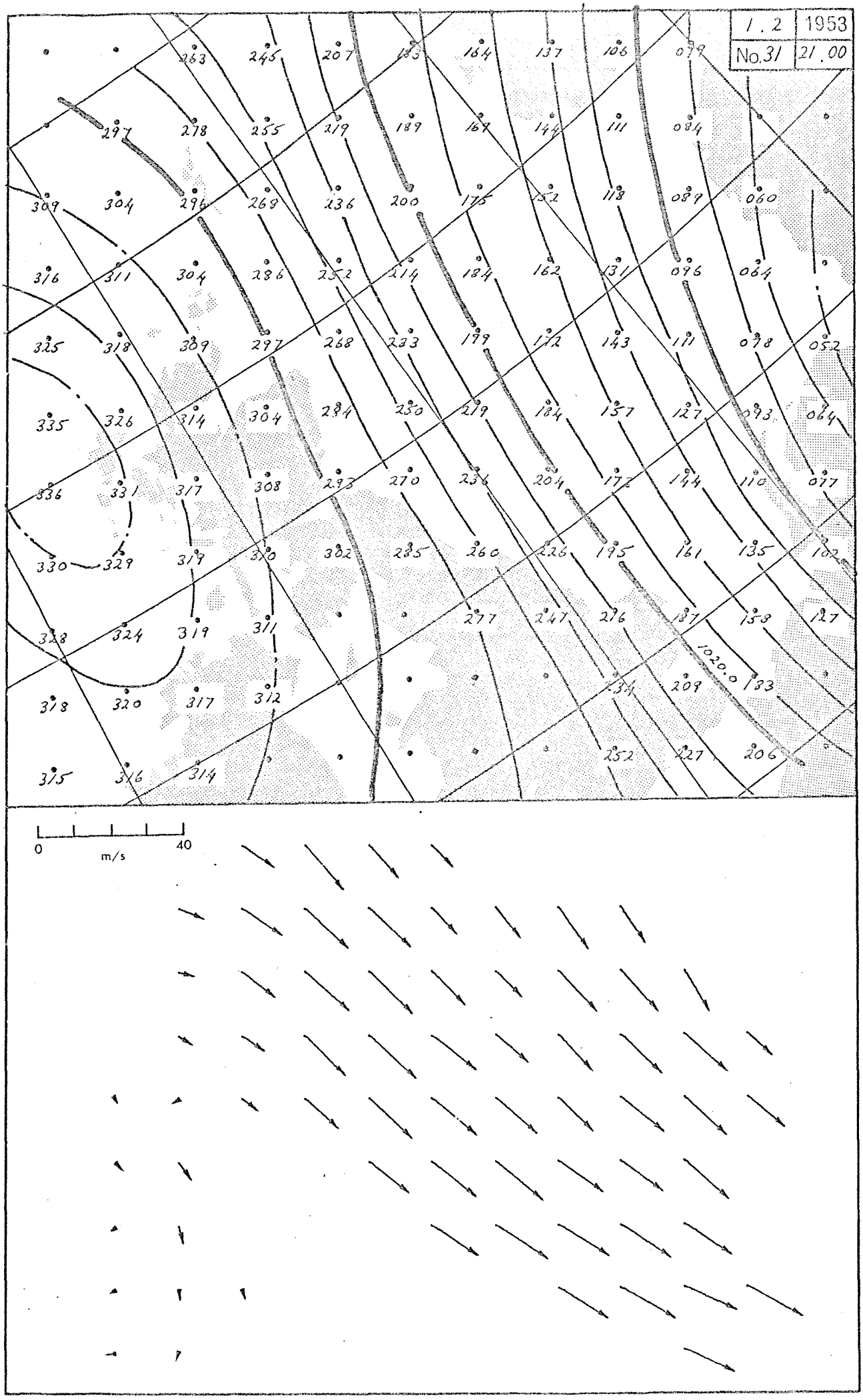
1.2 1953
No.31 21.00
1020.0
0
40
m/s

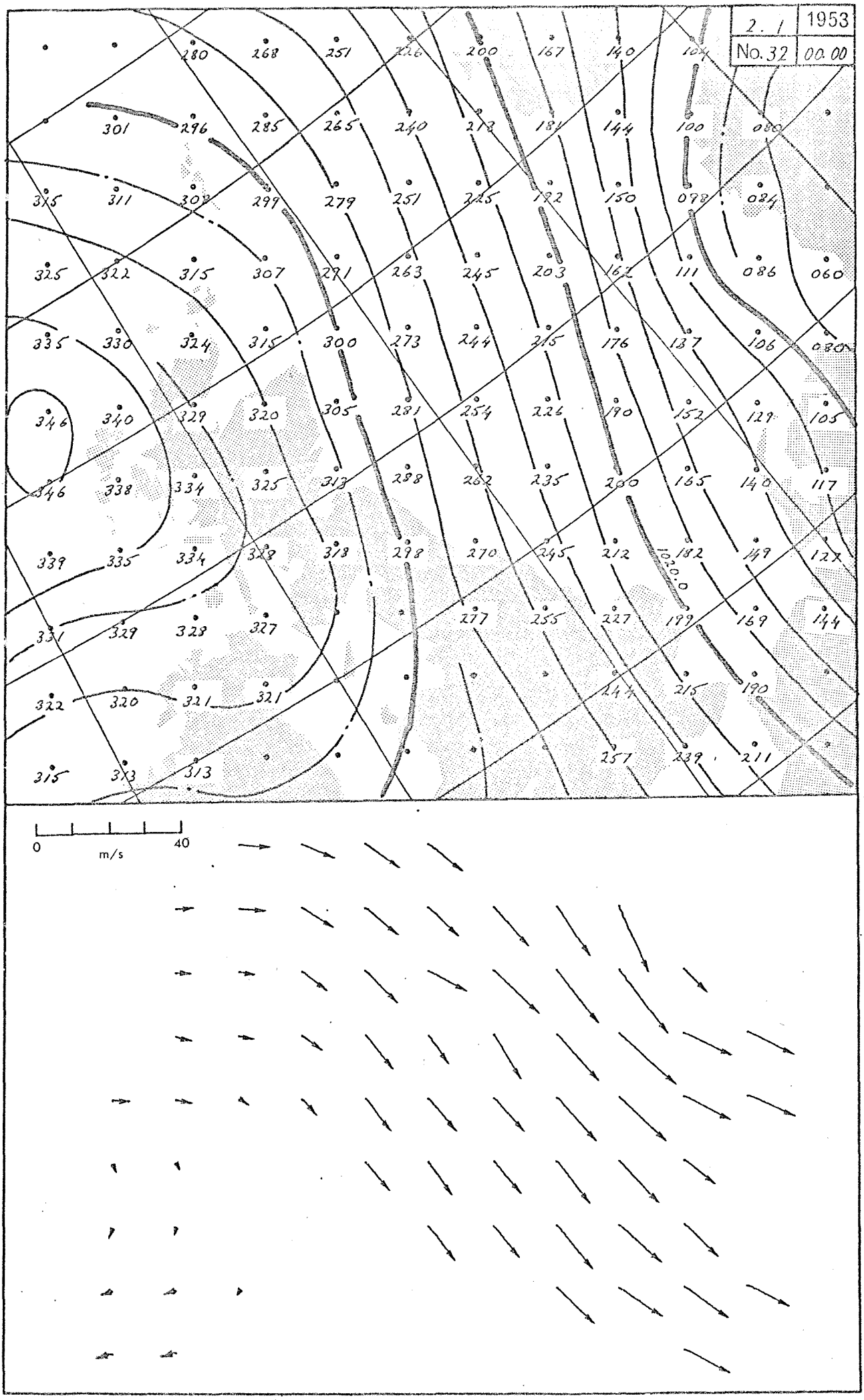
2. 1
1953
No. 32
00.00
0
40
m/s

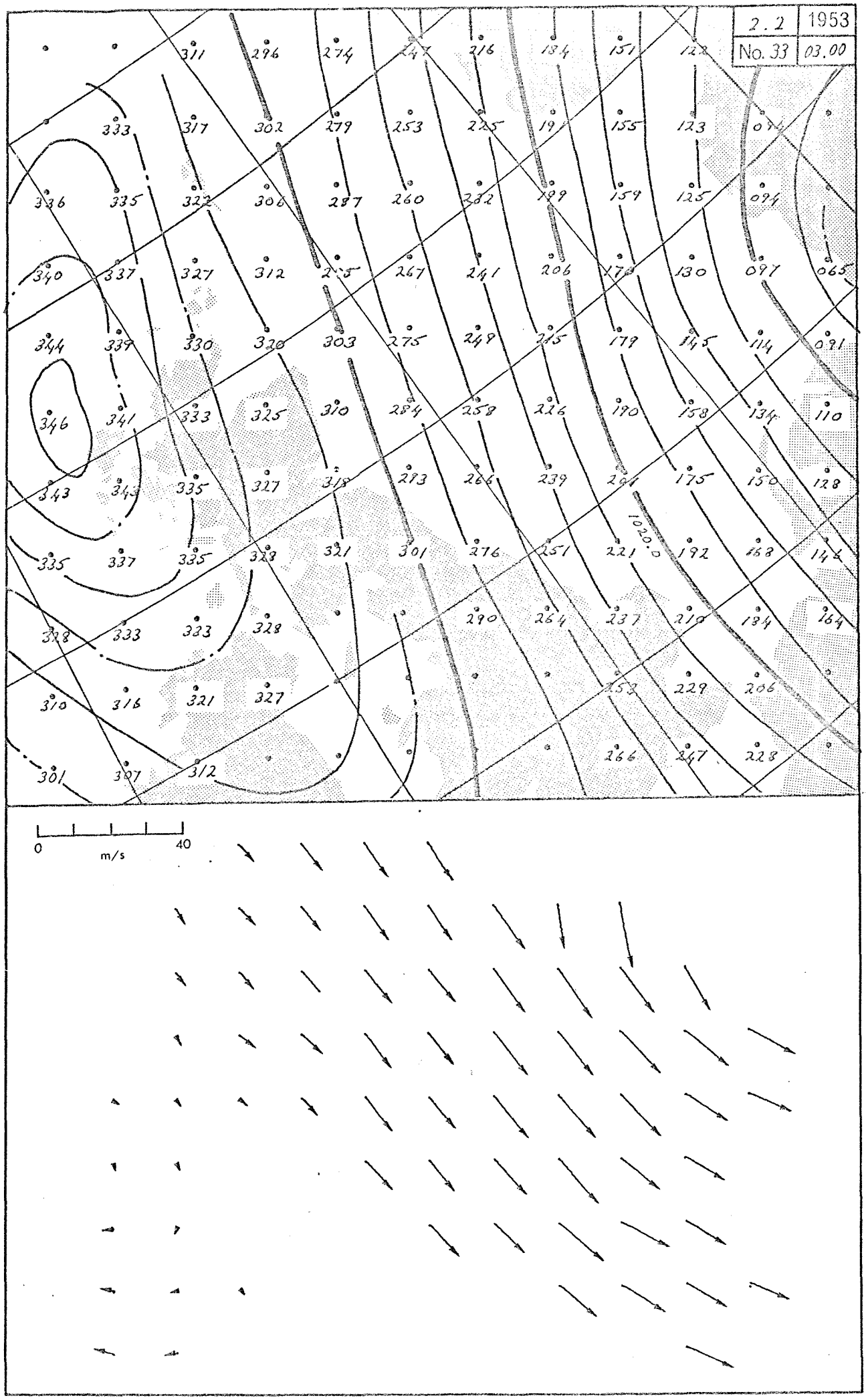
2.2
1953
No. 33
03.00
1020.0
0
40
m/s

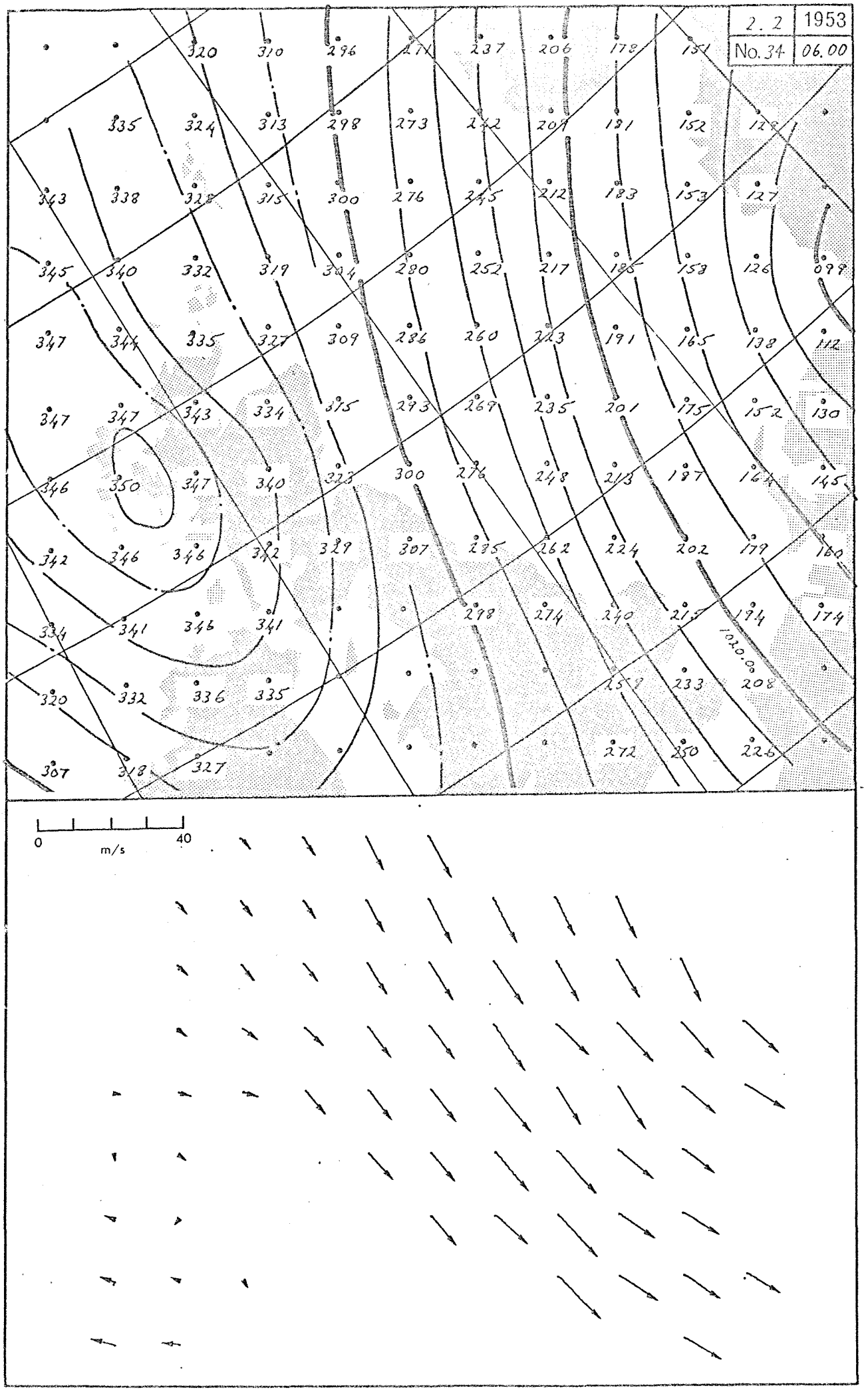
2. 2
1953
No. 34
06.00
0
m/s
40
1020.0

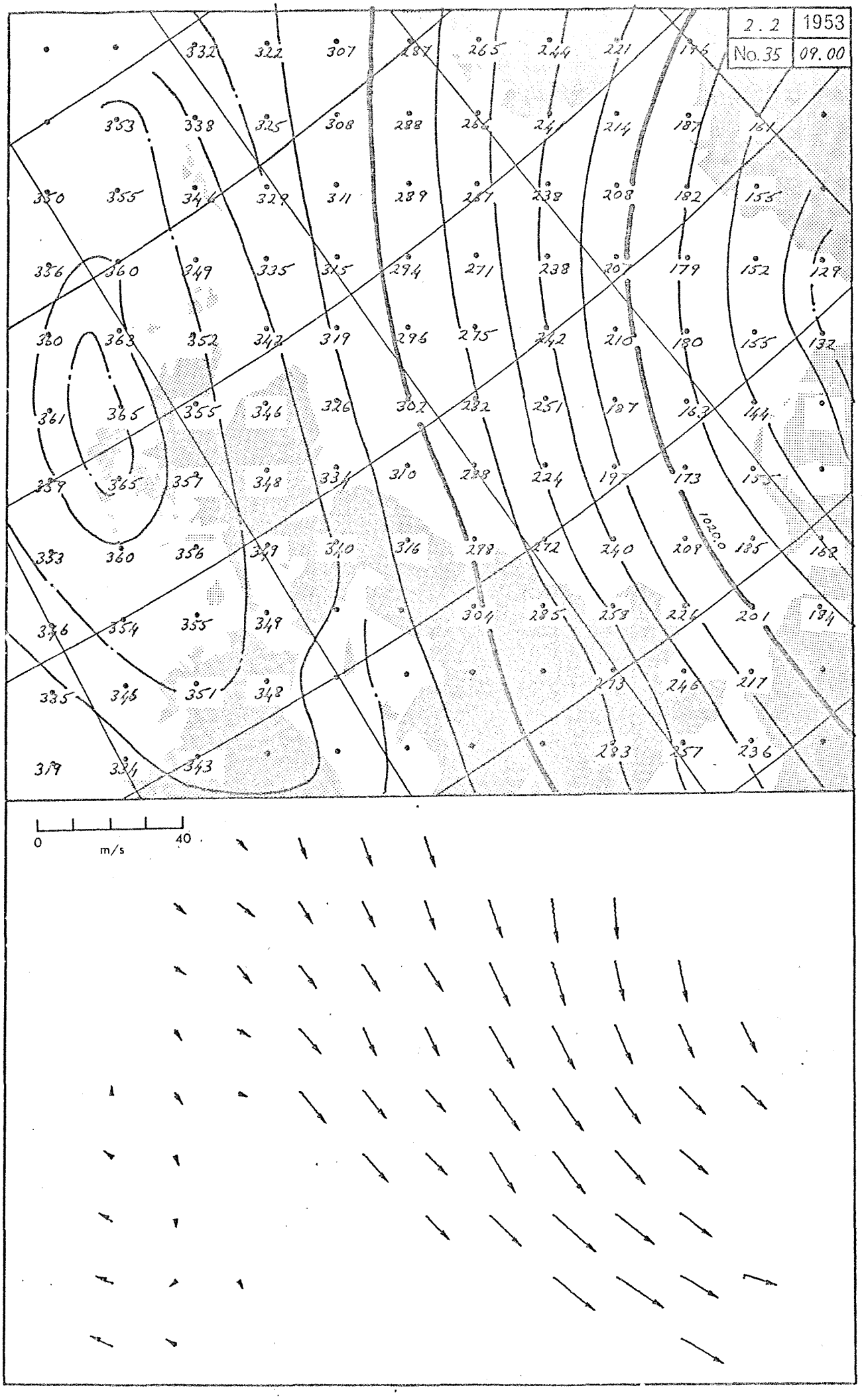
2.2
1953
No. 35
09.00
1020.0
0
40
m/s

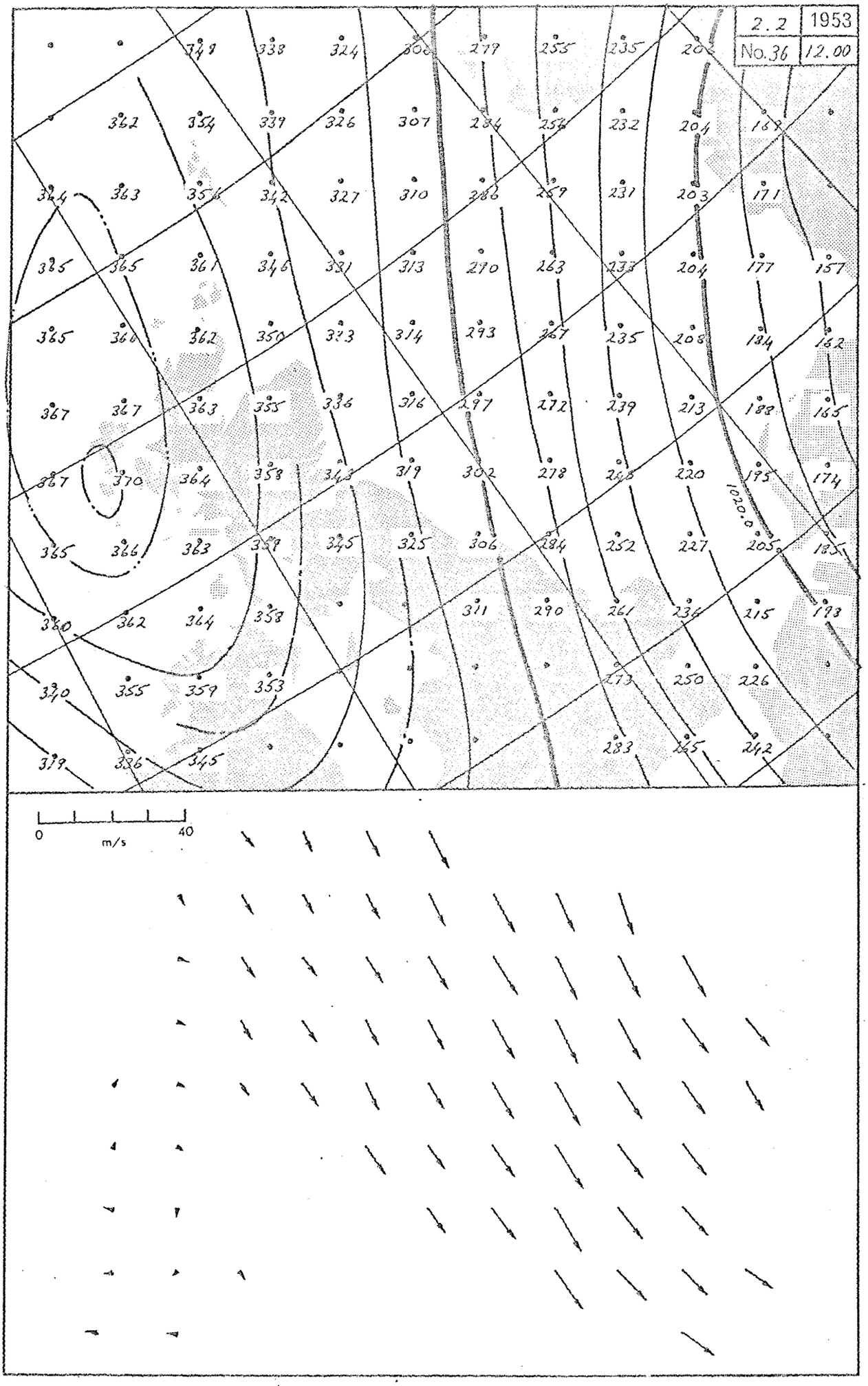
2.2
1953
No.36
12.00
1020.0
0
m/s
40

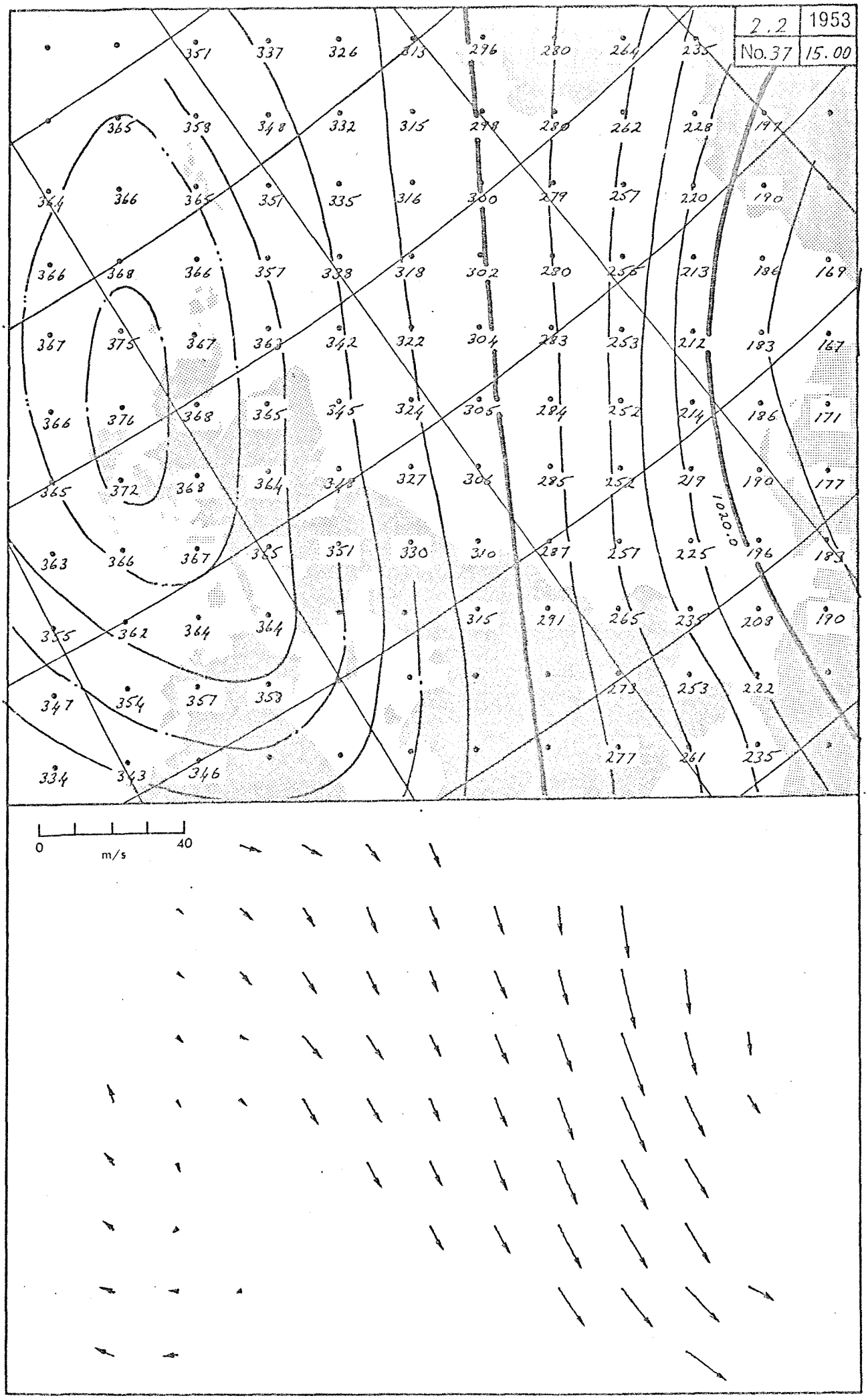
2.2
1953
No.37
15.00
1020.0
0
40
m/s

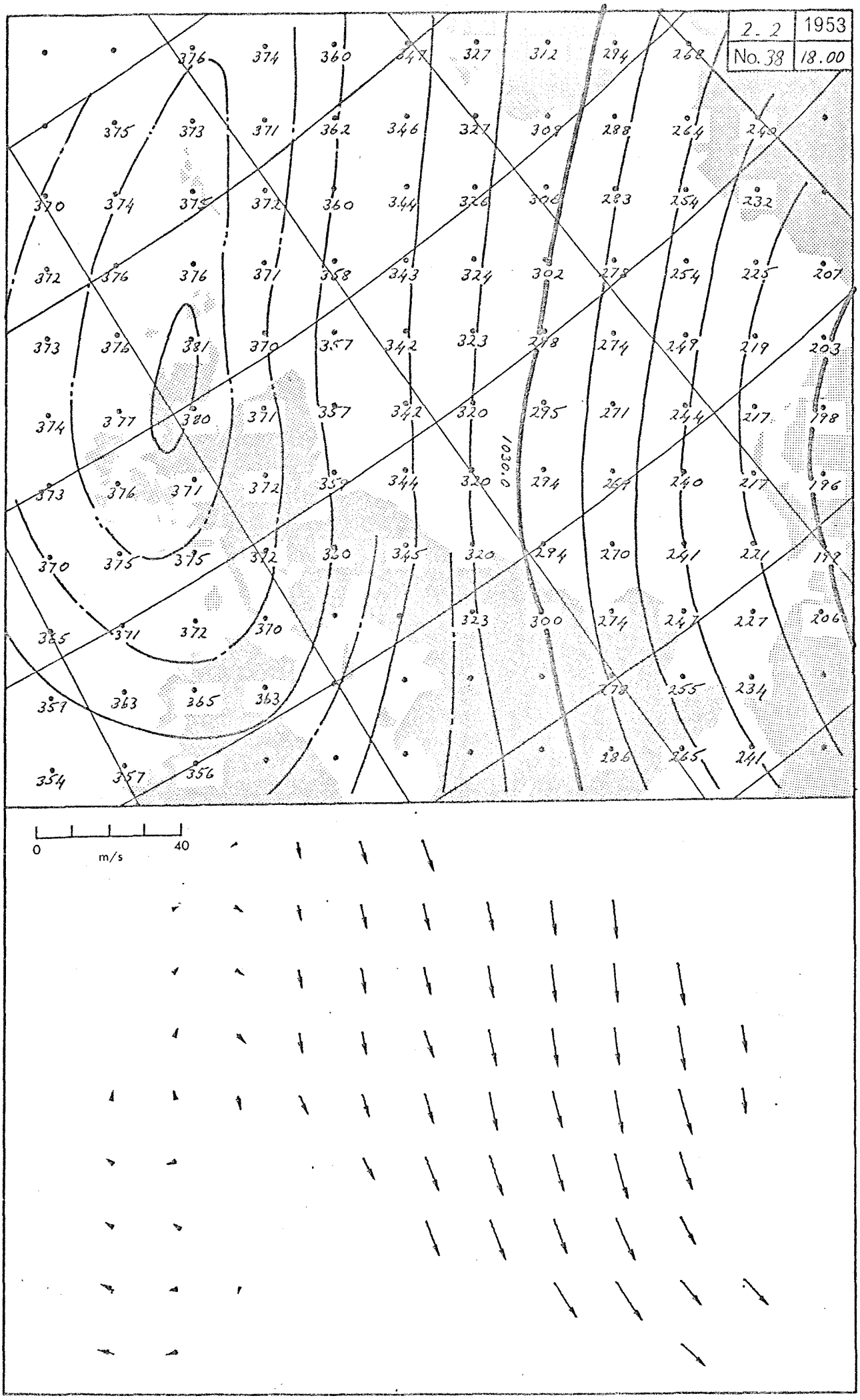
2. 2
1953
No. 38
18.00
1030.0
0
40
m/s

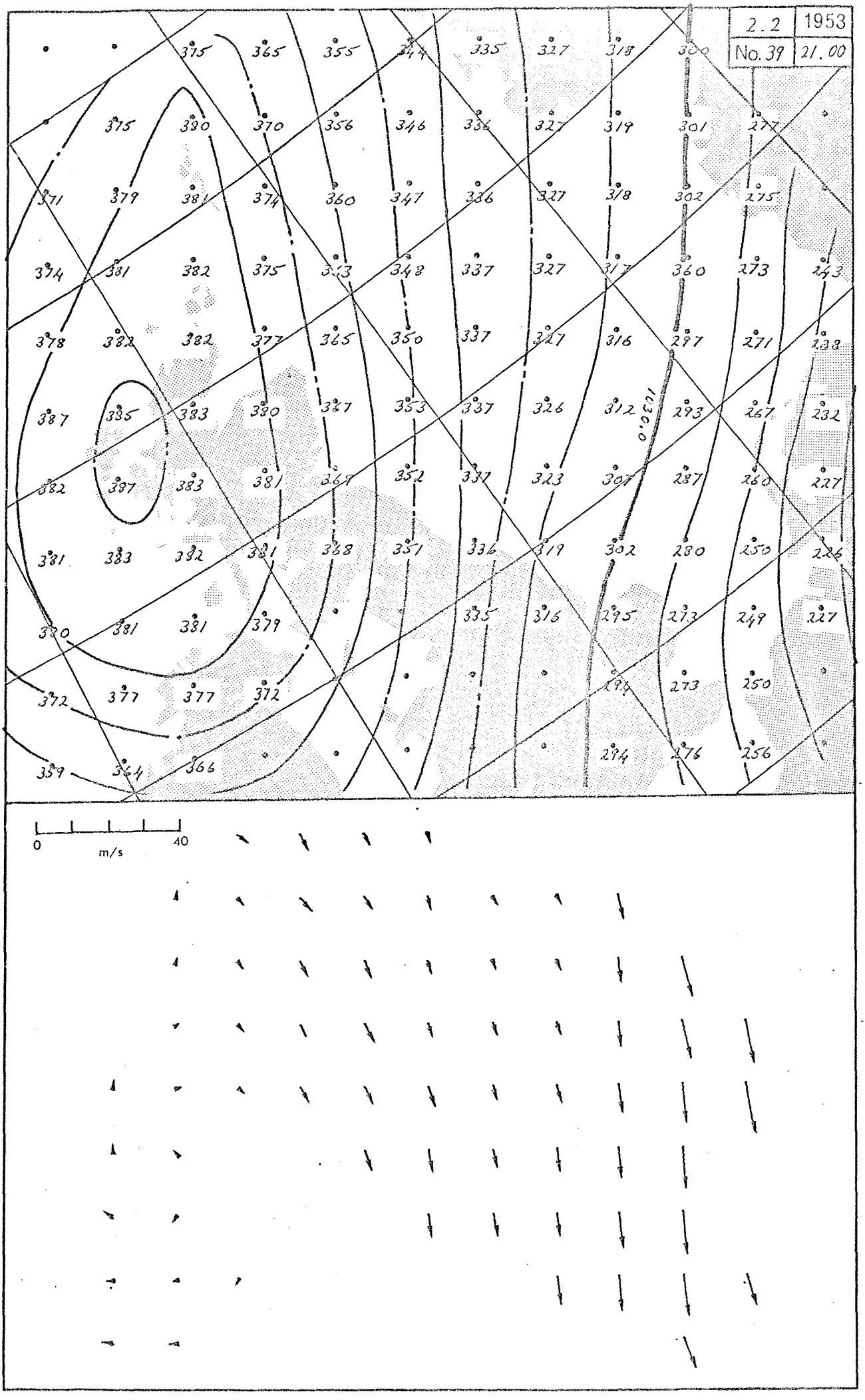
2.2
1953
No. 39
21.00
0
40
m/s

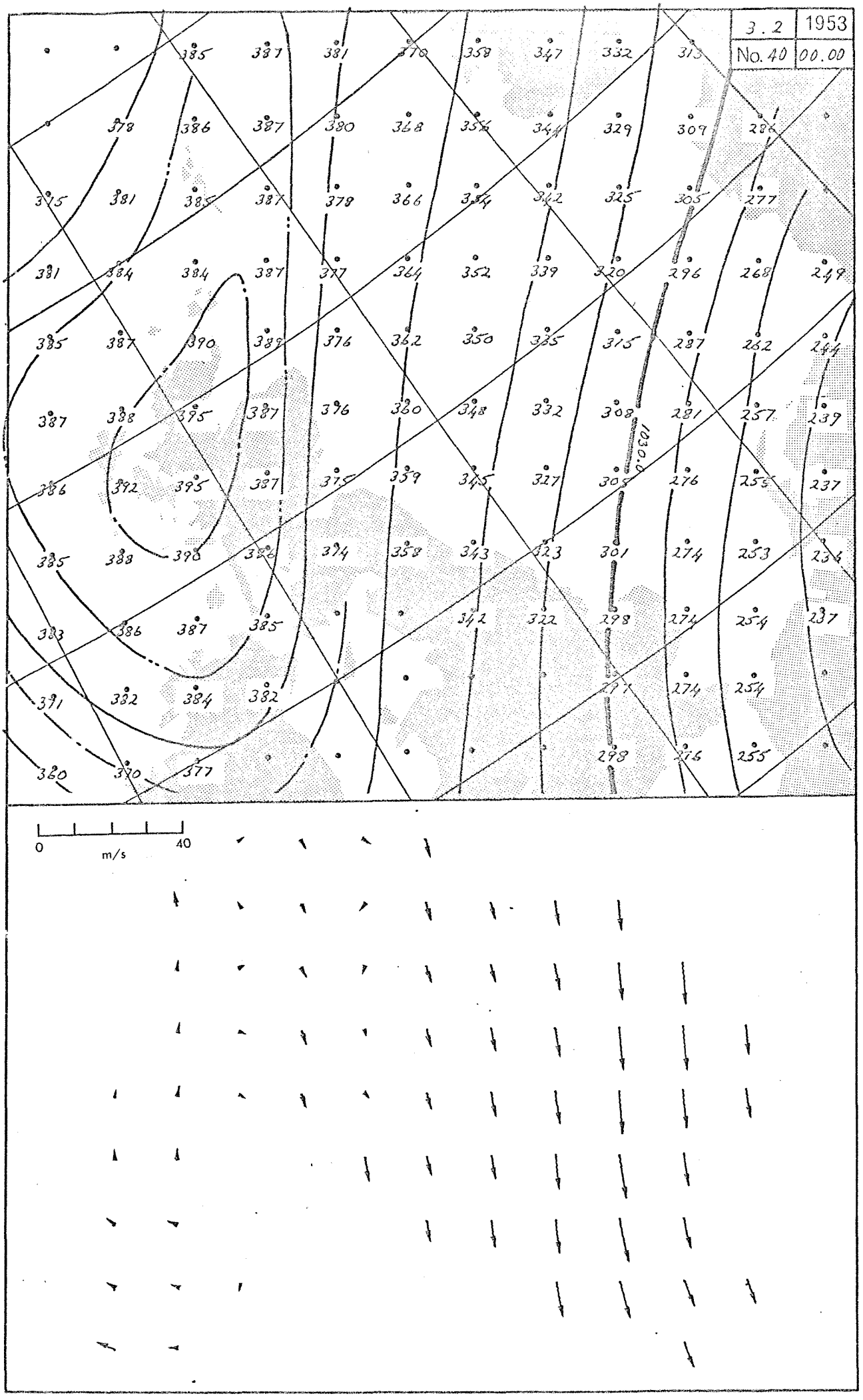
3.2
1953
No. 40
00.00
1030.0
0
40
m/s

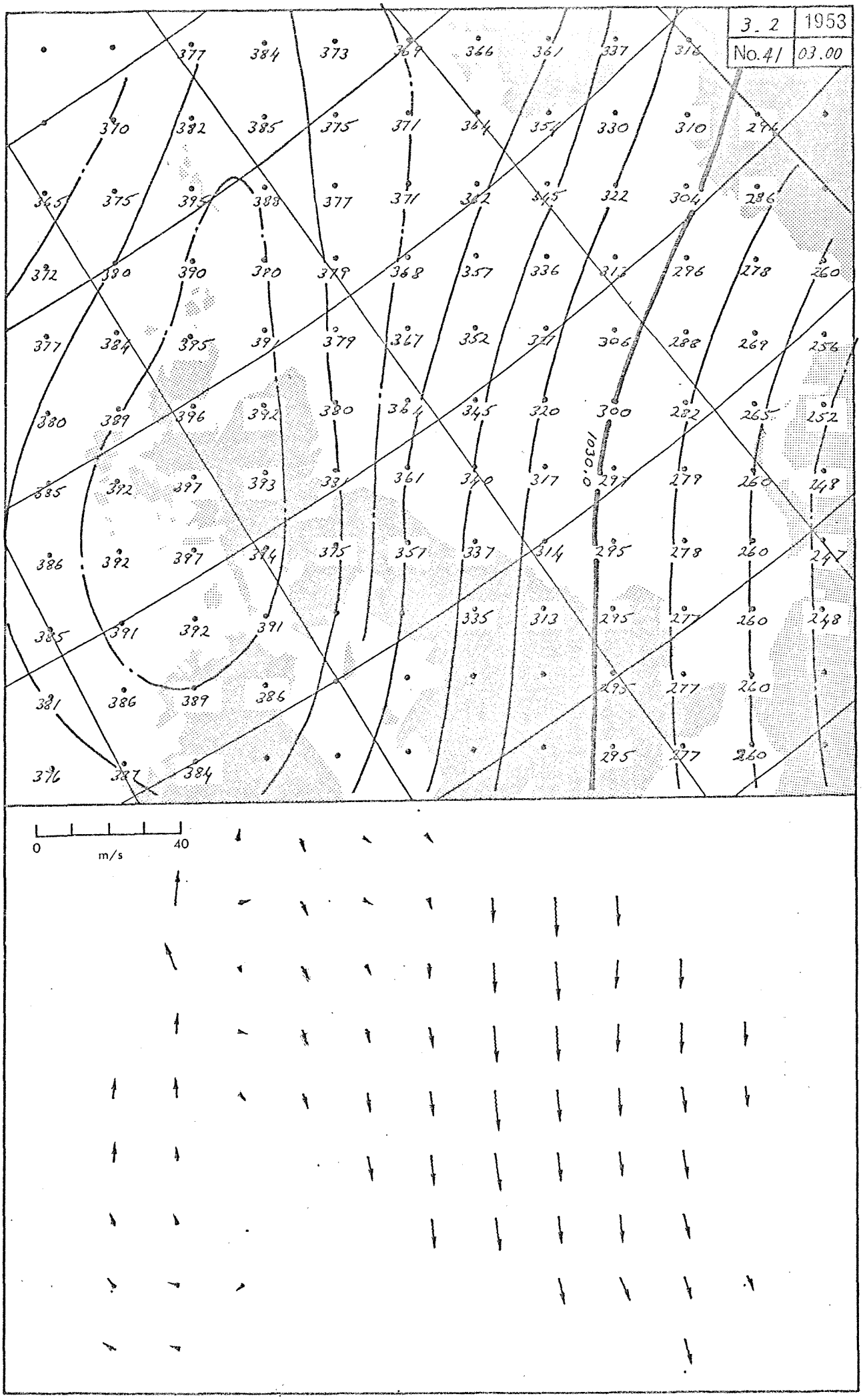
3. 2
1953
No. 41
03.00
1030.0
0
40
m/s

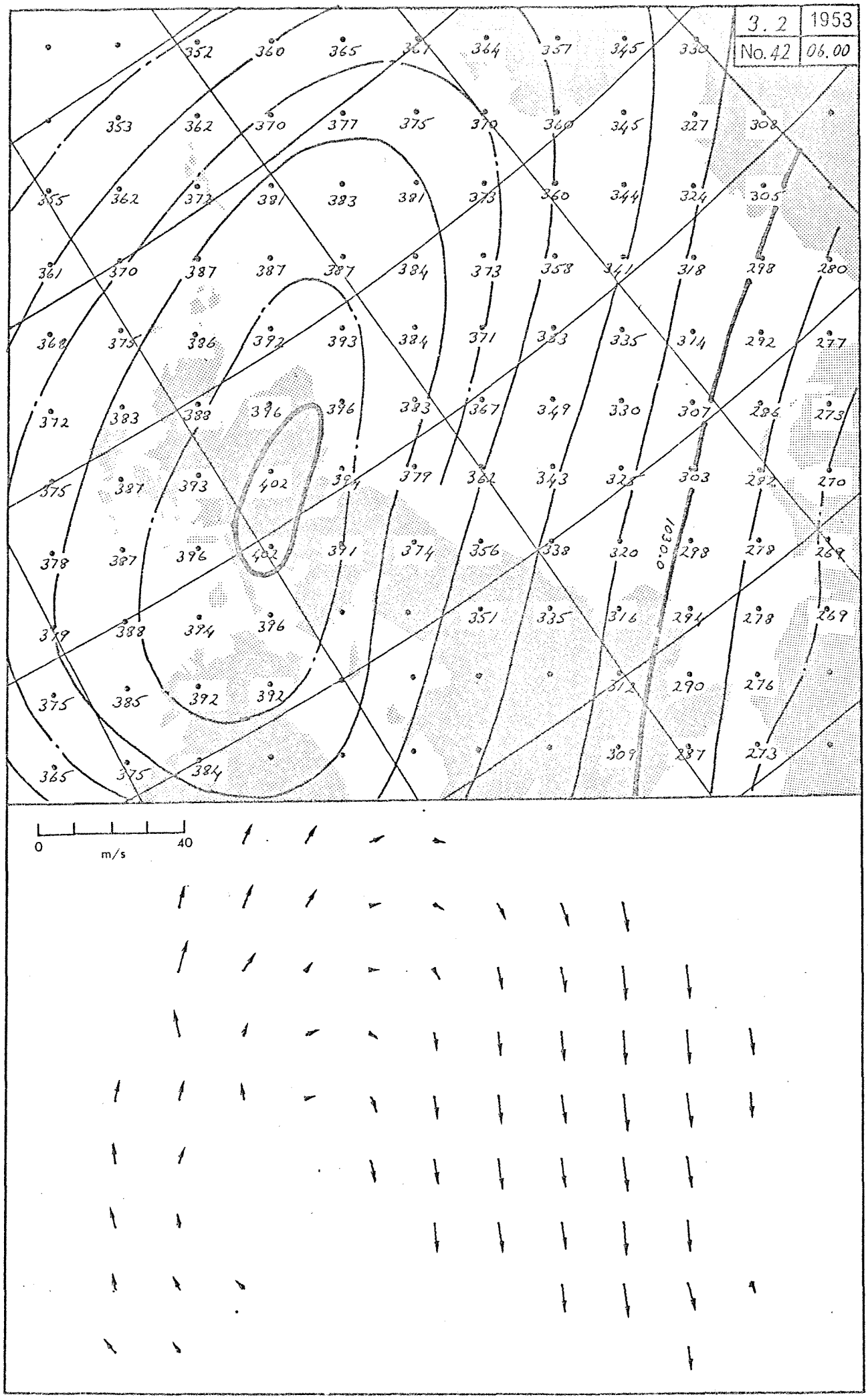
3. 2
1953
No. 42
06. 00
1030.0
0
40
m/s

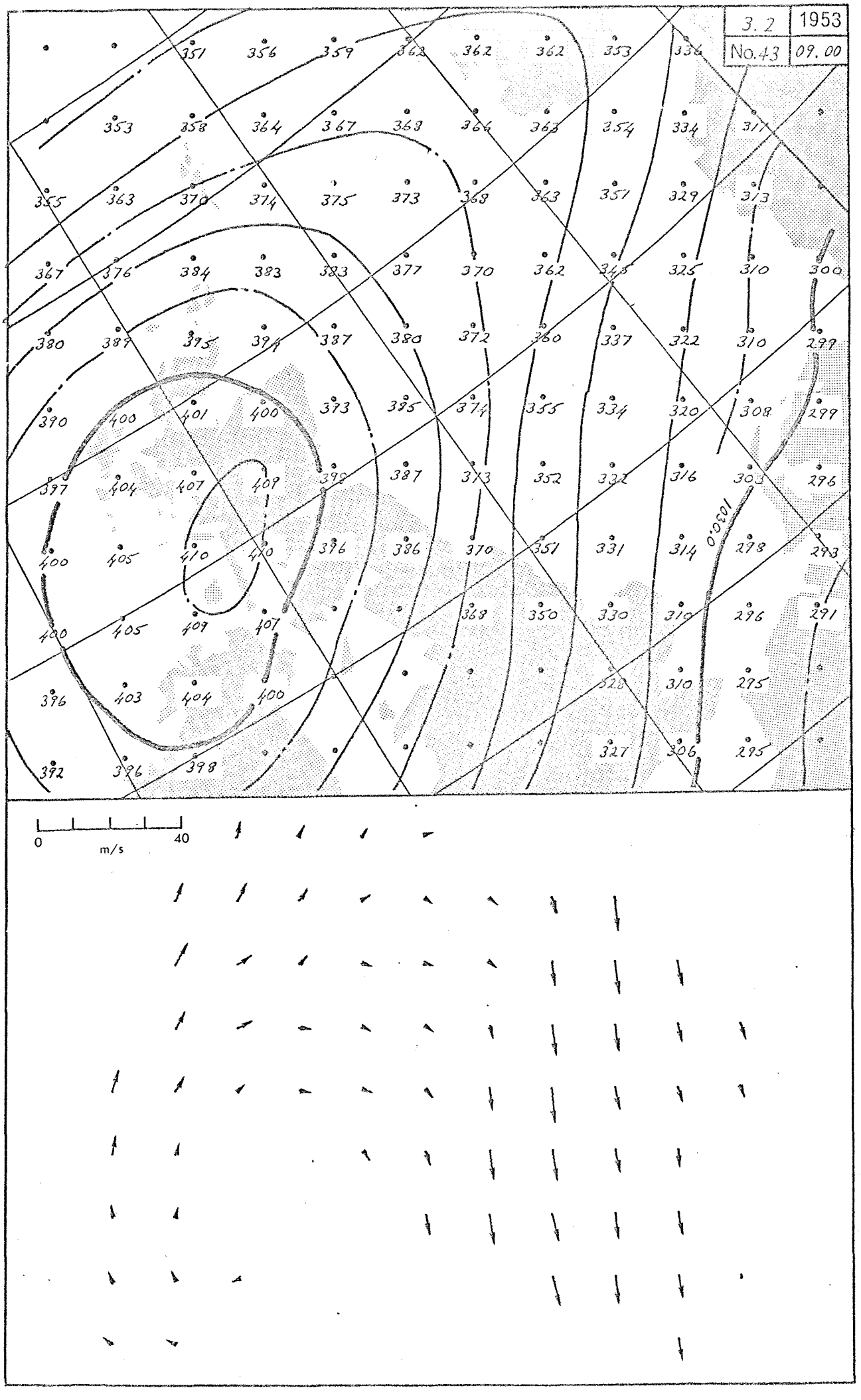
3. 2
1953
No. 43
09. 00
1030.0
0
40
m/s

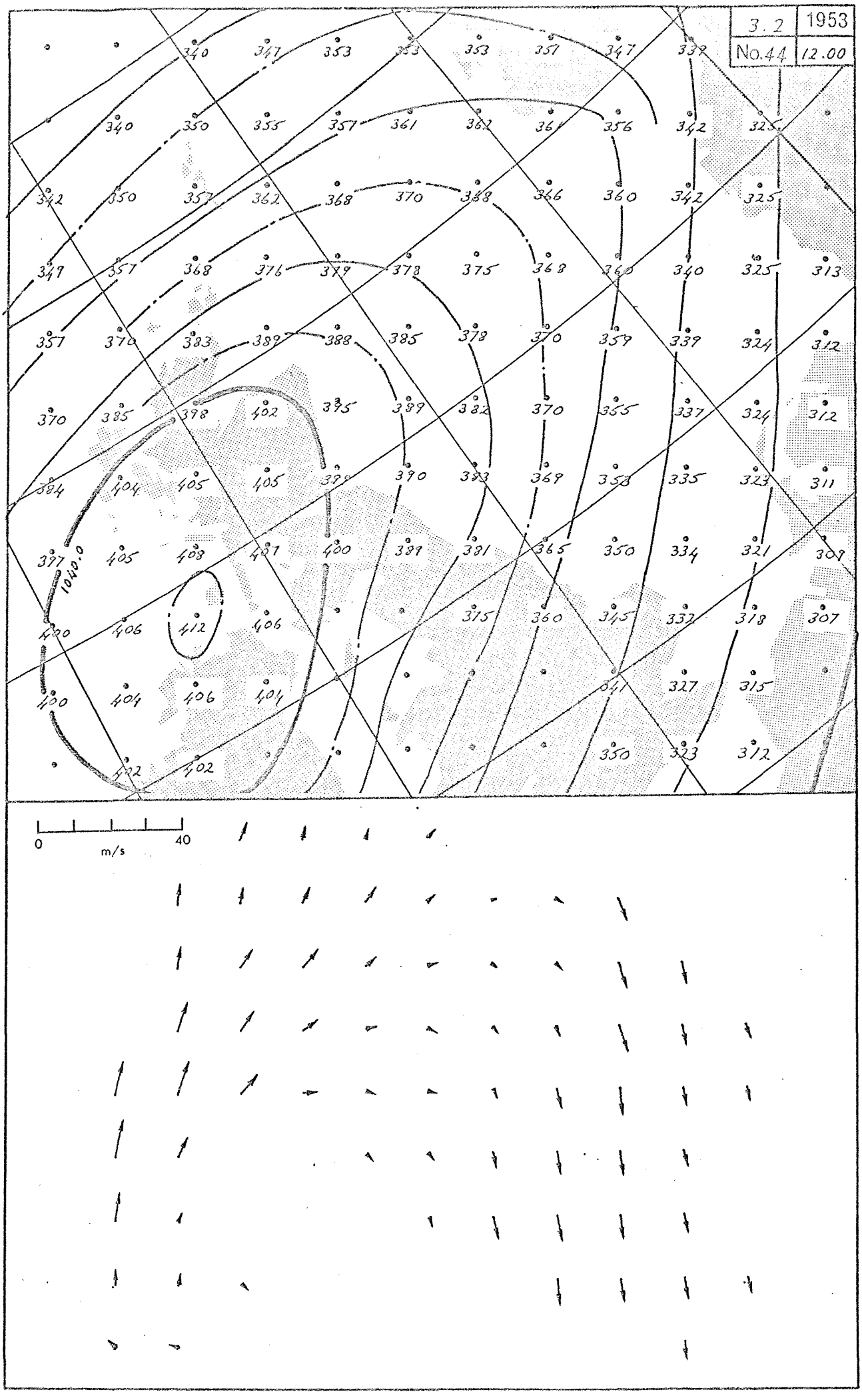
3. 2
1953
No.44
12.00
1040.0
0
40
m/s

Appendix Outline of the meteorological input-data processing system

The new electronic model for tides and storm surges contains a 'meteorological input-data processing system' (MIP) by which available meteorological input data is converted into a usable form for the electronic model. The MIP consists of several computing circuits, memories, and a XY plotter driving circuit, and is supported by an external numerical keyboard, tape-reader, tape-punch, and XY plotter. The main part of the apparatus is contained in a case 7.5 × 21 × 32 cm^3, and operated by a 240V AC power line.

The computing circuits are versatile within the data processing required for this application. By setting a few controls, several different modes of operation can be carried out. For example,

Re-arrangement of the order of data or combining data;

Computing the data of a wind field from the data of a pressure field;

Computing a wind-generated surge within each grid*;

Computing a pressure-generated surge within each grid*; and

Computing a pressure-and-wind generated surge within each grid*.

Since the speed of a computation is much faster than that of the peripheral instruments, the overall processing speed is limited by each peripheral instrument used. In practice, when input data is fed into the system, the output data is obtained at the same time. The output is obtained in two forms:

(a) A form which can be used directly by the main computation circuit of the model; or

(b) A form which is suitable for the XY plotter.

(b) is used for intermediate checking of the data being processed, or for displaying a particular factor, such as the wind-vector diagrams shown in this paper.

---

* 'A surge within each grid' means 'a surge which is directly generated by an external force (e.g. wind stress) acting within the grid at an instant'. The actual surge is the integration of many such surges over the whole sea surface and the time involved. The main computation circuit of the electronic model has been prepared to carry out such an integration continuously.